DISCRETE ELEMENT MODELING OF INFLUENCES OF AGGREGATE GRADATION AND AGGREGATE PROPERTIES ON FRACTURE IN ASPHALT MIXES

A Dissertation

by

ENAD MUHIB AHMAD MAHMOUD

Submitted to the Office of Graduate Studies of
Texas A&M University
in partial fulfillment of the requirements for the degree of

DOCTOR OF PHILOSOPHY

May 2009

Major Subject: Civil Engineering

DISCRETE ELEMENT MODELING OF INFLUENCES OF AGGREGATE GRADATION AND AGGREGATE PROPERTIES ON FRACTURE IN ASPHALT MIXES

A Dissertation

by

ENAD MUHIB AHMAD MAHMOUD

Submitted to the Office of Graduate Studies of
Texas A&M University
in partial fulfillment of the requirements for the degree of

DOCTOR OF PHILOSOPHY

Approved by:

Chair of Committee,	Eyad Masad
Committee Members,	Robert Lytton
	Amy Epps Martin
	Bruce Herbert
Head of Department,	David Rosowsky

May 2009

Major Subject: Civil Engineering

ABSTRACT

Discrete Element Modeling of Influences of Aggregate Gradation and Aggregate Properties on Fracture in Asphalt Mixes. (May 2009)

Enad Muhib Ahmad Mahmoud, B.S., University of Jordan;

M.S., Texas A&M University

Chair of Advisory Committee: Dr. Eyad Masad

Aggregate strength, gradation, and shape play a vital role in controlling asphalt mixture performance. Many studies have demonstrated the effects of these factors on asphalt mixture performance in terms of resistance to fatigue cracking and rutting. This study introduces numerical and analytical approaches supported with imaging techniques for studying the interrelated effects of aggregate strength, gradation, and shape on resistance of asphalt mixtures to fracture. The numerical approach relies on the discrete element method (DEM). The main advantage of this approach is the ability to account for the interaction between the internal structure distribution and aggregate properties in the analysis of asphalt mixture response and performance. The analytical approach combines aggregate strength variability and internal force distribution in an asphalt mixture to predict the probability of aggregate fracture.

The numerical and analytical approaches were calibrated and verified using laboratory tests on various aggregate types and mixtures. Consequently these approaches were used to: (1) determine the resistance of various mixture types with different

aggregate properties to fracture, (2) study the effects of aggregate strength variability on fracture, (3) quantify the influence of blending different types of aggregate on mixture strength, (4) develop a mathematical expression for calculating the probability of aggregate fracture within asphalt mixture, and (5) relate cracking patterns (cohesive: aggregate – aggregate and matrix – matrix, and adhesive: aggregate – matrix) in an asphalt mixture to internal structure distribution and aggregate properties.

The results of this dissertation established numerical and analytical techniques that are useful for developing a virtual testing environment of asphalt mixtures. Such a virtual testing environment would be capable of relating the microscopic response of asphalt mixtures to the properties of the mixture constituents and internal structure distribution. The virtual testing environment would be an inexpensive mean to evaluate the influence of changing different material and design factors on the mixture response.

DEDICATION

I dedicate my dissertation work to my loving parents, Muhib Mahmoud and Amal Abdelhadi; my grandfather, Nayef Hassan; my sisters, Aseel and Renad; and my brother, Eyad.

ACKNOWLEDGEMENTS

I would like thank my committee members who were more than generous with their expertise and precious time. A special thanks to Dr. Eyad Masad, my committee chairman, for his countless hours of reflecting, reading, encouraging, guidance, and most of all patience throughout the entire process. Thank you Dr. Robert Lytton, Dr. Amy Epps Martin, and Dr. Bruce Herbert for serving on my graduate committee and for very helpful comments on the dissertation.

I would like to thank Dr. Nazarian from the University of Texas at El Paso, and his entire research group for their precious help and cooperation in conducting laboratory testing as part of this research. I would like to thank the Texas Department of Transportation (TxDOT) for providing the funding for this research.

Special thanks go to the Texas Transportation Institute (TTI) and Zachry Department of Civil Engineering for supporting me as a student at Texas A&M University. I would like to particularly thank Cathy Bryan, Pam Kopf, Teresa Boriski, and Pam Fritcher for their great help. In addition, I would like to express my gratitude for my colleagues: Veronica Castelo Branco, Kamilla Vasconcelos, Emad Kassem, Chien Wei Huang, Silvia Caro, and Hassan Ghanem for the support and insightful technical discussions.

Finally, I would like to thank Leslie Gates, James Miles II, Paige Rieck, Stephanie Payne, Stephen Kirksey, and Ashlyn Kelbly for their remarkable help in all the laboratory testing and the different research tasks.

TABLE OF CONTENTS

CHAPTER Page

CHAPTER Page

LIST OF FIGURES

FIGURE Page

FIGURE Page

FIGURE Page

FIGURE Page

LIST OF TABLES

TABLE Page

CHAPTER I

INTRODUCTION

PROBLEM STATEMENT

An asphalt mixture is a combination of aggregates, asphalt binder, and air voids that consists approximately of 85% aggregates by volume. With increasing traffic volumes, asphalt pavements are exposed to higher stresses, which could lead to pavement distresses such as rutting and fatigue cracking. In order to improve the resistance to these distresses, improvements in the mixture design and material properties are sought. The new generation of asphalt mixtures such as stone matrix asphalt (SMA) and porous friction course (PFC) rely primarily on stone-on-stone contact to develop a strong coarse aggregate structure that can sustain and distribute applied loads. These mixtures, however, generate higher stresses in the aggregate structure, compared with conventional dense graded mixtures. Consequently, there is a concern that some aggregates in these new generation of mixtures might break and degrade under high stone-on-stone contact stresses.

The resistance of aggregate structure to degradation is function of the interrelated effects of aggregate gradation, shape, and strength. The degradation of the aggregate structure alters the mixture gradation and renders it weaker in withstanding applied traffic loading and more prone to pavement distresses such as rutting and fatigue cracking. The effect of gradation on asphalt mixture performance has long been recognized as an

---

This dissertation follows the style of *Journal of Materials in Civil Engineering*.

important factor because it influences the stress transfer mechanism within the mixture. However, there are no conclusive findings in the literature in regard to the type of gradation that provides the best performance.

Aggregate shape, angularity, and texture are believed to be key factors affecting asphalt mixture performance. These geometric characteristics affect the friction between aggregate particles, dilation of the aggregate structure, and directional distribution of material properties. Aggregate mechanical strength is another key factor in determining the resistance of aggregate particles to abrasion or breakage.

Accounting for the influences of all of these aggregate properties and characteristics (gradation, geometry, and strength) and their interactions through experimental methods is extremely hard because it would require a very comprehensive, time consuming, and labor extensive set of experiments. A major drawback of using only experimental methods is that these methods do not provide insight on the influence of these aggregate properties and characteristics on the internal structure distribution and its relationship to performance. Such an insight is needed to understand the mechanical behavior of asphalt mixtures in relationship to mixture design, and to optimize the internal structure to improve performance.

With the day-to-day advancement in computers speed, accuracy, and storage capacity, the use of analytical and numerical approaches to solve engineering problems is more compelling than ever. Such approaches provide a precise control over almost every single variable of the problem being studied, and thus allow researchers to develop a virtual testing environment that could cover as many variables as needed. Once an approach is calibrated, it can be used to run as many simulations as required.

OBJECTIVES OF THE STUDY

In this study, the discrete element method (DEM) is coupled with image processing techniques to model aggregate fracture within asphalt mixtures. This method allows accounting for the interrelated effects of gradation, shape, and strength of aggregate on asphalt mixture internal structure resistance to loading. Image analysis techniques will be used to transform the internal structure of an asphalt mixture into a discrete element model. DEM is then used to model the interaction between the mixture phases and apply various loading conditions to study the influence of mixture design, blending of aggregates with different properties, and variability in strength of aggregates on mixture strength and cracking patterns. The DEM results will be coupled with a probabilistic analytical method to calculate the probability of aggregate fracture given internal force distribution in the mix and aggregate strength.

The specific goals of this study are:

- Develop an approach to determine the internal forces developed within asphalt mixtures using the DEM. Magnitude and distribution of these internal forces are very important in affecting fracture initiation and propagation.
- Study the effect of the variability of aggregate properties on asphalt mixture performance.
- Study the effect of blending different types of aggregates on asphalt mixture performance.
- Develop an analytical approach that relates aggregate gradation and properties to resistance of aggregate structure to fracture. This analytical approach is formulated based on probability theory.

- Study the fracture patterns in asphalt mixture in relationship to internal structure distribution and their influence on mixture strength.

DISSERTATION ORGANIZATION

This dissertation is organized in seven chapters as follow:

- Chapter I introduces the main motivation of this study, followed by the objectives and the outline of the dissertation.
- Chapter II contains background on the technical topics relevant to the research documented in this dissertation. These topics include the DEM and its applications in asphalt mixtures, aggregate properties that affect asphalt mixture performance, and fracture and cracking patterns in asphalt mixtures.
- Chapter III presents the development of discrete element models for aggregates and asphalt mixtures. These models allowed the analyses of both the internal forces developed in asphalt mixtures and the effect of aggregate variability on asphalt mixtures. This chapter also includes a brief description of laboratory tests conducted to aid in the development and calibration of the models.
- Chapter IV presents a discrete element model that was developed to specifically assess the effect of blending aggregates with different properties in asphalt mixtures. The chapter includes a comparison between the model's results and laboratory experimental results.
- Chapter V introduces an analytical-probabilistic approach developed to calculate the probability of aggregate fracture in asphalt mixtures.

- Chapter VI utilizes the discrete element model of asphalt mixtures to analyze the different types of cracking patterns within asphalt mixtures and relate them to the strength of these mixtures.
- Chapter VII includes the conclusions and recommendations of this dissertation.

CHAPTER II

BACKGROUND AND LITERATURE REVIEW

INTRODUCTION

This chapter includes some background on the development and principles of discrete element method (DEM). This is followed by a literature survey of the topics relevant to the research documented in this dissertation, with emphasis on DEM applications in asphalt pavements and granular media; the effect of aggregate properties on asphalt pavement performance; and fracture and cracking patterns in asphalt mixtures.

BACKGROUND ON THE DISCRETE ELEMENT METHOD

The DEM is a finite difference scheme used to study the interaction among assemblies of discrete elements. DEM was introduced by Cundall (1971), and later in 1979 this method was proposed by Cundall and Strack for the simulation of two-dimensional non-continuous materials (Cundall and Strack, 1979). Cundall and Hart (1992) summarized the advancements in discrete element codes. They proposed that the name "discrete element method" should only apply to codes that allow finite displacements and rotations of discrete objects, including full detachment, and recognize new contacts automatically as the calculation progresses. As discussed by Abbas (2004), the DEM has been applied to study different types of geotechnical problems, such as the deformation mechanisms in geomaterials and flow of granular media.

DEM Principles

In the DEM the interaction between the discrete elements is a dynamic process in which equilibrium occurs when the internal forces balance. Tracking the movements of individual discrete elements within a stressed assembly of elements allows defining the contact forces and displacement of such an assembly. Movements occur as a result of disturbances that are caused by motion and/or body force of either a discrete element or a wall.

The DEM concept is simple in principle; it is based on successively solving the law of motion (Newton's second law) and the force-displacement law for each element. Figure 2.1 represents this concept; an explicit time-stepping scheme is employed to integrate Newton's second law for each element, given a set of contact forces acting on the discrete element. This leads to updated elements' positions and velocities. Based on the new positions, the relative displacements of each element are calculated and used to calculate the contact forces. The DEM is based upon the idea that the time step chosen is sufficiently small so that during a single time step, disturbances cannot propagate from any element farther than its immediate neighbors. Therefore, at all times the forces acting on any element are determined exclusively by its interaction with elements that it is in contact with (PFC2D, 2004).

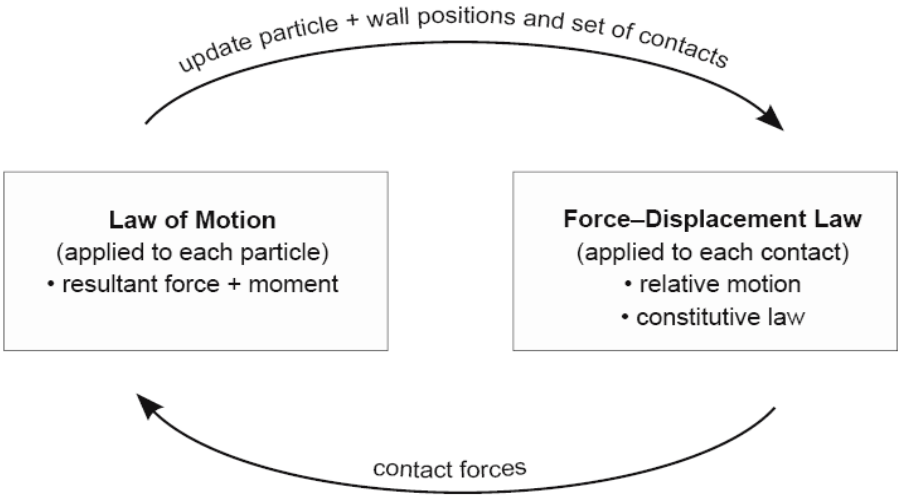

Figure 2.1. Calculation Cycle in Discrete Element Method (after PFC2D, 2004).

Particle Flow Code in Two Dimensions (PFC2D)

In this study a commercially available DEM code called Particle Flow Code in 2-Dimensions (PFC2D Version 3.1) developed by Itasca Consulting Group was used. This code includes a user-friendly graphical interface, linear and non-linear contact models, and linear and curvilinear boundary conditions. Several publications (e.g., Abbas [2004], Cheng et al. [2003], and You and Buttlar [2004]), including PFC2D manuals (PFC2D, 2004), include a description of this code. However, a brief description of the features of this code is discussed here for completeness.

In PFC2D, elements are circular (disks). They are allowed to overlap at the contact points, which occur over a very small area (i.e., at a point). The amount of overlap is related to the contact force via the force-displacement law. All overlaps are assumed to be small in relation to element sizes.

Contact Behavior

A contact between two elements exists whenever the distance between the centers of two adjacent elements is equal to or less than the summation of their radii (i.e., the two elements are just touching or overlapping).The contact behavior in PFC2D is described using up to three models (these models are activated for all contacts):

1. Contact Stiffness Models,
2. Slip Models, and
3. Bonding Models.

Contact Stiffness Models

The contact stiffnesses relate the contact forces and relative displacement in the normal and shear directions (normal and shear stiffness). The linear contact model is the simplest stiffness model (Figure 2.2). An effective normal and shear contact stiffness between elements is calculated from the elements' stiffnesses assuming that they act in series:

$$K^n = \frac{k_n^{[A]} k_n^{[B]}}{k_n^{[A]} + k_n^{[B]}} \tag{2.1}$$

$$k^s = \frac{k_s^{[A]} k_s^{[B]}}{k_s^{[A]} + k_s^{[B]}} \tag{2.2}$$

where k_s: shear stiffness, k_n: normal stiffness, K^n: effective normal stiffness, k^s: effective shear stiffness, and A & B: element designation.

Slip Model

This is an essential model between two elements in contact, and it becomes active once a contact bond is broken. The input parameter for this model is the friction coefficient (μ) at contact (dimensionless). It provides no normal strength in tension and allows slipping

to occur by limiting the shear force. The maximum allowable contact shear force is equal to the coefficient of friction multiplied by the normal force ($\mu \times F_n$) at that contact. Once the shear force (F_s) at the contact exceeds the value of this multiplication slipping will occur.

Bonding Models

Bonds can be added to the contacts between elements to either increase the stiffness of the contact and/or to include a strength parameter above which a bond breaks. PFC2D allows different types of bonds to be assigned. The two basic models are contact-bond model and parallel-bond model (Figure 2.3).

The contact bond effect is similar to a point of glue between two elements; it posses a constant shear and normal stiffnesses at the contact as well as specified shear and normal strengths. The bond will break once either the contact shear force equals or exceeds the contact bond shear strength, or the contact normal tensile force exceeds the contact bond normal strength.

On the other hand, the parallel bond effect is similar to the effect of a finite-sized bonding material (glue) between two elements, which also have constant shear and normal stiffness that is uniformly distributed throughout the size of the contact as well as specified shear and normal strengths. Again, if any of the contact forces (shear and tensile) exceed the assigned strength, the bond will break.

The main differences between the contact bond and parallel bonds are: 1) the parallel bond transmits both forces and moments between elements, while only forces are transmitted in the case of a contact bond, and 2) the stiffnesses of the parallel bond will act in parallel with the contact point stiffnesses, while the contact bond stiffnesses are the

same as the contact point stiffnesses. Thus, a parallel bond will have a stiffening effect at the contacts.

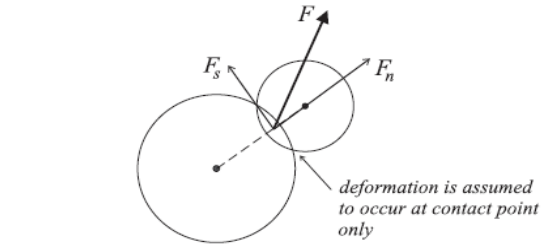

Linear contact law

$$F_n = k_n U_n$$

$$\Delta F_s = k_s \Delta U_s$$

Slip condition *friction coefficient*

$$F_s \leq \mu F_n$$

Figure 2.2. Linear Contact Model in the Discrete Element Code PFC2D (after PFC2D, 2004).

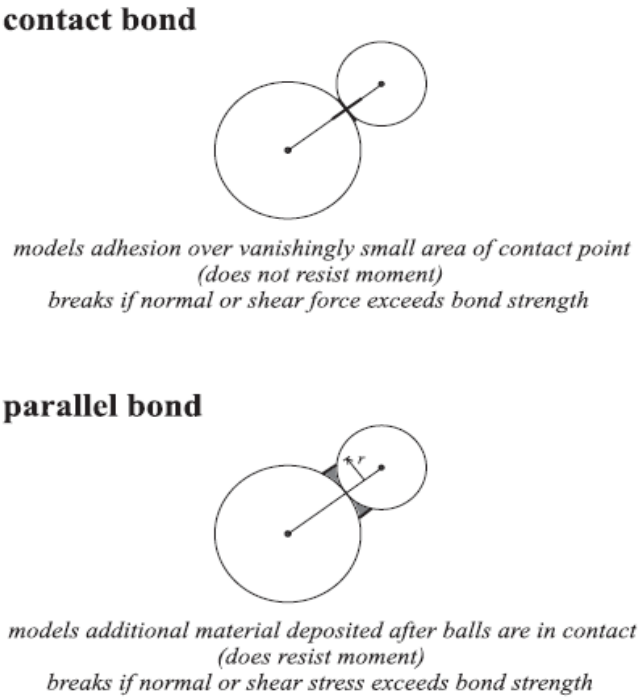

Figure 2.3. Contact Bonds and Parallel Bonds in PFC2D (after PFC2D, 2004).

Model Geometry

The model geometry in PFC2D is defined using an arrangement of circle elements (i.e., disks), which can be either defined directly by the user or created using the built-in generation algorithms of the software. When using the built-in generation algorithms, the location of the element is chosen at random. If the newly generated element is found to overlie a formerly generated one, another location is randomly selected. The number of trials to fit each element is 20,000 by default; however, the user could choose to change this number. This technique makes it not possible to describe materials of known geometry, but it is functional in describing materials with random element distributions. The other way to describe the geometry is to generate several element arrangements by defining their radii and x and y coordinates. Generally for this case, the user can write a code using the PFC2D built-in programming language (FISH).

Boundary and Loading Conditions

As mentioned previously, the basic components in PFC2D are circular elements (disks). To load the model both forces and velocities can be applied to a disk or a set of disks. Generated elements are not fixed, by default. Walls are used as the boundaries of the discrete element model. The walls are defined by specifying their end-points. According to the order in which the end-points are entered, only the left side of each wall is active. Walls do not interact with one another but interact with balls. Intersecting walls produce no problems, as no interaction will occur. Generated walls are fixed by default, but can be assigned a velocity, either an angular and/or translational. The equation of motion is not solved for walls, and thus forces cannot be directly assigned for them. In order to

apply stresses, a numerical servo-control mechanism can be used in which the wall velocity is updated at each cycle to meet the targeted stress level (PFC2D, 2004).

DEM APPLICATIONS FOR GRANULAR MATERIALS AND ASPHALT MIXTURES

DEM has been used in many different fields to study engineering problems. As such, there are many examples of DEM applications to problems related to flow of elements under different static and dynamic loadings. DEM has been used in soil dynamics, earthquakes, mining and tunneling, rock mechanics, powders and grains, concrete and asphalt behavior, and many other engineering fields. This section focuses on the applications that are directly relevant to the research conducted in this dissertation, namely granular materials and asphalt mixtures.

DEM Applications for Granular Materials

Evaluation of granular material crushing under direct shear test conditions was studied by Guerrero and Vallejo (2005) using DEM. They simulated the direct shear test with the use of a simple circular geometry for the granular material. As the elements in the model are unbreakable, the authors defined a failure criterion based on contact forces that is equivalent to a predefined element strength, and modified the model to replace any element that fulfilled the failure criterion by a group of eight smaller elements (Figure 2.4). This representation of the granular material and the crushing is not desirable, as this method is assuming a perfect circular shape to represent granular materials; of course, this assumption is far from true. The crushing criterion reduces the amount of the

material each time an element undergoes crushing, as the eight small elements are smaller (in total) than the original element, and this is another limitation of this proposed method.

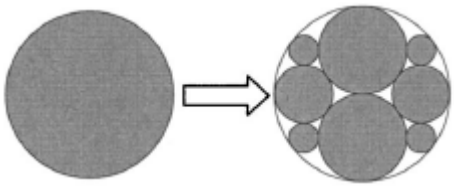

Figure 2.4. Crushing of a Granular Material (after Guerrero and Vallejo, 2005).

Cheng et al. (2003) performed DEM simulations of crushable agglomerates (i.e., aggregates). Aggregates in this study were made by bonding DEM elements, and simple contact bonds were used. The authors used a three-dimension model, and thus the DEM elements were spheres and the aggregates were generated with a shape of a sphere; however, 20% of the elements of each aggregate were deleted based on a random selection. The authors suggested this method to introduce variability and a more realistic shape to the DEM simulation. Two tests were simulated: the first was single aggregate crushing in which each aggregate was crushed between two plates; the second test was isotropic compression of a cubical arrangement of aggregates. The simulation results matched the crushing strength from laboratory samples of sand grains. This representation of aggregates (bonding DEM elements) allows crushing to be defined in a more realistic manner as it's simply the loss of bond between elements inside the aggregate. However, aggregate shape was not realistically represented, and the strength variability could have been introduced by varying the bond strength instead of randomly deleting DEM elements.

Marketos and Bolton (2007) utilized DEM to quantify the extent of crushing in granular materials. They used DEM along with probabilistic analysis to predict crushing within granular media. Their approach was based on combining a strength distribution of the granular material with an internal force distribution within the granular material system. A particle within the granular material system crushes when an internal force becomes higher than its strength.

The authors applied different levels of loading to a granular system using DEM without allowing any crushing to occur and studied the internal forces distribution. For each load level, the internal forces were normalized to the average internal force; this allowed fitting one distribution to all the internal forces from the different loading levels. Then by using a predefined strength distribution, along with the internal forces distribution, the crushing probability was studied both numerically and using DEM simulations.

Although the procedure followed by Marketos and Bolton (2007) to predict the crushing probability within granular material is sound and based on strong probabilistic basis, the DEM simulations were simplified by two assumptions. The first assumption was to use perfect spherical shapes to represent aggregates, and the second assumption was to remove particles once they reached the crushing criteria, as that was the only way crushing could be introduced since each aggregate particle was represented by a single DEM element. A similar approach is used in Chapter V of this dissertation to predict the probability of aggregate crushing within asphalt mixtures; however, the approach is modified to avoid these two simplifications in the DEM simulations.

DEM Applications for Asphalt Mixtures

Several research studies utilized DEM to characterize asphalt mixtures' behavior. The following part of this section summarizes some of these recent studies. These studies were selected to cover a wide range of the different tests/behavior of asphalt mixtures.

You and Buttlar (2004) used DEM to predict the modulus of asphalt concrete mixtures across a range of loading frequencies and test temperatures in both extension and compression. Internal structure of the asphalt mixture was captured by optical scanning of sawn test specimen. These images were then processed and analyzed in order to facilitate transferring them into DEM elements for PFC2D software. Elastic models were used to describe the contact behavior in this model, and so in order to capture the mixture modulus dependency, mastic properties were varied for the different temperatures and frequencies at which the mixture modulus needed to be determined. The predicted modulus values were reasonable at low temperatures. However, at higher temperatures the predicted values were lower than the measured ones. The authors explained this by noting that the model is a 2-D approximation and neglected the aggregate-to-aggregate contact in the third dimension. To overcome this, aggregates were expanded by a fixed proportion (particle dilation). Figure 2.5 shows the model geometry before and after aggregate dilation. This calibration technique matched the experimental data more closely. The authors explained the better results based on the assumption that dilation is expected to add more contacts between the aggregate in the 2-D model and thus better approximate the 3-D case. However, by examining Figure 2.5, it is obvious that the effect of aggregate particle dilation was mainly merging most of the aggregate particles rather than establishing more contacts, and thus it actually affected the ability of

the model to capture the real aggregate particles' shape. The increase in the modulus is expected in this case because the dilation increased the amount of material with high stiffness within the mixture.

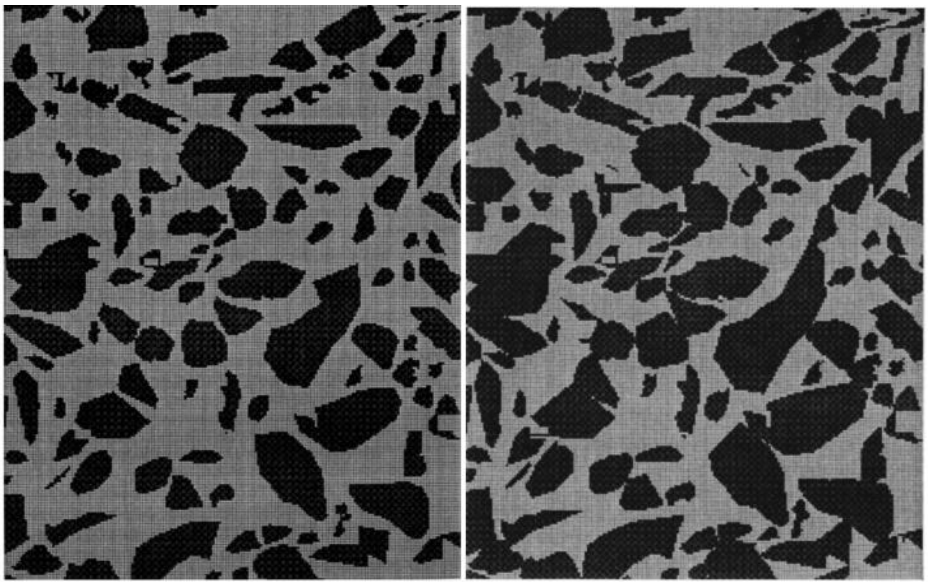

Figure 2.5. DEM Geometry: Before Aggregate Dilation (left) & After Aggregate Dilation (right) – aggregate particles in black – (after You and Buttlar, 2004).

Abbas et al. (2005) used DEM along with micromechanical-based models to determine asphalt mastic stiffness. The DEM was used to simulate the dynamic mechanical behavior of asphalt mastic measurements acquired using the dynamic shear rheometer (DSR). The discrete element model geometry used simple circular discrete elements to represent the filler material within the asphalt. The use of circular aggregate particles was justified by the small sizes (100 μm) of aggregate particles in asphalt mastics. However, filler shape could affect stiffness especially at high volumetric concentration of fillers. A linear contact model and a contact bond were used to represent the interaction between the elements. The analysis was done using three different asphalt

binders and four different aggregates from the SHRP materials reference library (MRL). The stiffening effect was also investigated at different concentrations of mineral fillers. The DEM was able to capture the stiffening behavior that was observed in the laboratory results. On the other hand, the micromechanical models (investigated in this particular study) underestimated the stiffening effect of the mineral fillers on the asphalt mastic behavior when compared to the experimental data.

Another study by You and Buttlar (2005) investigated the use of DEM to simulate a hollow cylinder tensile (HCT) test. This test applies internal pressure in the inside of a hollow cylindrical specimen. In this study, experimental measurements were conducted at different temperatures and load ranges in order to measure the asphalt mixture dynamic modulus. The discrete element model used the same procedure of You and Buttlar (2004) to capture the internal structure of an asphalt mixture. Figure 2.6 shows a laboratory specimen of the HCT test and its DEM representation. The dynamic modulus predicted from DEM simulations was in good conformity with the laboratory results for the coarse-graded mixtures. However, the model underestimated the asphalt mixture modulus for the fine-graded mixtures. The authors believe that this phenomenon was expected, as in the coarse-graded mixtures the model is able to provide the physical representation of internal forces developing within the aggregate skeleton (i.e., aggregate-to-aggregate contact). However, the model did not capture the aggregate skeleton for the fine-graded mixtures. The authors, just as in You and Buttlar's (2004) model, used elastic contact models to predict the dynamic modulus. However, it is necessary to represent the mastic properties using a viscoelastic contact model in order to represent the mixture response as a function of temperature and frequency.

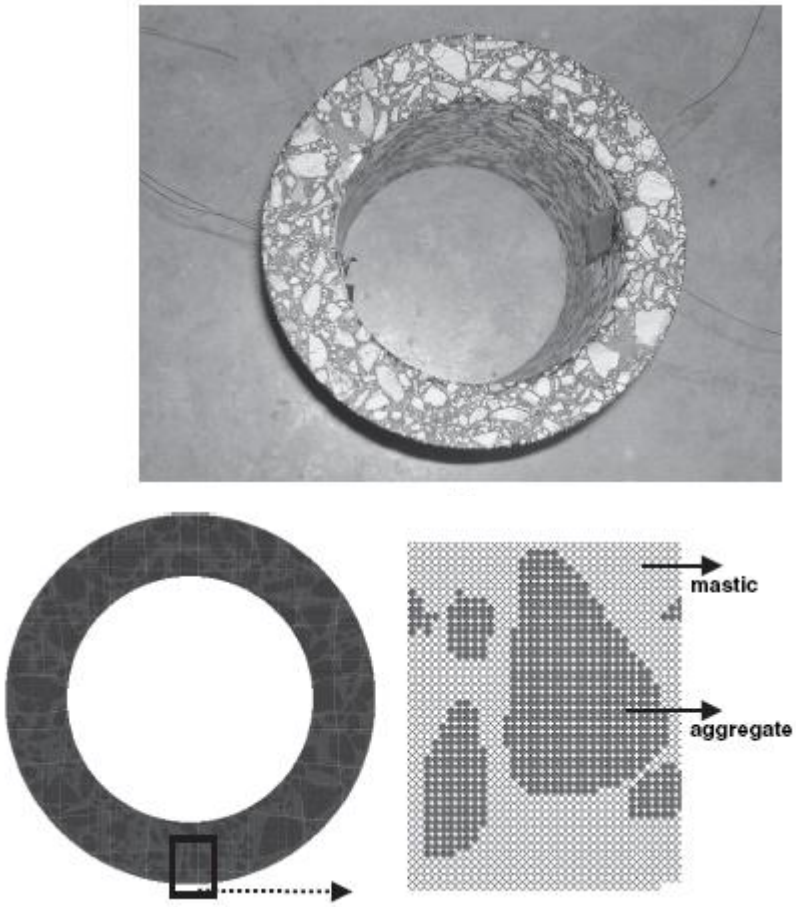

Figure 2.6. HCT Test Laboratory Specimen (upper part) and its DEM Representation (lower part) (after You and Buttlar, 2005).

Dai and You (2007) used the DEM to predict the creep stiffness of asphalt mixtures. Laboratory measurements of asphalt mixture creep stiffness were conducted in order to provide a comparison for the DEM predictions. The experimental measurements were conducted at three temperatures, 0, -10, and -20^{o}C, for up to 100 s of loading time. The creep stiffness was obtained from the inverse of creep compliance at different loading times and temperatures. The 2D internal structure of the asphalt mixtures was captured from digital images of sawn laboratory asphalt samples. The DEM results were

compared to finite element (FE) analysis of the response of asphalt mixtures. For the FE model, elliptical fitted aggregates were used (Figure 2.7) and were assumed to be rigid with infinite stiffness. However, the discrete element model utilized images of the internal structure (Figure 2.8) with a typical stiffness value. The laboratory results fell between the two model predictions with the FE overestimating the stiffness at lower reduced times, while the DEM underestimated the mixture creep stiffness at higher reduced times. The authors attributed the under-prediction of DEM results to the use of a 2D model, which underestimates the aggregate-to-aggregate contact (interlocking) that could be captured by a 3D model.

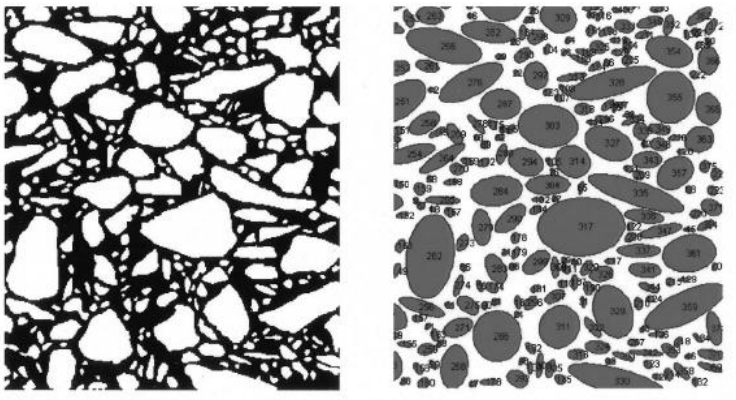

Figure 2.7. Aggregate Representation by Elliptical Fitted Shapes for FE Model: Mixture Internal Structure (left) & Aggregate Representation (right) (after Dai and You, 2007).

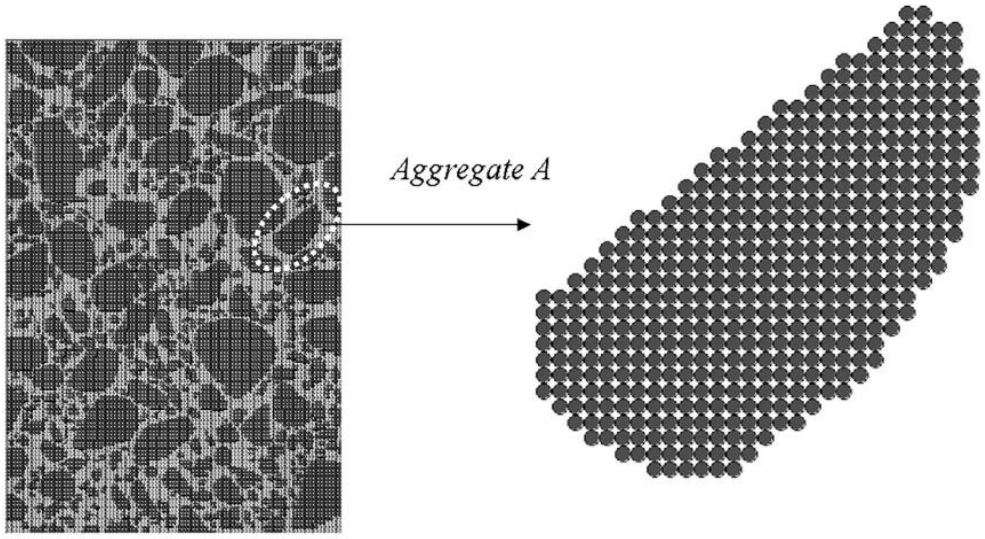

Figure 2.8. Aggregate Representation by Real Shapes for DEM (with one aggregate particle enlarged) (after Dai and You, 2007).

The viscoelastic behavior of asphalt mixtures using DEM was studied by Abbas et al. (2007). In this study, the discrete element model was developed to predict the asphalt mixture response under sinusoidal loading similar to laboratory measurements of the dynamic modulus of asphalt mixtures. The experimental tests were conducted on mixtures with nine different binders, both modified and unmodified, with one aggregate gradation from one source. Asphalt mixtures cylindrical samples of 100 mm (4 in.) diameter and 150 mm (6 in.) height were tested to measure the dynamic modulus and phase angle at a temperature of 50^{o}C over the following range of frequencies: 0.1, 0.5, 1.0, 10.0, and 25.0 Hz. As in the previously discussed studies, digital images were used to capture the internal structure of the asphalt mixtures. The DEM predicted the dynamic modulus of seven out of the nine mixtures. On the other hand, the phase angles were overestimated by the DEM for all nine mixtures. The authors attributed these results to the use of a 2D representation of the geometry and the low resolution of the model.

Kim et al. (2008) used DEM to study the fracture behavior in asphalt concrete mixtures. The authors used a disk-shaped compact tension geometry to determine the fracture energy of asphalt concrete mixtures. The loading in this test was in tension through the loading holes with a constant crack mouth opening displacement (CMOD) rate of 1 mm/min. This loading/geometry configuration induces a mode I fracture. A discrete element model of similar geometry was developed with a heterogeneous cohesive zone implemented within the discrete element model. This zone was implemented by the use of the "Displacement-Softening" model supported by PFC2D software in this model. Once the contact force exceeds the contact bond strength, the contact starts to yield until it reaches a maximum predefined displacement, and then it breaks. A digital image was used in this study as well to capture the internal structure of the asphalt mixture samples (Figure 2.9). The simulation results compared very well to the laboratory results in terms of initial stiffness, peak load, and the CMOD that corresponds to this specific test.

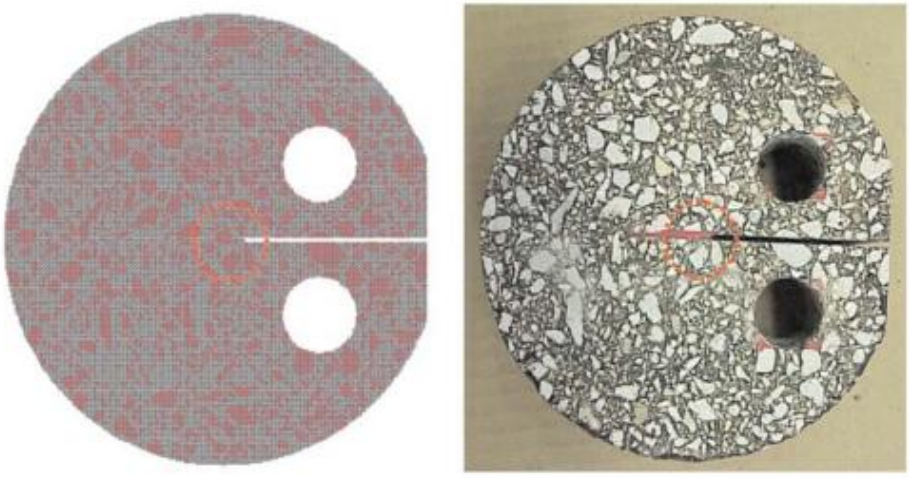

Figure 2.9. DC (T) Test Geometry: DEM Representation (left) & Laboratory Sample (right) (after Kim et al., 2008).

AGGREGATE PROPERTIES' EFFECT ON ASPHALT PAVEMENT PERFORMANCE

Aggregate characteristics such as gradation, shape, stiffness, and strength are all important factors that affect the performance of asphalt pavements. There has been discussion in the literature on the influence of gradation on asphalt mixture performance (Hand et al., 2002). However, there is no consensus on a certain type of gradation that would provide the best performance. This is caused by the fact that the selection of aggregate gradation depends to a large extent on the local experience with different gradations; properties of available aggregates; and the priorities of performance measures, such as resistance to fatigue cracking, resistance to rutting, drainage of surface water, etc. For example, open-graded (such as PFC) mixtures are applied primarily to provide drainage of surface water, while gap-graded (such as SMA) mixtures provide high resistance to deformation and very good durability.

The role of aggregate shape in controlling performance, such as fatigue and rutting resistance, of asphalt mixtures is emphasized by many research studies. Aho et al. (2001) indicated that aggregate shape characteristics are the second most important parameters after gradation in affecting asphalt mixture performance. Based on modeling the influence of aggregate structure on performance, Cheung and Dawson (2002) concluded that "roundness and angularity are the major factors affecting the ultimate shear strength and permanent deformation."

Sanders and Dukatz (1992) studied the effect of coarse aggregate angularity on permanent deformation. The study was conducted on four interstate sections, and the one section that developed permanent deformation was the one with lower quantities of

angular coarse aggregates when compared to the other three sections. A study by Barksdale et al. (1992) showed that aggregate shape properties correlate statistically with selected asphalt mixtures' rutting behavior.

The Aggregate Imaging System (AIMS) was developed in recent years to measure aggregate shape properties using image capturing and processing techniques (Masad, 2003). AIMS is capable of measuring aggregate angularity, form, and texture of various sizes of aggregates. Masad (2003) provided the details of the design of AIMS hardware and the mathematical methods used for calculating the aggregate shape properties.

In addition to gradation and shape, aggregate stiffness and strength are important properties that provide resistance to crushing and abrasion during construction (stockpiling, placing, and compaction) and under traffic loading (Wu et al., 1998). This is necessary to avoid changes in asphalt mixture gradation during construction, resulting in a mixture that does not meet the desired volumetric properties (Prowell et al., 2005) or deforms excessively under traffic loads (Cheung & Dawson, 2002).

Mahmoud and Masad (2007) developed experimental methods for evaluation of aggregate resistance to polishing, abrasion, and breakage. The proposed methods utilized the Micro-Deval machine to induce abrasion, breakage, and polishing of aggregates. The AIMS system was used to obtain the shape properties of the aggregates (angularity and texture) before and after the Micro-Deval test. The weight loss in the Micro-Deval combined with a drop in angularity was used to assess the aggregate breakage and abrasion, while the texture of aggregates at three different points, namely before Micro-Deval, after Micro-Deval, and after an extended run on Micro-Deval, were used to

capture the polishing of the aggregate. The use of three texture points allowed capturing both the loss in texture, i.e., polishing amount, and the rate that the aggregate lost its texture, i.e., polishing rate.

New-generation asphalt mixtures such as PFC and SMA rely on stone-on-stone contact between coarse aggregates in resisting applied loads. However, these contacts generate high localized stresses that necessitate careful evaluation of the properties of coarse aggregates (strength, gradation, and shape) needed to prevent fracture of aggregate particles and resultant degradation of mixture properties. It would be difficult to account for all these characteristics using experimental methods, as a comprehensive experimental testing would be expensive and yet fall short of affording a full explanation of the different interactions that occur.

FRACTURE AND CRACK PATTERNS IN ASPHALT MIXTURES

Cracking in asphalt pavements is dependent on the localized internal forces within its structure. Different studies have attempted to study cracking by treating asphalt mixture as a binder with rigid inclusions (aggregates). This section will briefly introduce some of the studies on crack propagation of two-phased materials in general. This will provide the background to discuss the studies that focus on the asphalt pavement mixtures.

One of the first studies that discussed the interaction of a crack front with a second-phase inclusion was conducted by Lange (1970). In this study, the second-phase inclusions were considered as obstacles that delay the moving crack front. This phenomenon was called “momentary pinning” by the author. The author presented observations of crack pinning using topography of fracture surfaces, which showed that

the crack front interacts with inclusions and increases its length during fracture. The author explained this as a bowing action that occurs in between the inclusions and pinning at the location of the inclusions, and thus the crack front length increases. This concept was used to derive an expression of fracture energy for composite brittle materials which shows that the fracture energy increases as a result of the inclusion and that it is a function of the spacing between the inclusions. The conclusion was that a brittle material can be strengthened by the addition of closely spaced inclusions, neglecting its role as a stress concentration point. A later study by Evans (1972) used the theory developed by Lange (1970) to study the strength of brittle material containing second-phase inclusions. The derivations in this study accounted for both the size and spacing of inclusions, compared to the derivation of Lange (1970), which only accounted for spacing. Including both the size and the spacing makes the problem more complicated. Such derivations are cumbersome and out of the scope of this review. The study by Evans (1972) concluded that the crack extension stress (which is the stress required to extend the crack) depends on the ratio between the inclusion dimension and the inclusion spacing, and it is larger than the stress to propagate the primary crack (before interacting with inclusions), except for high values of inclusions' spacing.

Rodriguez et al. (1996) studied the low temperature fracture performance of asphalt binders and asphalt mixtures. It was found that asphalt binder toughness increases with addition of fillers, that the theory developed by Evans (1972) could predict this increase, and that this increase is a function of the volume fraction of the filler only. As the filler becomes coarser, the Evans theory underestimates the increase in the fracture toughness. This can be seen in Figure 2.10, which is extracted from that study. The two

curved lines, “a and b,” represent the theoretical estimation of the fracture toughness using Evans’ theory. Line “a” assumes a non-interacting semi-elliptical crack, while line “b” assumes interacting secondary cracks. The limestone #2 and the granite have a coarser gradation compared to the limestone #1 and the calcium carbonate cases, and it shows that Evans’ theoretical prediction underestimates the coarser fillers, especially at higher volume fractions. The authors attributed this to a change in the fracture mechanics from crack pinning to crack blunting and/or bulk plastic yielding. The authors also emphasized the importance of the adhesive bonding between the asphalt binder and the filler, as the fracture toughness increases with higher adhesive bonding.

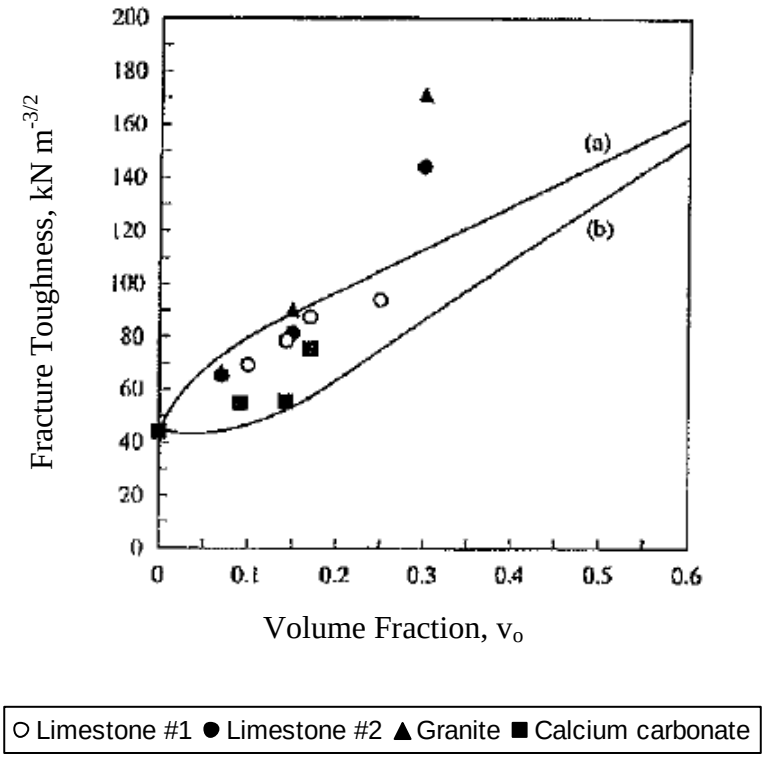

Figure 2.10. Fracture Toughness Increase in Asphalt Binder as a Function of Filler Volume Fraction (after Rodriguez et al., 1996).

Smith and Hesp (2000) expanded the work by Rodriguez et al. (1996) by using crack pinning theory to explain the fatigue behavior in both asphalt mastic and mixtures at low temperatures. Fatigue performance was evaluated experimentally for mastics using a dynamic rheometer by applying a constant torsional strain for the different specimens at 10^{o}C and 40 Hz and at different strain levels. For the asphalt mixtures, a constant stress fatigue test was conducted on mixtures of both gap-graded and dense-graded samples. The fatigue life of asphalt mastic increased with a decrease in the filler size, and this is in agreement with Evans' (1972) crack pinning theory. Conversely, the particle size did not significantly affect the fatigue life of asphalt mixtures. The authors explained the general behavior of fatigue performance based on the type of crack propagation that occurs. If the propagation is slow and through numerous micro-cracks, then the filler size will affect the fatigue performance; however, in the case of a single crack causing failure through the sample, then the size of the filler will not affect the fatigue performance (i.e., Evans' theory is not applicable).

Jacobs (1995) used a three-phase crack propagation theory to explain crack growth in asphalt mixtures. The three phases are: (1) cohesive crack growth, which is the crack growth within the asphalt matrix (binder + fine aggregates); (2) adhesive crack growth, which is the crack propagation due to the bond loss between the aggregate particles and the binder (pealing); and (3) crack retarding in the case of crack direction change (crack tip hitting an aggregate particle). The work of Jacobs (1995) differs from crack pinning theory as it does not attribute the increase in fracture energy to plastic energy dissipation at the crack tip due to crack pinning.

SUMMARY

This chapter included a brief summary of the DEM background that covers the basic calculations, as well as the different models that can be used to utilize this method with the commercially available software (PFC2D). The second part of this chapter summarized some of the studies covering the applications of the DEM in engineering problems with emphasis on evaluation of asphalt mixture performance, aggregate properties that influence asphalt mixture performance, and theories that used to explain the crack propagation within asphalt mixtures.

Based on the literature review, the use of DEM to predict and/or model asphalt mixture performance seems to be promising. It allows for representation of the internal structure of the mixtures with the realistic shape of aggregate particles. Also, it was successful in modeling a wide range of performance tests on both asphalt mixtures and mastic, and it was able to capture the response reasonably.

The review also showed how aggregate characteristics play a vital role in controlling asphalt mixture performance. Aggregate characteristics such as angularity, size, shape, strength, and toughness, as well as gradation, all showed significance in different asphalt performance aspects, such as fatigue, rutting, and durability.

Finally, crack pinning is believed to be one of the fracture modes that controls cracking in asphalt mixtures; however, the results presented in the literature supporting this hypothesis were all based on asphalt mastics (fine fillers), and a different mechanism is expected to be dominant in the presence of coarse aggregates.

CHAPTER III

INFLUENCE OF AGGREGATE INTERNAL STRUCTURE, PROPERTIES, AND VARIABILITY ON FRACTURE OF ASPHALT MIXTURES

INTRODUCTION

Increased loads on asphalt pavements have necessitated the use of new-generation mixture designs that rely on stone-on-stone contact of the coarse aggregates. Coarse aggregate gradations, shape, stiffness, and strength play a vital role in these new-generation asphalt mixtures in resisting and distributing applied loads during construction and under traffic. It is imperative that the contribution of the aggregate properties to asphalt mixture performance is understood and that methods are developed to analyze this contribution during mixture design.

This chapter introduces an approach that combines the DEM and image processing techniques to account for aggregate strength, gradation, and shape in modeling asphalt mixture resistance to fracture. The DEM input parameters were determined from testing aggregate and asphalt mixtures. The developed approach was used to determine the internal forces within the aggregate structure in asphalt mixture under loading and to relate them to aggregate structure and properties. In addition, the approach was used to analyze the influence of variability in aggregate strength in a mixture on asphalt mixture resistance to fracture. The approach developed in this chapter

can be summarized in the following steps:

1. Design asphalt mixtures with different gradations and different types of aggregates in the laboratory.
2. Obtain aggregate stiffness and strength from laboratory tests.
3. Conduct DEM simulations of aggregate laboratory tests in order to determine the DEM input parameters.
4. Capture the internal structure of the different asphalt mixtures through image processing techniques.
5. Transfer the internal structure of asphalt mixture to a discrete element model, and simulate asphalt mixture resistance to fracture.
6. Analyze the influence of variability in aggregate strength and blending of different types of aggregates on asphalt mixture resistance to fracture.

MATERIALS AND LABORATORY TESTING

Materials

Five different aggregate types were selected – granite, hard limestone, soft limestone, gravel, and sandstone – in preparing asphalt mixtures with different gradations. As shown in Table 3.1, three or four aggregate gradations were used in this study for each of the five aggregate sources. A total of 17 mixtures were evaluated.

The gradation curves are illustrated in Figure 3.1. These gradations provide significantly different aggregate structures. The designations of these mixtures follow the Texas Department of Transportation (TxDOT) classification of mixtures. The PFC is sometimes referred to as open-graded friction course (OGFC). It is an open-graded

mixture with a high percentage by weight of coarse aggregates. It is composed of 89% aggregates larger than a No. 8 sieve. The Superpave-C mixture is a well-graded mixture that consists of 35% coarse aggregates and 65% fine aggregates. The Type-D mixture is also a well-graded mixture, but it has a smaller maximum size than Superpave-C. It includes 40% coarse aggregates and 60% fine aggregates. The coarse matrix high binder (CMHB-C) mixture is a gap-graded mixture that is very similar to SMA in its volumetrics. It is composed of 63% coarse aggregates and 37% fine aggregates. The same binder (PG 76-22) was used for all the mixtures to minimize the impact of binder grade on the results.

Table 3.1. Selection of Aggregates and Mixtures.

Aggregate Type	Superpave-C	CMHB-C	PFC	Type-D
Granite	×	×	×	
Hard Limestone	×	×	×	
Soft Limestone	×	×	×	
Gravel	×	×	×	×
Sandstone	×	×	×	×

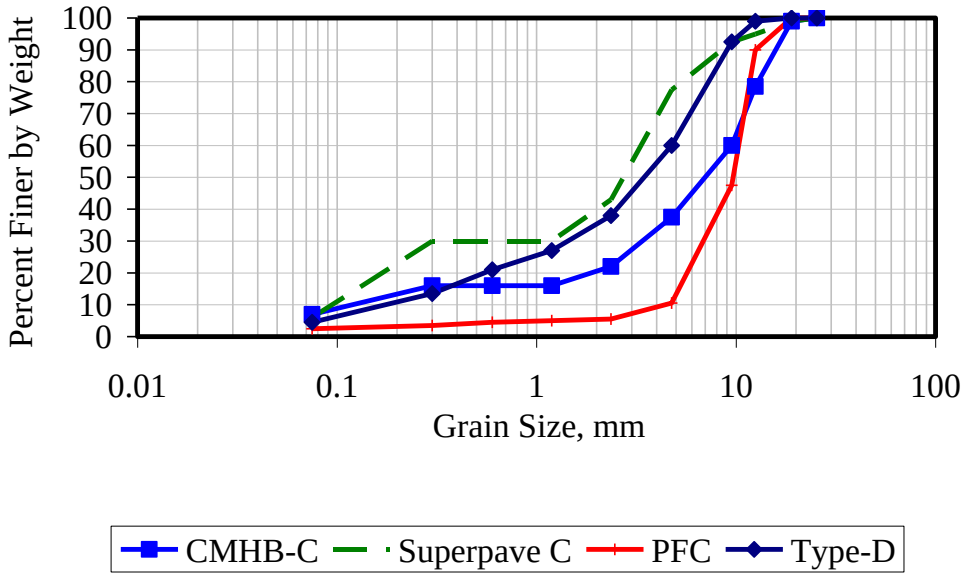

Figure 3.1. Aggregate Gradation Used in this Study.

Aggregate Tests

Splitting tensile tests (indirect tensile tests) on cores from rock masses retrieved from quarries were carried out to determine the potential tensile strength of the aggregates. Split tensile strength is a measure of a material's ability to resist a diametric compressive force. The rock specimens tested were cylinders approximately 5.8 cm (2.3 in.) in diameter and 5 cm (2 in.) in height. Diametrical lines were drawn on each end of the specimen to insure that they were in the same axial plane. Diameter and height of each sample were measured at three different locations to obtain an average height and diameter. Then, the specimen was positioned with its axis placed horizontally with two bearing strips placed between the specimen and both the upper and lower bearing blocks of the compressive machine. The bearing strips were 0.32 cm (1/8 in.) nominal

thickness, 2.5 cm (1 in.) wide, and of length equal or slightly larger than that of the specimen. Once in place, a continuously increasing compressive load was applied to the test specimen until splitting or rupture occurred. This load was applied at a nominal constant rate of loading of 1724 kN/m^2 (250 psi) per minute.

Rock cores similar to those for the indirect tensile tests (extracted from bulk rocks) were used to determine the unconfined compressive crushing strength of the aggregates. Two bearing blocks were used in this test (upper and lower), both cylindrically shaped, with a minimum dimension 3% greater than the diameter of the test specimen, and at least 2.5 cm (1 in.) thick. The lower bearing block was placed on the testing table directly under the seated upper bearing block. The axis of the specimen was aligned with the center of the bearing block, and the upper bearing block was then brought to bear on the specimen. Once in place, the load was continuously increased until crushing failure occurred.

Moduli of aggregate rocks were obtained using a nondestructive testing technique based on ultrasonic testing (V-meter). The V-meter is an ultrasonic device that measures the travel time of compressive waves by means of electric impulses. In this device, a transmitting transducer is securely placed on the top face of the specimen. The transducer is connected to the built-in high-voltage electrical pulse generator of the device. The electric pulse transformed to mechanical vibration is coupled to the specimen. A receiving transducer is then placed on the bottom face of the specimen, opposite the transmitting transducer. The receiving transducer, which senses the propagating waves, is connected to an internal clock of the device. The clock automatically displays the travel time of the compression wave. By dividing the length

of the specimen by the travel time, the compression wave velocity and, thus, the modulus of the material are determined. In this case, the two opposite faces of each rock mass were made smooth using a band saw. Table 3.2 summarizes the experimental results of the different aggregate tests.

Table 3.2. Experimental Results of the Aggregates.

Material	Compressive Strength, kN/m^2	Tensile Strength, kN/m^2	Modulus, MN/m^2
Hard Limestone	71892 (38%)*	9735 (20%)	71209 (13%)
Granite	96761 (7%)	7322 (23%)	46098 (6%)
Soft Limestone	48056 (8%)	4702 (-)**	37735 (11%)
Sandstone	96196 (31%)	11563 (11%)	59702 (7%)
Gravel	Not Feasible		

*** Numbers in the parentheses are the coefficients of variation from triplicate tests.**
**** Only one specimen was tested for the soft limestone.**

Asphalt Mixture Tests

For the asphalt mixtures, the indirect tensile test was conducted by applying a compressive load to a cylindrical specimen through two diametrically opposed, arc-shaped steel loading strips 12.7 by 12.7 mm (0.5 x 0.5 in.). Each specimen, which was nominally 10 cm (4 in.) in diameter and 5 cm (2 in.) thick, was compacted to 93±1% density. Test specimens were placed in a constant temperature apparatus for a long enough time to ensure a consistent temperature of 25±1^{o}C (77±2^{o}F) throughout the test. The specimen was then placed on the lower loading strip; the upper loading strip was then brought into light contact with the specimen by slowly lowering it and then loaded at a 5 cm (2 in.) per minute rate. Table 3.3 summarizes the asphalt mixture test results.

Table 3.3. Experimental Results of the Asphalt Mixtures.

Material	Mixture Type	Tensile strength at failure, kN/m^2
Hard Limestone	CMHB-C	731
	Superpave-C	827
	PFC	455
Granite	CMHB-C	572
	Superpave-C	800
	PFC	421
Soft Limestone	CMHB-C	648
	Superpave-C	862
	PFC	345
Sandstone	CMHB-C	1427
	Superpave-C	1558
	PFC	538
	Type-D	1427
Gravel	CMHB-C	1407
	Superpave-C	1262
	PFC	400
	Type-D	1400

DEM OF AGGREGATES

The PFC2D software was used to model the modulus test, compressive strength test, and indirect tensile strength of rock samples representing aggregates used in this study. The compressive test geometry was a rectangle that represents a vertical cross section of the laboratory specimen. The splitting tensile test was represented by a circular geometry, which is the vertical cross section of the specimen tested in the laboratory. Each model consisted of elements or balls with a density of 2560 kg/m^3. The dimension of the square geometry and the diameter of the circular geometry was 50 mm.

Two walls were added at the top and the bottom of the sample; the walls allow and define how the load is applied. In PFC2D, the law of motion is not solved for walls, but the walls are assigned a constant or variable velocity. The walls interact with the

balls only. In turn, the wall movement introduces loading on the aggregate particles. A specific stress can be applied by calculating the total force reacting on each wall, and then adjusting the velocity to produce a specific force (stress). This can be done by writing a servo-control code in the PFC2D. Applying constant velocity is equivalent to applying a continuously increasing load. This approach was used in this model; however, the servo-control code was used to track the force applied by the walls onto the samples as the test progressed.

A bonding model, stiffness model, and slip model are included in the constitutive representation of contact points between the discrete elements (i.e., the building blocks of the model). The bond model can be envisioned as elastic springs at the contact point. This bond represents the maximum shear and normal forces the contact can carry before breaking. The bond will break if either the shear force or the normal tension force exceeds its limit. In the linear stiffness model, an effective normal and shear contact stiffness is calculated from the elements' stiffness assuming that they act in series. The mathematical expressions for the stiffness parameters are:

$$K^n = \frac{k_n^{[A]} k_n^{[B]}}{k_n^{[A]} + k_n^{[B]}}, \quad K^s = \frac{k_s^{[A]} k_s^{[B]}}{k_s^{[A]} + k_s^{[B]}}$$

where k_s: shear stiffness of elements, k_n: normal stiffness of elements, K^n: effective normal stiffness, K^s: effective shear stiffness, and A & B are the designations of elements in contact.

The slip model, which becomes relevant once the bond between two adjacent elements breaks, allows slipping between elements to occur as soon as the shear force

between them exceeds the allowable shear force. The allowable shear contact force is the friction coefficient multiplied by the magnitude of compressive normal component of the force.

Aggregate contact stiffness and strength in the model were determined such that the model results matched the experimental measurements on aggregate samples (Table 3.2). Following the work that was conducted by McDowell and Harireche (2002) and Cheng (2004), the simulation was conducted using a value of unity for the ratio of the normal stiffness to shear stiffness. The coefficient of friction between the model elements was set to a small value such that sliding could occur after the bond broke. The friction between the loading walls and the model elements was set to 0.5, as recommended by Cheng (2004).

Considerable attention was placed on determining the appropriate value for the approaching velocity used in loading. A higher velocity means less loading time and reduction in the simulation time. However, there is a limit on the maximum velocity that can be used without introducing inertia due to high loading speed (Cheng et al., 2003).

The appropriate approaching velocities for the compression and tension tests were determined by increasing them until the peak forces started to diverge. Based on the results in Figures 3.2 a and b, a rate of loading of 30.5 mm (1.2 in.) per second was selected for the modulus and compressive strength tests, and 51 mm (2 in.) per second was chosen for the tensile strength test. These two rates of loading limited the numerical errors to an acceptable level and could be run within reasonable computational time.

Using a very high bond strength that prevents breakage, the contact stiffness among the model elements was varied until the aggregate modulus of the model matched the experimental modulus measurements in Table 3.2. The next step was to vary the normal and shear bond strengths until the compressive and indirect tensile strengths from the model matched the experimental strength measurements in Table 3.2. This required conducting iterative analysis to determine the parameters that had the best match with both tests. The experimental and numerical results compare quite well, as shown in Figure 3.3 a, b, and c.

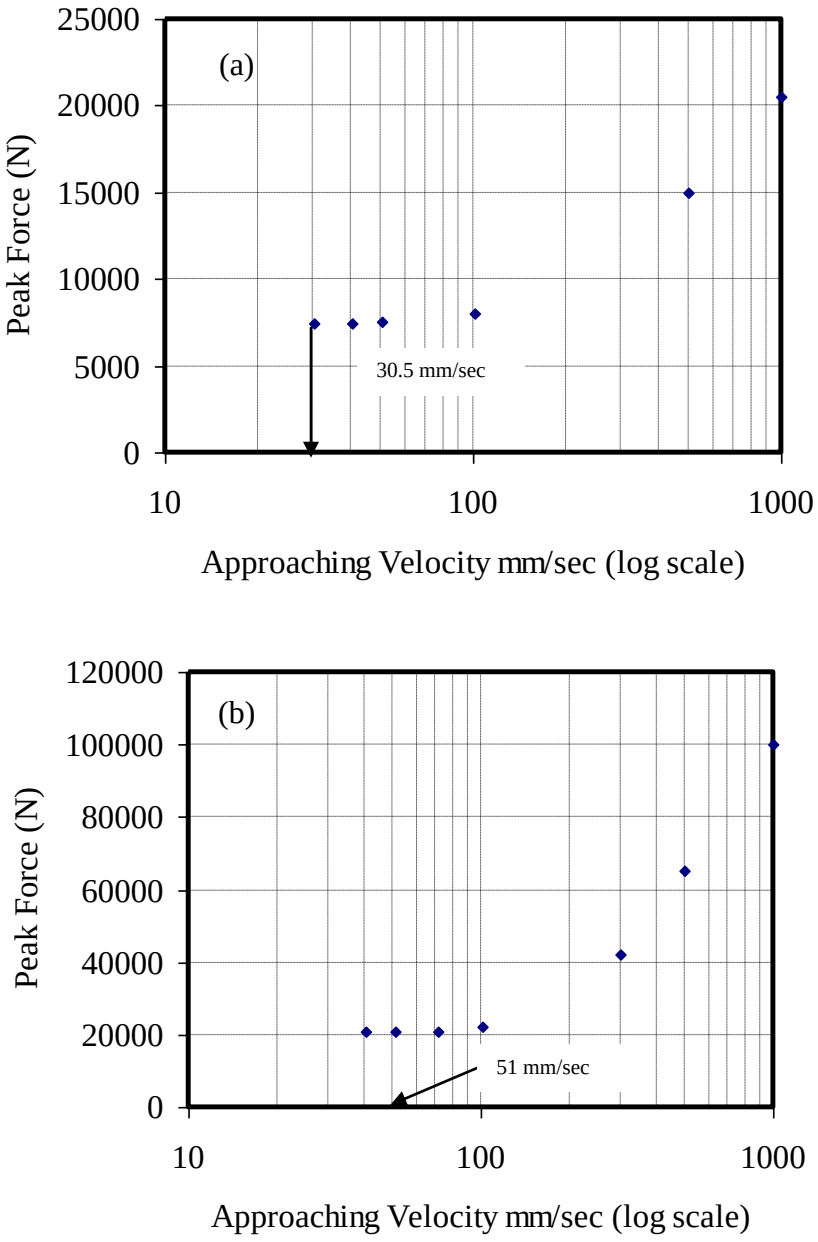

Figure 3.2. Effect of Approaching Velocity on the Peak Force: (a) Compression Test and (b) Splitting Tensile Test.

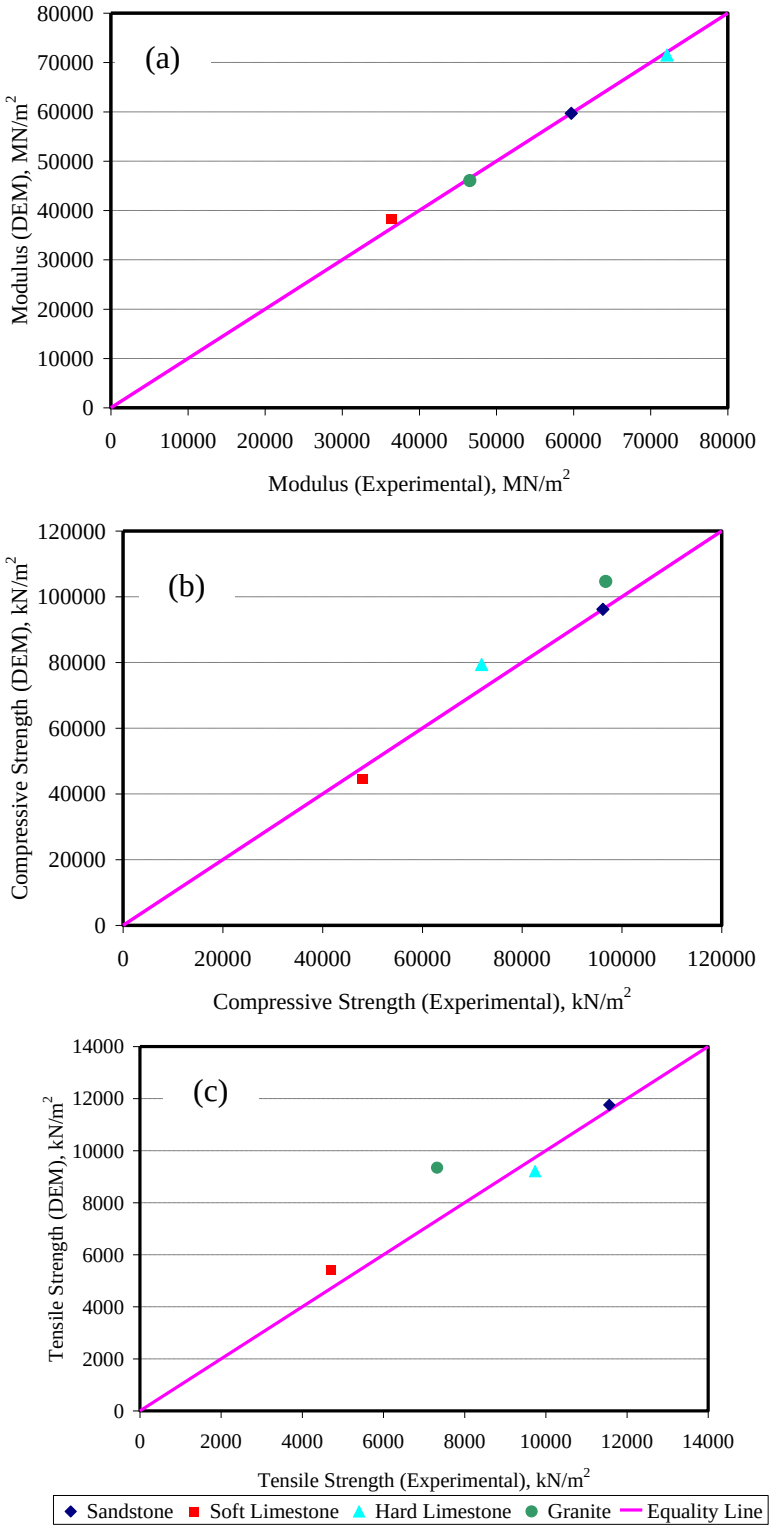

Figure 3.3. Comparison of Modeling and Experimental Results of: (a) Aggregate Modulus, (b) Compressive Strength, and (c) Tensile Strength.

DEM OF ASPHALT MIXTURES

Indirect tensile test results of the asphalt mixtures were modeled as well; however, such modeling cannot be accomplished by using simple geometry assignment because of the irregular shapes of aggregates and the fact that there are two major phases (matrix and aggregates) in the mixture. In order to distinguish between aggregate particles and matrix, X-ray computed tomography (CT) was used to take an image of the internal structure of an asphalt mixture that could be transferred to represent the model geometry in PFC2D.

Images were converted to a binary format (i.e., 0 for matrix and 255 for aggregate) first. The image pixels become the elements in the PFC2D model. The *Image-Pro Plus* (IPP) image analysis package was used to identify the outline pixels of each aggregate particle, and a FORTRAN code was used to group the elements of each aggregate particle in one group. The FORTRAN code checks in all four directions (up, down, right, and left) whether the adjacent pixels are aggregate or matrix (Abbas, 2004). Figure 3.4 shows the discrete element model after differentiating between matrix and aggregate. Each of the model phases can be assigned specific properties, such as bond strength and type, friction coefficient, and density. The input parameters for the aggregate phase were selected from the aggregate tests' calibration, as discussed in the previous section. The matrix phase parameters were selected such that each mixture matched the experimental results of the indirect tensile (IDT) from the laboratory (i.e., peak force and stiffness). The bond and stiffness models for the matrix were the same as those for the aggregate models. The force displacement curve for each mixture was the main output of the model. The model also tracked the internal shear and normal forces (both in compression and tension) developed among the discrete elements during different loading

stages. Figure 3.5 shows the calibration results for the different mixtures and aggregates. The discrete element model results matched the laboratory test results quite well.

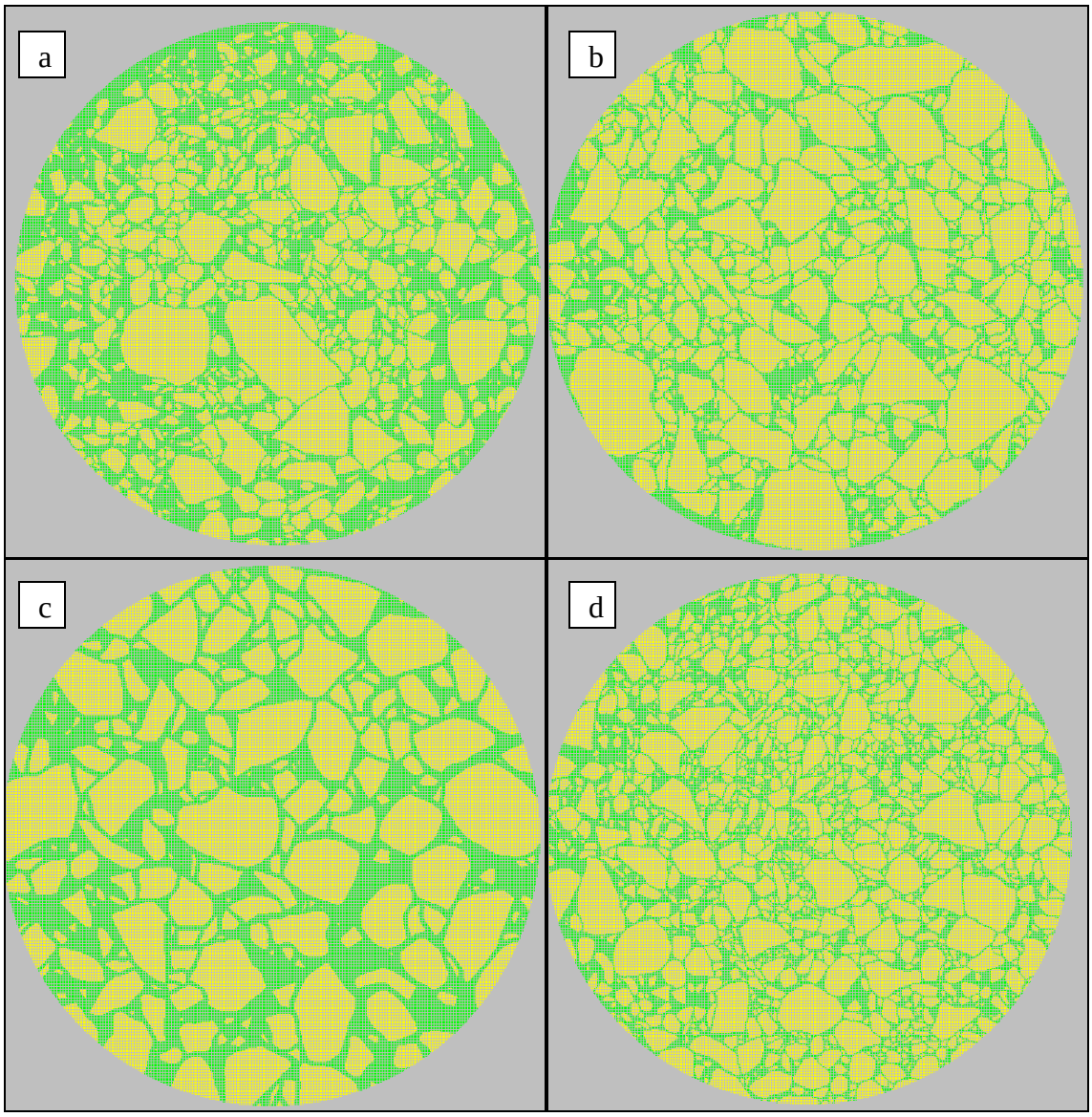

Figure 3.4. DEM of Internal Structure of Asphalt Mixture: (a) Superpave, (b) CMHB-C, (c) PFC, and (d) Type D.

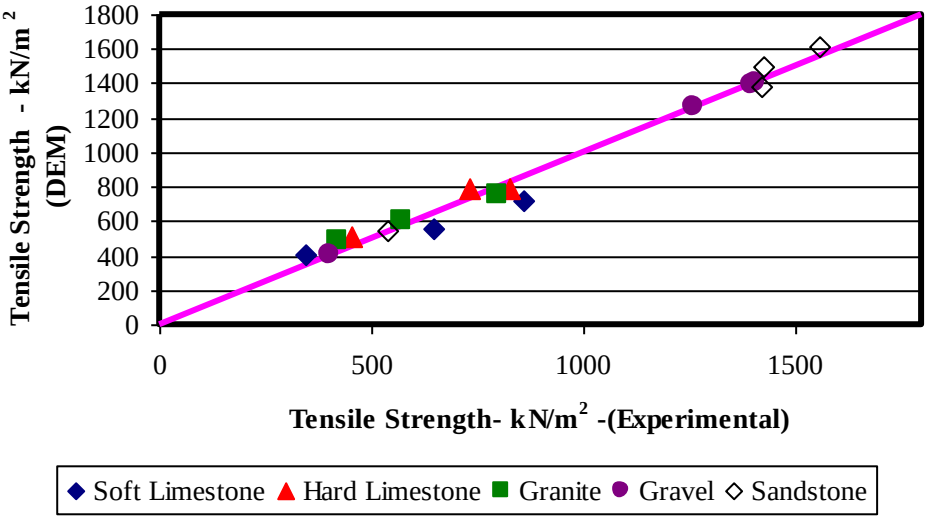

Figure 3.5. Comparison of Modeling and Experimental Results of Asphalt Mixtures' Tensile Strength.

ANALYSIS AND RESULTS

Internal Forces Distribution Analysis

The internal forces in the mixtures are extremely important since they control stress localization and mixture fracture. The internal forces in the mixture models were studied at three stages of loading. Case I was selected at the peak force (just before failure). Case II represented an intermediate force equal to 50% of the peak force. Case III was selected at a force of 2 kN (450 lb), where the cracking and bond loss were minimal for all mixtures.

Table 3.4 presents the maximum internal forces within each of the mixtures for the three different cases. The PFC mixtures typically exhibited the highest maximum internal forces among all mixtures when compared at the same level of loading. The ratio of the maximum internal force in PFC to the maximum internal force in the other

mixtures ranges from 1.1 to 2.0 with an average of 1.36. This indicates that aggregates in the PFC mixtures experience higher internal forces than the other mixtures.

The average and third quartile of internal forces from Case III are summarized in Tables 3.5 and 3.6, respectively. The average and third quartile values are higher for the PFC mixtures, while there are smaller differences in forces among the remaining mixtures. Based on the data in Tables 3.5 and 3.6, the internal forces' ratios between the PFC and the remaining mixtures are about 1.2.

Table 3.4. Maximum Internal Force at Different Loading Stages (N).

Aggregate	Mixture	Loading Stage		
		Case I	Case II	Case III
Hard Limestone	CMHB	446	349	230
	PFC	510	504	503
	Superpave	551	463	300
Granite	CMHB	600	424	202
	PFC	709	278	297
	Superpave	864	377	256
Soft Limestone	CMHB	296	208	196
	PFC	300	218	287
	Superpave	393	268	260
Gravel	Type D	2500	601	193
	CMHB	1456	657	184
	PFC	396	176	228
	Superpave	1351	590	219
Sandstone	Type D	1017	570	206
	CMHB	976	657	189
	PFC	529	299	266
	Superpave	787	514	242

Table 3.5. Average Values of Internal Forces (N).

Aggregate	Mixture	Compression	Shear	Tension
Hard Limestone	CMHB	94	30	6
	PFC	129	33	14
	Superpave	108	28	8
Soft Limestone	CMHB	83	29	7
	PFC	112	29	18
	Superpave	93	28	13
Granite	CMHB	83	26	4
	PFC	112	30	19
	Superpave	92	27	12
Gravel	CMHB	81	26	4
	PFC	92	30	19
	Superpave	83	24	4
	Type-D	84	26	4
Sandstone	CMHB	82	26	4
	PFC	100	30	15
	Superpave	89	26	5
	Type-D	86	27	4

Table 3.6. Third Quartile of Internal Forces (N).

Aggregate	Mixture	Compression	Shear	Tension
Hard Limestone	CMHB	100	31	6
	PFC	132	37	17
	Superpave	114	30	6
Soft Limestone	CMHB	87	32	4
	PFC	119	33	20
	Superpave	89	28	12
Granite	CMHB	92	28	4
	PFC	120	33	20
	Superpave	97	29	12
Gravel	CMHB	85	26	4
	PFC	97	33	21
	Superpave	90	22	4
	Type-D	90	29	4
Sandstone	CMHB	87	27	5
	PFC	106	33	17
	Superpave	99	24	5
	Type-D	94	30	5

Figures 3.6 and 3.7 show examples of the relationships between the maximum internal forces for the three cases representing low (Case III), medium (Case II) and high (Case I) applied external forces. The maximum internal forces increase with an increase in applied load for the different mixtures. The rate of increase in the internal forces with an increase in the applied loads is influenced by the aggregate resistance to breakage within the mixture. In a displacement-controlled test or simulation, breakage of particles reduces the ability of the mixture to sustain applied loads and causes a reduction in the internal forces among aggregate particles. From the aggregate tests and models, the gravel is a much stronger aggregate than the soft limestone, which is reflected in a better ability to sustain applied loads and a higher rate of increase in build-up of internal forces. It is interesting to note that, for a given aggregate type, the PFC has the smallest rate of increase in the internal forces among the mixtures, which is an indication that aggregate breakage in PFC is more probable than in other mixtures. This can be attributed to the difference in gradation between the difference mixtures, as the Superpave mixture is a more uniform mixture with both fine and coarse aggregate sizes, while the PFC is an open-graded mixture. The well-graded aggregate within the Superpave mixture leads to a more uniform distribution of internal forces, as opposed to the uniform gradation in the PFC mixture.

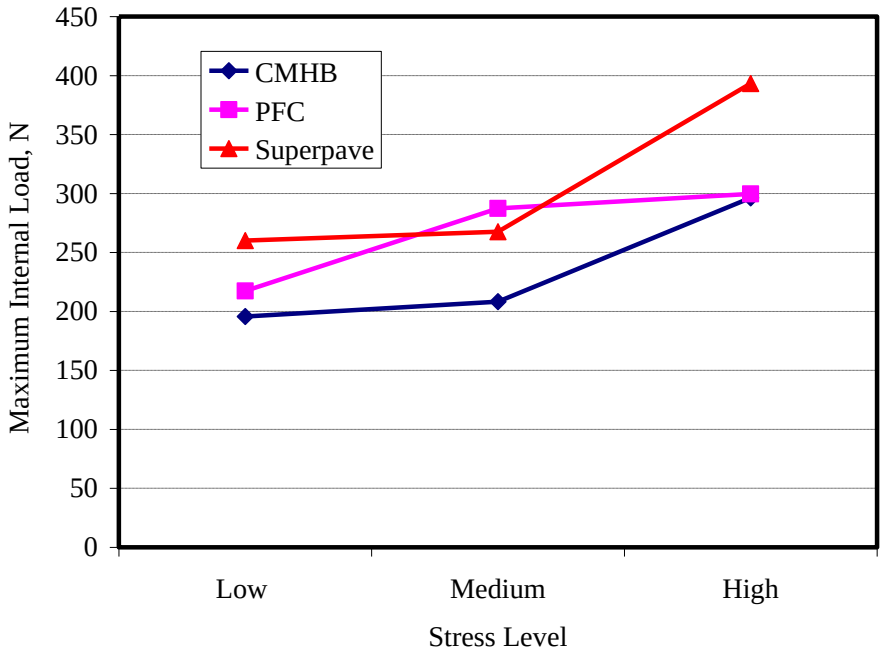

Figure 3.6. Internal Force Changes with Change in Applied Load for Soft Limestone Mixtures.

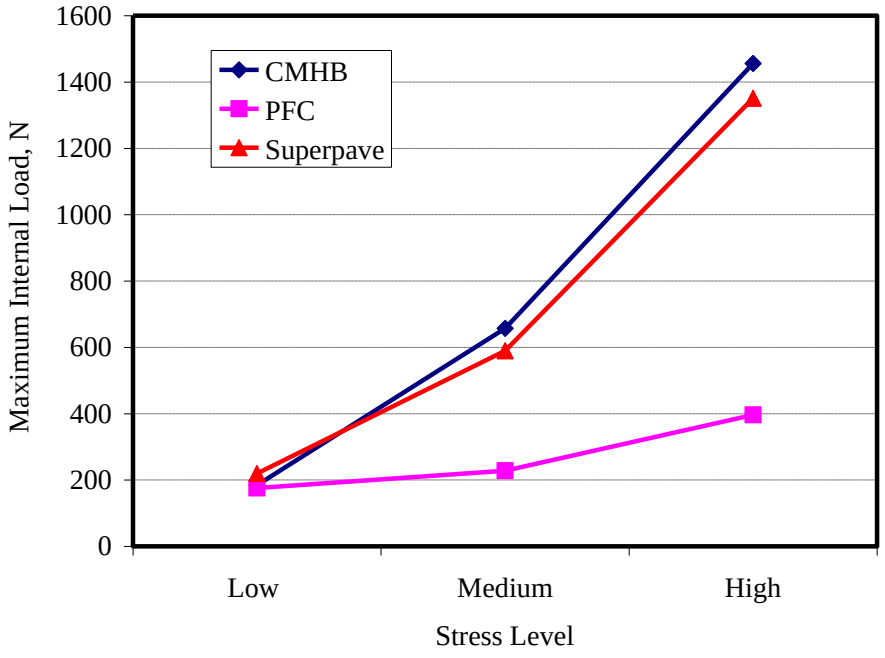

Figure 3.7. Internal Force Changes with Change in Applied Load for Gravel Mixtures.

The complete distributions of internal forces were also evaluated. These distributions confirmed the finding that PFC mixtures had higher internal forces than the other mixtures. Graphical illustrations of forces are shown in Figure 3.8 for Type-D and PFC mixtures using gravel as coarse aggregate. The black color represents compression forces, while the red color represents tension forces. Higher forces are represented by thicker lines in these plots. As evident in the thicker black lines (higher forces) in PFC, Figure 3.8 indicates that there is less uniform distribution of forces within the PFC mixtures compared to the Type-D mixture. Similar results were also fund for the other mixtures for all the aggregates.

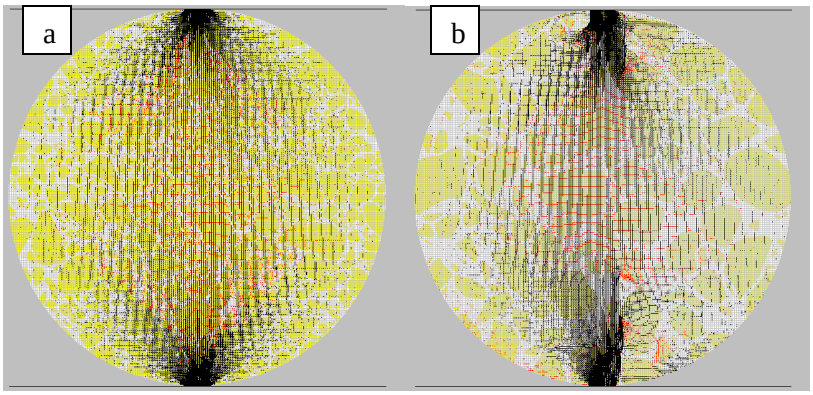

Figure 3.8. Internal Forces Distribution within Two Different Mixtures at 2 kN (450 lb) Stress State: (a) Type-D, (b) PFC.

In summary, no matter how the internal forces (whether the maximum, average, third quartile, or the distribution of forces) are analyzed, the results indicate that the aggregates in the PFC mixtures experienced higher internal forces and resulted in more aggregate fracture. This matter is very important when specifying the minimum requirements for aggregate strength in PFC mixtures.

All of the previous analyses focused on comparing the different mixtures within each aggregate type. The following analysis will evaluate the response of different aggregates within each mixture type. Figure 3.9 presents the normalized compressive force distributions within the different aggregate types for the CMHB-C mixtures. The normalized compression force is calculated as the ratio of the contact force to the compressive strength of the aggregate. The normalized values, instead of the absolute values, were used in order to account for the strength of aggregates in comparing aggregate performance. For example, for a high-strength aggregate, high contact forces may not be of concern for aggregate fracture. The use of normalized forces allows comparing aggregates based on how far they are from reaching their compressive strength and fracture condition.

As shown in Figure 3.9, the soft limestone experienced the highest normalized internal forces compared to the other aggregates. On the other hand, the gravel experienced the lowest normalized internal forces. Hard limestone exhibited higher internal forces than the granite and the sandstone, but still below the soft limestone. Finally, the sandstone and granite exhibited similar internal forces. Similar trends were observed for other mixture types.

Based on these results, aggregates can be ranked for the different mixtures (Table 3.7). This helps in selecting which type of aggregate should be used with a specific mixture. It is very important to mention that this ranking is based only on the strength criteria and ability of the aggregate to resist fracture within a mixture. Other important aspects, such as resistance to moisture damage or other distresses, should also be considered in selecting aggregate type.

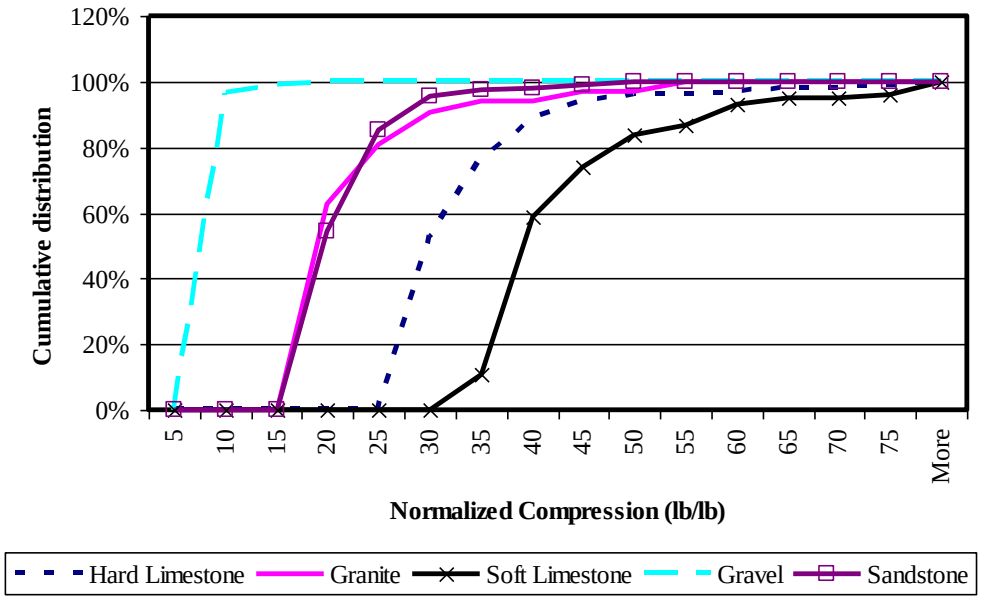

Figure 3.9. Internal Compression Force Distribution within Different Aggregates (CMHB-C).

Table 3.7. Aggregate Ranking for the Different Mixtures.

Aggregate	Mixture Design		
	CMHB-C	Superpave	PFC
Hard Limestone	4*	4	4
Soft Limestone	5	5	5
Granite	2	2	2
Gravel	1	1	1
Sandstone	2	2	2

* A value of 1 represents the best aggregate and a value of 5 indicates the least desirable aggregate.

Influence of Variability in Aggregate Properties

All the analyses presented thus far assumed one average value for the bond strength within the aggregates. However, aggregate particles from the same source may exhibit variations in their properties. In order to account for such variability in the model, aggregate bond strength was assumed to follow a normal probabilistic distribution. The

means and standard deviations for the distributions were taken to be equal to those obtained from the experimental measurements summarized in Table 3.2.

The analysis was repeated seven times for each mixture and aggregate type. In each execution, the locations or positions for the various bond strength values were determined using a random number generator. In essence, all repeated executions represented the same aggregate type and had the same mean and standard deviation, but the positional distributions of the bonds were different among the different repeated executions. This procedure allowed for the introduction of a variability factor into the model.

The distributions of the strengths are summarized in Figure 3.10 a and b. The means and the standard deviations from the means (represented by the error bars) from the experimental results are compared to those from the model. The experimental and the numerical values compare reasonably well. The differences in variation between the model and the experimental results could be due to a number of factors, including the assumption of normal distribution, attributing all the variability in the experimental strength measurements to variability in only aggregate particles' bond strengths, and assuming no variability in matrix properties. Re-calibrating the matrix properties based on the distribution of aggregate properties may help in obtaining better agreement between the experimental and numerical results.

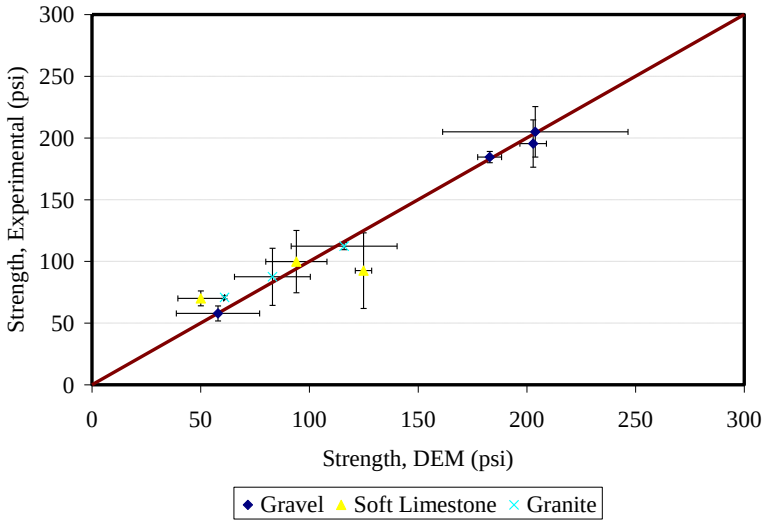

(a)

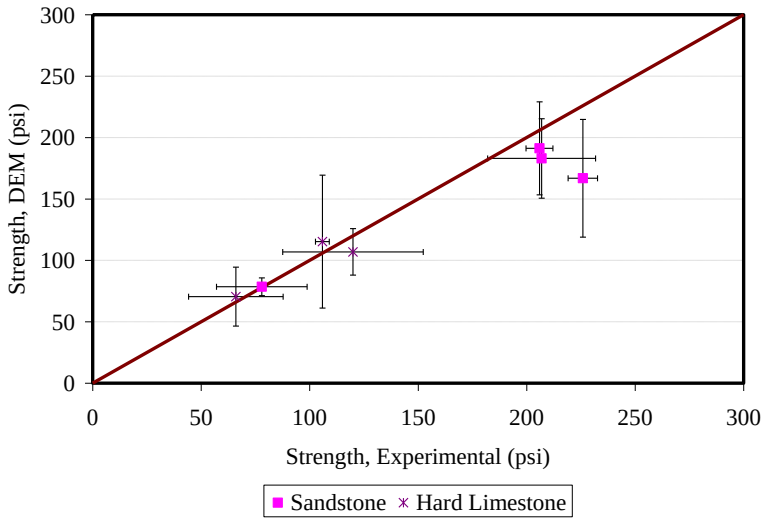

(b)

Figure 3.10. Influence of Variability in Aggregate Bond Strength on Mixture Strength.

SUMMARY

The developed approach that combines the DEM and image processing techniques was useful in simulating the resistance of asphalt mixtures to fracture. This approach accounts for the combined effect of aggregate gradation, shape characteristics, and

strength. There are significant interactions among these properties that make it difficult to study the effects of these factors on asphalt mixture performance individually.

After proper calibration, the model allowed for quantification of the internal forces in asphalt mixtures, which cannot be accomplished by conventional experimental methods. The model was successful to a large extent in representing the variability in aggregate properties and the influence of this variability on mixture response.

Analysis of internal forces revealed that the PFC mixtures experienced higher stresses than all other mixtures. Based on the results, it is recommended that aggregate strength for the PFC mixtures should be about 25% more than the aggregates used in other mixtures. However, with the exception of the PFC mixtures, the internal forces were comparable for all other mixtures for a given aggregate type.

The soft limestone experienced the highest internal forces compared to the other aggregates. The ranking of aggregates based on internal forces can be used to select the appropriate aggregate type for a given mixture design. The rate of increase of internal force with an increase in applied loads is an indication of the aggregate resistance to fracture. A high rate of increase in forces indicates less breakage of aggregates. PFC mixtures experienced the least rate of increase, indicating more aggregate breakage when compared to the other mixtures.

The model allowed for assignment of variable bond strength instead of a single average value. This allowed producing different samples of a mixture of one aggregate without the need to physically prepare the extra samples in the laboratory. The variability that resulted in using the model compared fairly to the variability of doing multiple samples and testing them in the laboratory.

CHAPTER IV

DISCRETE ELEMENT ANALYSIS OF THE INFLUENCE OF AGGREGATE BLENDING ON ASPHALT MIXTURE STRENGTH

INTRODUCTION

Although aggregate is a low-cost bulk material, it is a non-renewable resource, and thus the demand has to be balanced against the available supply (Rajaram and Hoagberg, 1984). Based on very conservative assumptions, a US geological survey (1999) projected that the production of gravel, sand, and crushed stone in the next 25 years will be equivalent to the total production in the past 100 years, and thus enormous quantities of aggregates will be needed in the future. The source of such quantities is yet to be identified (USGS, 1999). To overcome the depletion of good-quality aggregate, many studies suggest either the use of waste material as a replacement of, or blended with, raw aggregate, or the utilization of lower-quality aggregates in blends with high-quality aggregates.

Aggregates are rated for quality based on their resistance to mechanical breakdown (under traffic loading) and chemical breakdown (weathering effect). Thus, based on road use and climate, the rating of an aggregate will change from one place to another. Construction and maintenance costs of highways can be minimized by utilizing locally available materials; the cost of imported materials is usually much higher due to the transportation costs (hauling costs are the highest component) (Foltz and Truebe, 2003).

Rajaram and Hoagberg (1984) conducted a study for the Minnesota Department of Transportation in order to inventory the aggregates in the expanding urban area in the state of Minnesota. The authors concluded that aggregate depletion is a major concern, as it is expected to increase the cost of this material and thus the construction costs in general. The land use regulation and transportation costs are the most important factors affecting the cost and availability of aggregates. Rajaram and Hoagberg (1984) suggested four different methods to enhance the aggregate supply in that area. These methods are defining aggregate quality and quantity, maximizing the utilization of mined aggregates, developing new specifications that allow maximum use of lower-grade aggregates and recycled materials, and revising land use regulations. The concept of blending low-quality aggregates with high quality aggregates without affecting performance would extend the supply of high-quality aggregate.

Collins (1976) studied the use of waste products as replacements for aggregates. The author discussed the aggregate production, usage, shortage, and different proposed solutions for the shortage. The author stated that aggregate is an exhaustible resource and should be used and re-used wisely. One of the important points this study shed light on is the fact that even if the overall national supply of aggregate is enough to meet all the demand, there are certain regions in the states with a shortage of aggregate supply. Collins (1976) believed that the following factors are the main reasons behind such shortages: 1) the lack of high quality aggregates naturally occurring in some places, 2) zoning restrictions that prohibit aggregate extraction in and around metropolitan areas, 3) pollution control policies, 4) expensive transportation costs for hauling aggregates to areas away from aggregate producing locations, 5) peak demands of aggregate due to

seasonal fluctuation (especially in the highway industry), and 6) excessively rigid quality control requirements for some uses of aggregate materials. Furthermore, the study suggested the following different solutions for the aggregate shortage: 1) increase production, 2) import aggregate by transportation from other areas, 3) use manufactured or synthetic aggregates, 4) utilize available by-products (waste materials), 5) modify current specifications to allow use of lower quality aggregates in certain applications, and 6) beneficiate lower quality aggregate materials after some processing such as crushing, screening, and blending.

Harra (1962) from the Oregon State Highway Department stated that fifteen million tons of aggregate are used annually for the highway construction in the state of Oregon. Many sources of good aggregates are already exhausted, and many others are being rapidly exhausted. This high demand along with land zoning restrictions requires the use of some inferior or substandard aggregate (lower quality) for economical reasons.

Aggregate supply shortage/depletion, as previously discussed, has been recognized for a long time; recent studies evaluated different ways to overcome this problem. Rakshvir and Barai (2006) suggested the use of recycled aggregates in order to reduce the extraction of raw materials, reduce transportation costs, reduce environmental impact, and reduce the depletion rates of conventional aggregate sources. Blending of different aggregate sources is also an appealing alternative approach for overcoming the shortage of locally available high-quality aggregates.

The effect of blending different types of aggregates on the behavior of unbound aggregate layers was studied by Pan et al. (2006) for resilient behavior and Tutumluer and Pan (2008) for strength and permanent deformation behavior. In both studies

uncrushed gravel was blended with another five types of aggregates: crushed granite, crushed limestone, crushed gravel, slag, and sandstone. The uncrushed gravel blending percentages were 100, 50, 33, 17, and 0. These two studies showed how blending can enhance the behavior of the uncrushed gravel; however, the different blends produced different results. The data extracted from these two studies for the resilient modulus and the maximum deviatoric stresses at failure are plotted in Figures 4.1 and 4.2. The x axis shows the percent of blended material with the uncrushed gravel, i.e., at 0% blended material all the material used is the uncrushed gravel.

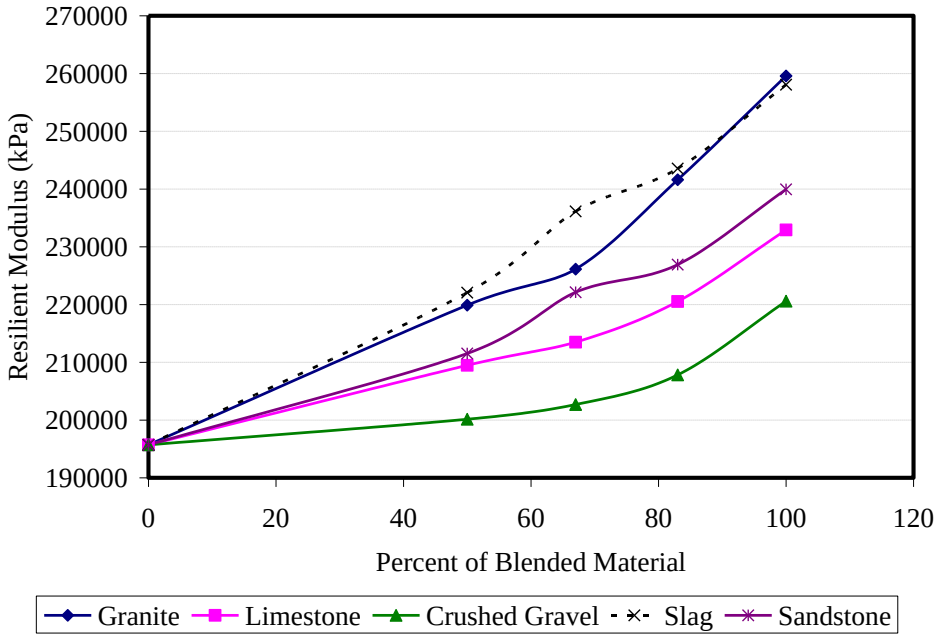

Figure 4.1. Blending Effect on the Resilient Modulus of Uncrushed Gravel (after Pan et al., 2006).

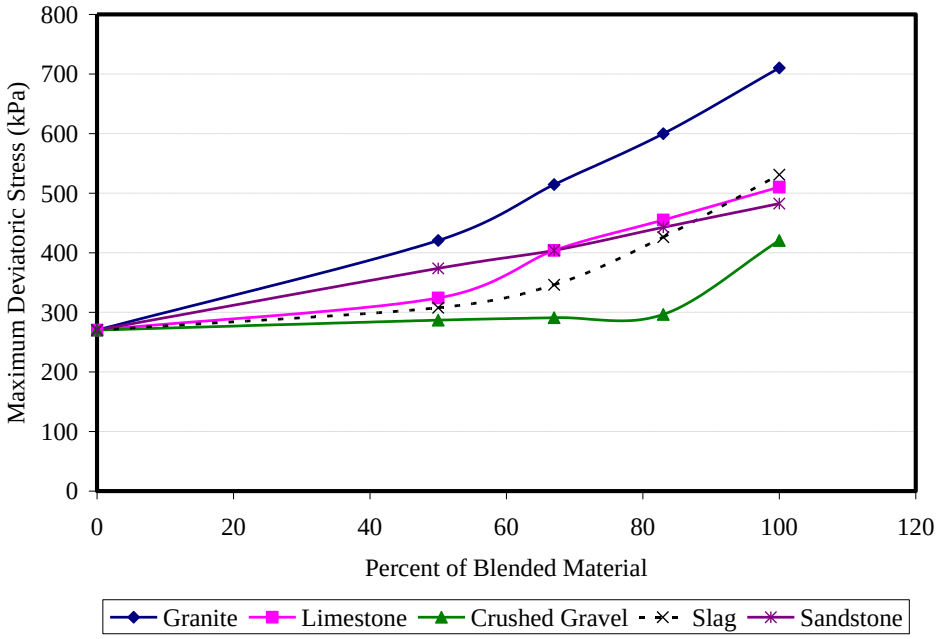

Figure 4.2. Blending Effect on the Max Deviatoric Stress of Uncrushed Gravel (after Tutumluer and Pan, 2008).

Blending aggregates with different properties to enhance the performance of asphalt mixtures is a common practice. The performance can be enhanced either by increasing the structural capacity of the pavement, or increasing its resistance to specific distress. One other application of aggregate blending is to enhance the surface properties of the pavement in order to achieve a higher skid resistance. In this case aggregates with higher surface texture are more desirable. This has been done for few years in different DOTs, such as TxDOT.

OBJECTIVES AND SCOPE

In this study, DEM is used to study the effect of blending two different types of aggregates on the strength of asphalt mixtures. An approach was developed using the

DEM to develop models in which aggregates (soft and hard) are distributed randomly within the structure. The discrete element models were first calibrated for different types of mixtures. Then, they were used to calculate the change in the strength of several mixtures with changes in percentages of blending two different aggregate types.

The DEM analysis was conducted for two different blends. The first blend consisted of hard limestone and soft limestone (Case I), and the second blend mixed sandstone with the soft limestone (Case II). As is indicated by its name, soft limestone is the soft material in the two blending cases. DEM results of Case II were compared to laboratory test results on asphalt mixtures prepared by blending the same two aggregates. The tests included were the IDT strength, dynamic modulus, Hamburg wheel (rut depth), and flow time maximum strain. The comparison was based on percent changes in the different test results, and the experimental results compared well with the DEM analysis. Finally, blending charts were developed to predict the behavior of different mixtures when two aggregates are blended.

A PROCEDURE FOR DISCRETE ELEMENT ANALYSIS OF BLENDING

The discrete element model developed in Chapter III was used to conduct the blending analysis. As discussed in Chapter III, the model uses image analysis techniques to convert black and white images to DEM elements. The model was calibrated for five different aggregates (granite, hard limestone, soft limestone, gravel, and sandstone). Each aggregate was used in three or four different gradations (Superpave, PFC, CMHB, and Type-D) for a total of 17 different mixture cases, simulating IDT strength of the asphalt mixtures. Table 3.1 summarizes the different analysis cases.

The method developed in Chapter III distinguishes between discrete elements that belong to the matrix and aggregate phases. However, in the blending analysis, the method was extended to identify aggregate particles that belong to each aggregate type. For this purpose, a method was used to identify and group discrete elements that belong to each aggregate particle (Abbas, 2004). In this method, the *Image-Pro Plus* (IPP) software was used to convert an image into pixels of black (belonging to aggregate particles) and white (belonging to the matrix). Then, a program was written to read and identify aggregate outline pixels (referred to as an object), and then add all the inside pixels to the same object. Each object or individual aggregate particle is assigned a number (starting from 1 and going up to the total number of aggregate particles (n) in an image) (Abbas, 2004).

Blending two types of aggregates within one mixture in the DEM was done at 11 different blending percentages from 0 to 100 with an increment of 10 (with the hard material percentage = 100 – soft material percentage). Examples of blends with different proportions are shown in Figure 4.3. The model selects a specific percentage of soft aggregate randomly from all aggregate particles within the mixture and assigns the soft material properties to it. The rest of the particles are then assigned the hard material properties. This random selection process is achieved using a program written for this specific purpose. The program performs the following steps:

1. Determine the number of aggregate particles (n) in the discrete element model (as described previously).
2. Assign a number to each particle (1, 2 …, n).

3. Calculate the number of aggregate particles that should fall into the soft material category (s = n*p/100), where p is the specific percentage of soft material.
4. Use a random number generator to generate a list of "s" integers between the values 1 and n. Aggregate particles with this designation number in the list are assigned to the soft material group.
5. Assign hard aggregate properties to the hard material group.

For each blending percentage from (hard/soft) 90/10 to 10/90, the analysis was conducted nine times. Each time, a random group of particles was selected to represent the soft aggregate. The randomness of the process comes from step 4, as each time this step is performed, even for the same s number, the selected aggregate particles will change. Figure 4.4 shows the six different distributions of soft/hard limestone of a blend that consists of 30% soft limestone and 70% hard limestone. The analysis of different random distributions of the same blend was necessary because the location distribution of soft particles in an asphalt mixture could affect the results of simulating mixture performance.

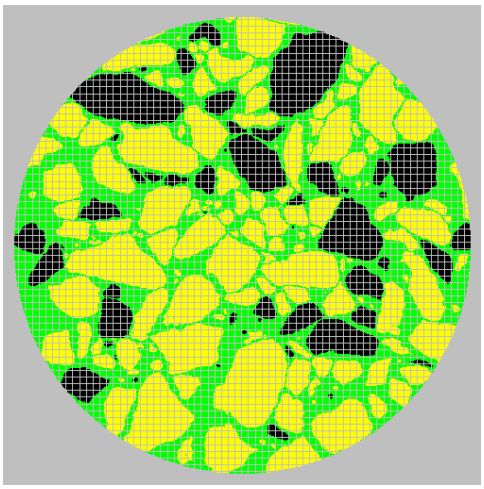

30% Soft

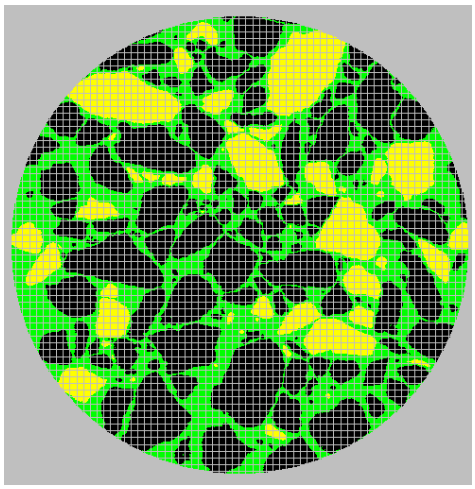

70% Soft

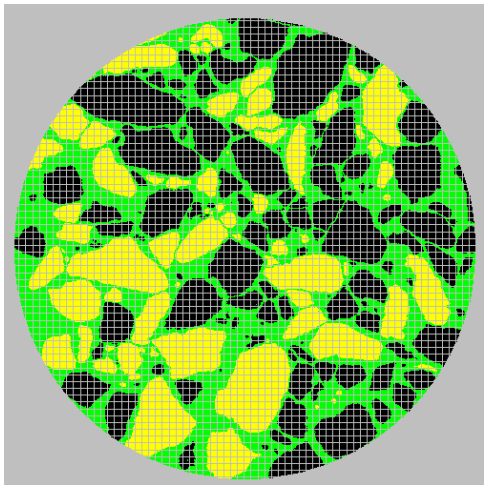

50% Soft

Black Particles: Soft Materials, Yellow Particles: Hard Materials

Figure 4.3. Different Percentages of Blends of Two Aggregate Types.

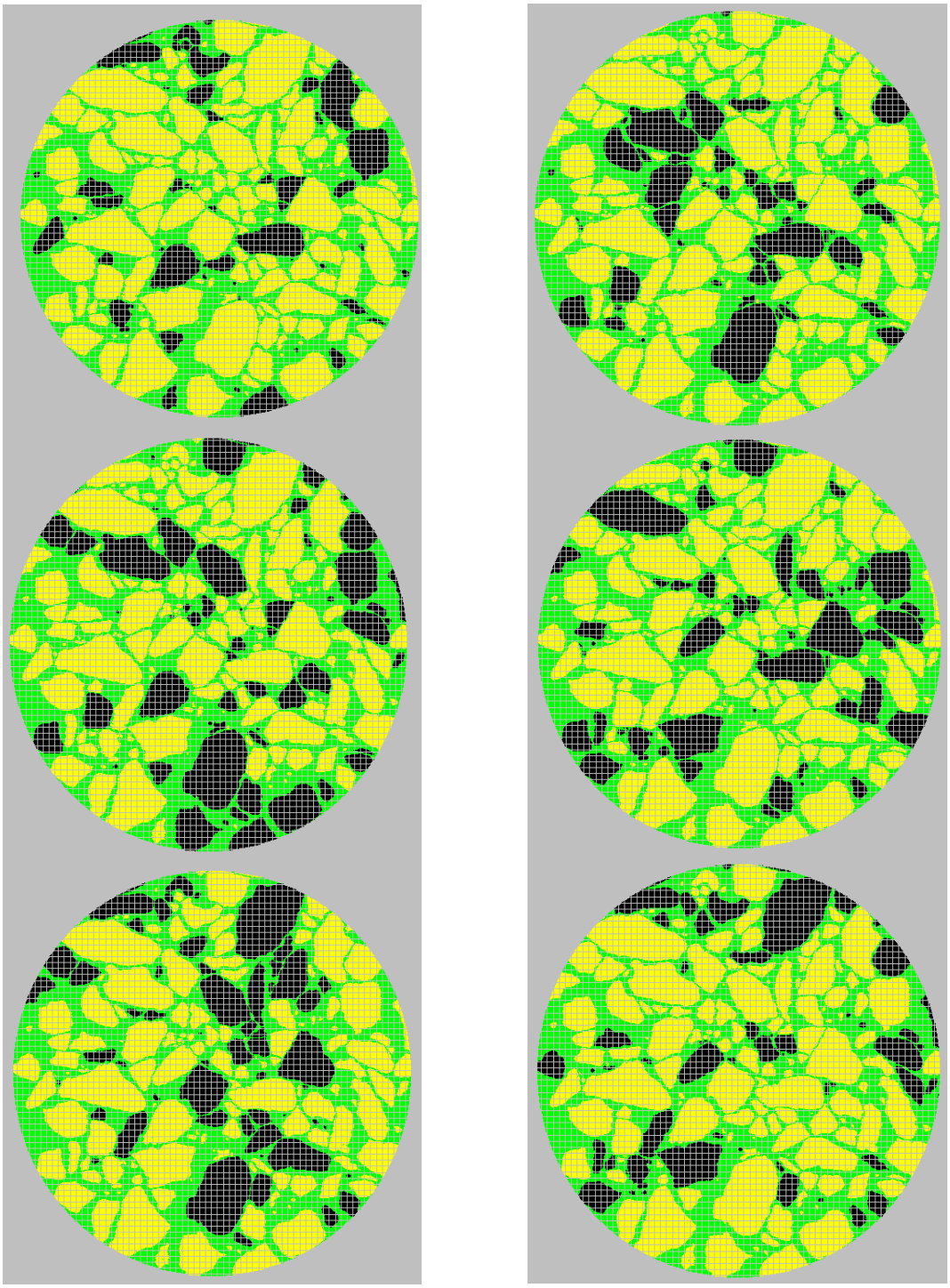

Black Particles: Soft Materials, Yellow Particles: Hard Materials

Figure 4.4. Different Random Distributions of 30% of Soft Limestone (70% Hard Limestone).

BLENDING RESULTS

Case I: A Blend of Soft Limestone and Hard Limestone

The blending procedure described previously was conducted for four different mixtures (PFC, CMHB, Type-D, and Superpave). Each blend percentage was repeated 9 times representing different spatial distributions of soft and hard aggregates within the mixture (a total of 324 analysis cases). Therefore, the analysis allowed calculating the mean and the standard deviation of mixture strength for each blend. Figures 4.5 through 4.8 summarize the results for the PFC, CMHB, Superpave, and Type-D mixtures, respectively. The error bars represent one standard deviation. For the PFC mixture (Figure 4.5) blending 10% to 50% of the soft aggregate did not seem to affect the strength of the mixture; however, the mixture strength dropped at 50% soft limestone. The strength remained almost constant after using more than 70% soft limestone. These results indicate that up to 50% of soft aggregate can be used without compromising the strength. In addition, the use of less than 30% hard material has no benefit in improving the strength.

The CMHB mixtures exhibited higher variability at the same blending percentage compared to other mixtures. As shown in Figure 4.6, the CMHB mixture strength did not change significantly until using 60% of soft limestone, after which the strength continued to decrease with an increase in the percentage of soft aggregate. The trend for the Type-D mixtures is shown in Figure 4.7. The strength values were constant up to a 30% blend of soft limestone. Between 30% to about 80% soft limestone, the strength decreased with an increase in the percentage of soft limestone. Strength reached a constant value after using 80% soft limestone.

Finally, the Superpave mixture (Figure 4.8) strength variability was rather small as judged by the length of the error bars. A linear decrease in the strength with an increase in the soft limestone percentage best described the behavior of this mixture.

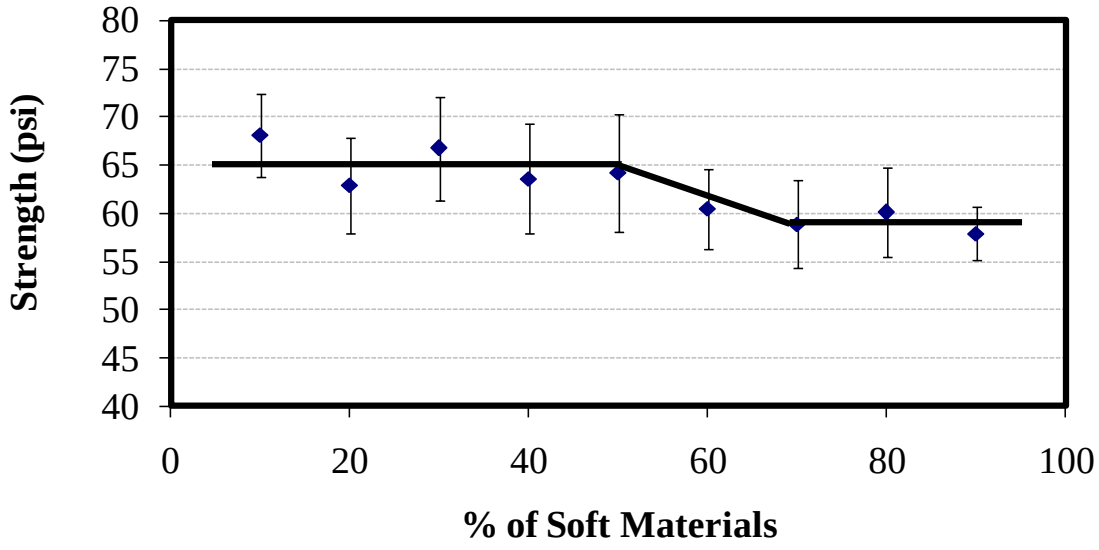

Figure 4.5. PFC Blending Results (Case I).

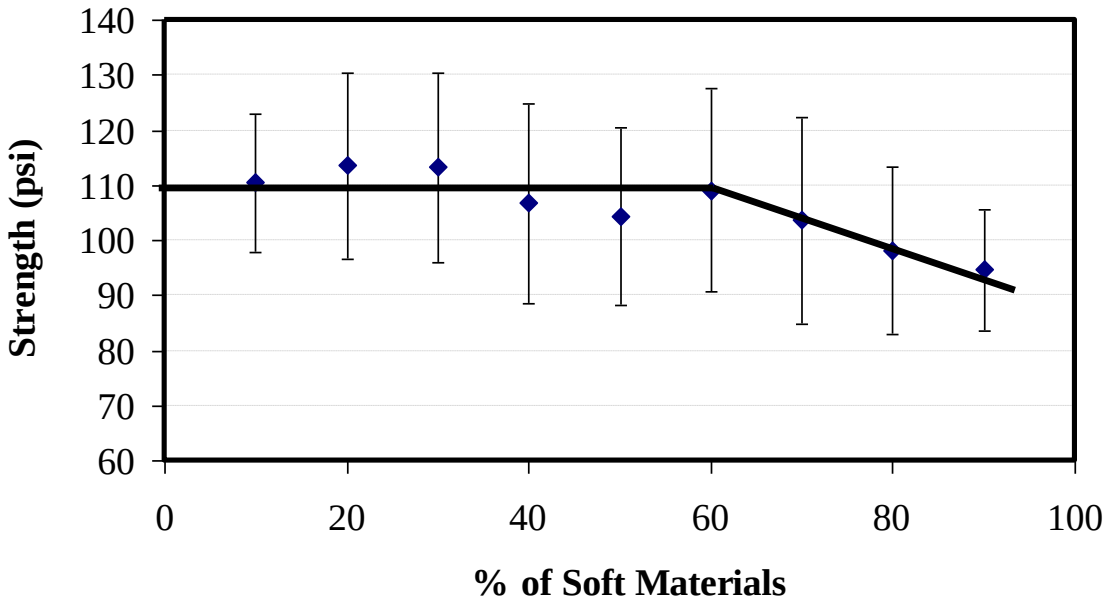

Figure 4.6. CMHB Blending Results (Case I).

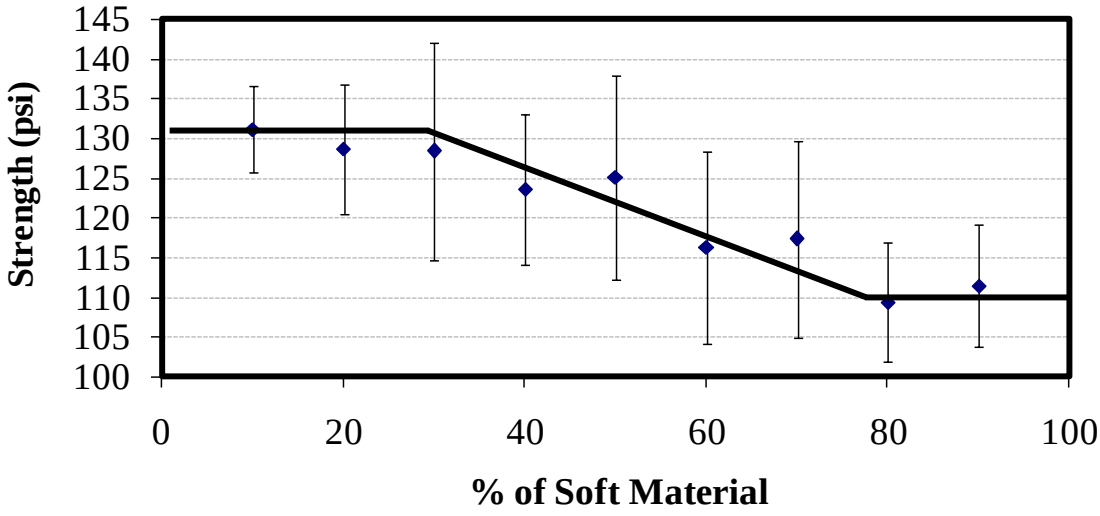

Figure 4.7. Type-D Blending Results (Case I).

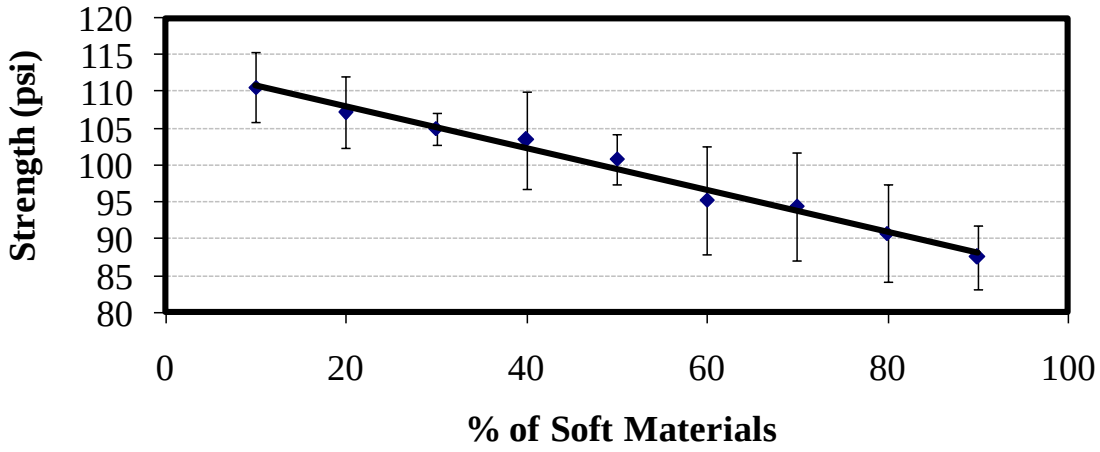

Figure 4.8. Superpave Blending Results (Case I).

The use of different spatial distributions at the same percentage revealed interesting information about the effect of mixture segregation on performance. This point can be illustrated by considering the two cases shown in Figure 4.9. These cases are for 70% soft limestone. The structure in Figure 4.9a had a tensile strength of 139 psi, while the structure in Figure 4.9b had a tensile strength of 82 psi. The difference in the

tensile strength is attributed to the location of soft and hard aggregate in a specimen. The maximum tensile stress in the IDT is in the center of the specimen. In Figure 4.9a, the center of the specimen has mostly hard limestone with high tensile strength, while the center of the structure in Figure 4.9b has mostly soft limestone with low tensile strength. These results demonstrate the significance of segregation on mixture response. The error bars shown in Figures 4.5 to 4.8 indicate that the Superpave mixture is the least sensitive to segregation (smallest error bars) compared to the other mixtures.

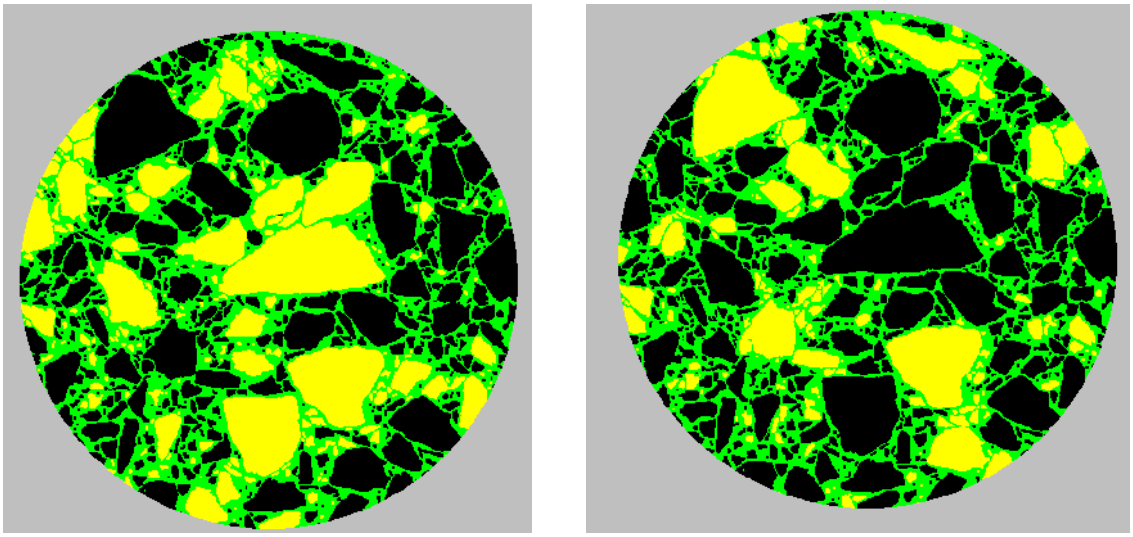

a) Highest Strength b) Lowest Strength

Black Particles: Soft Materials, Yellow Particles: Hard Materials

Figure 4.9. Different Mixture Strengths at Same Blending Percentage.

Case II: A Blend of Sandstone and Soft Limestone

The same procedure used in Case I was repeated herein but for a blend of sandstone and soft limestone. Figures 4.10 through 4.13 summarize the results for the PFC, CMHB,

Superpave, and Type-D mixtures, respectively. In the PFC mixture, blending 10% to 40% of the soft limestone did not seem to affect the strength of the mixture; however, for the blending percentages between 40% and 70% the mixture exhibited a drop in its strength, and the strength remained almost constant after using more than 70% soft limestone. The trend for the PFC is the same in the two cases (hard limestone with soft limestone, sandstone with soft limestone); however, the drop in the strength started at 40% for Case II, while it started at 50% for Case I. This can be attributed to the fact that there is a larger difference in strength in the two aggregates used in Case II compared to the aggregates used in Case I.

For the CMHB mixture, blending 10% to around 40% soft limestone did not affect the strength of the mixture; however, further addition of soft materials resulted in a drop in the mixture strength. This drop stopped after 70% soft limestone blending point. It is noted that the CMHB behavior in Case II (Figure 4.11) differs from Case I (Figure 4.6). This indicates that the mixture response to blending could depend not only on the proportions of aggregates but also on the properties of the aggregates.

The Superpave mixture results are summarized in Figure 4.12. The effect of blending on the Superpave mixture is a linear decrease in mixture strength with an increase in the soft material; this is the same as in Case I. Finally, the trend for the Type-D mixtures, as shown in Figure 4.13, is similar to the Superpave mixture. This is different than the behavior of the Type-D mixture for the Case I aggregates. This supports the point that the mixture behavior does not only depends on the blending percentages but also on the aggregate properties.

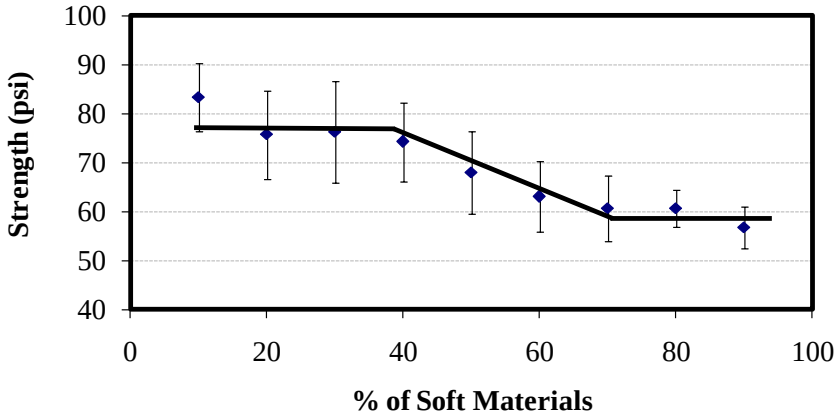

Figure 4.10. PFC Blending Results (Case II).

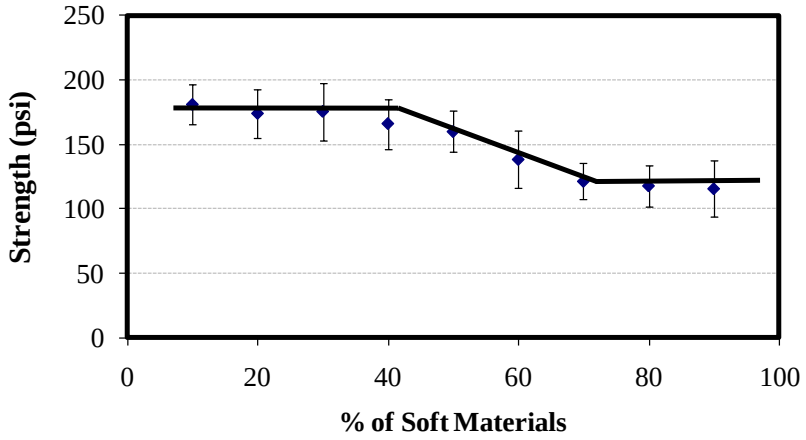

Figure 4.11. CMHB Blending Results (Case II).

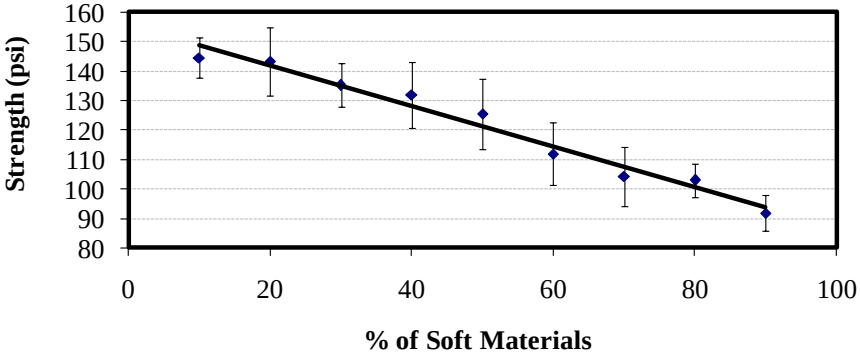

Figure 4.12. Superpave Blending Results (Case II).

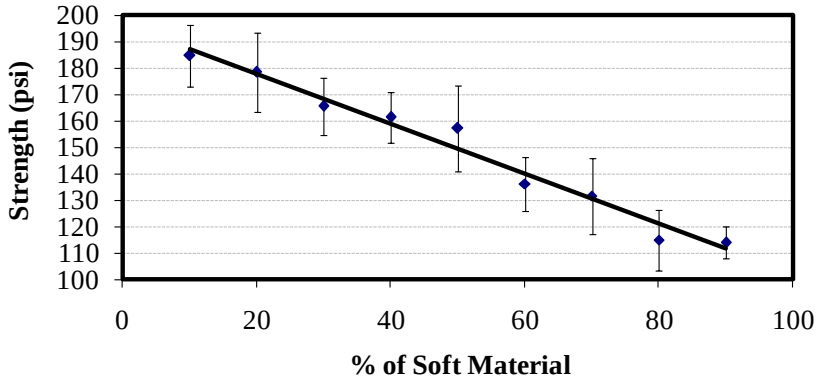

Figure 4.13. Type-D Blending Results (Case II).

Comparison of Case I and Case II Results

For a better understanding of the differences between the Case I and Case II results, Figure 4.14 a, b, c, and d were generated for the four mixtures to compare the effect of blending on the mixtures. In all four mixtures, the Case II curve is higher than the Case I curve. This is attributed to the fact that the sandstone used in Case II has a higher strength than the hard limestone used in Case I.

The PFC and CMHB mixtures exhibited no drop in strength for at least 40% of soft material. However, the curves for both cases almost meet at about 70% soft limestone. This indicates that this aggregate dominates performance at a percentage higher than 70% regardless of the strength of the harder aggregate. For these mixtures, the use of 30% or less of harder material does not contribute to improving performance. This 30% cut off point can be generalized for all four mixtures. As shown in Figure 4.14, the mixture strength either drops or stays constant when 70% soft material or more (30% hard material or less) is used.

The Superpave mixture curves in both cases are linear indicating that this mixture did not accommodate blending of soft aggregate, as CMHB and PFC mixtures did.

Finally, the Type-D curves coincide at the 90% point. This means that an addition of hard aggregate of more than 10% improves mixture strength.

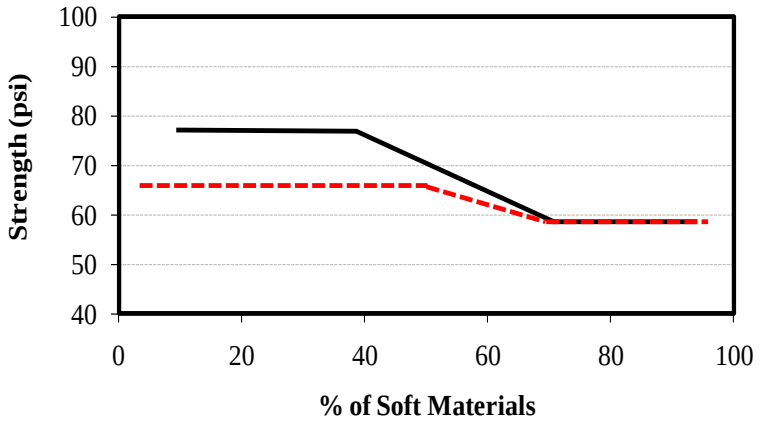

(a) PFC Mixture

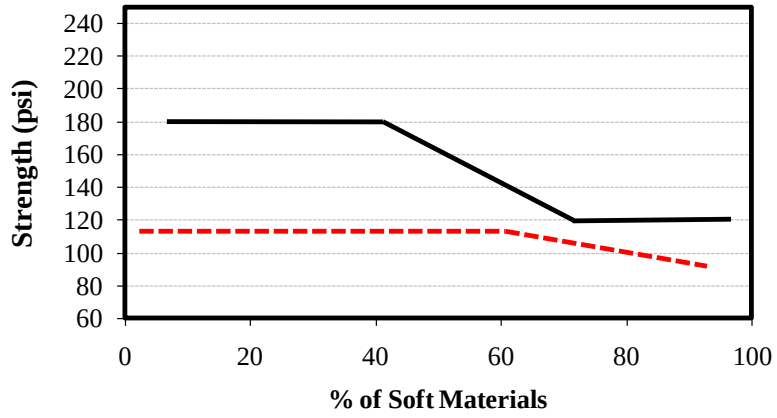

(b) CMHB Mixture

Figure 4.14. Case I and II Blending Trend Results.

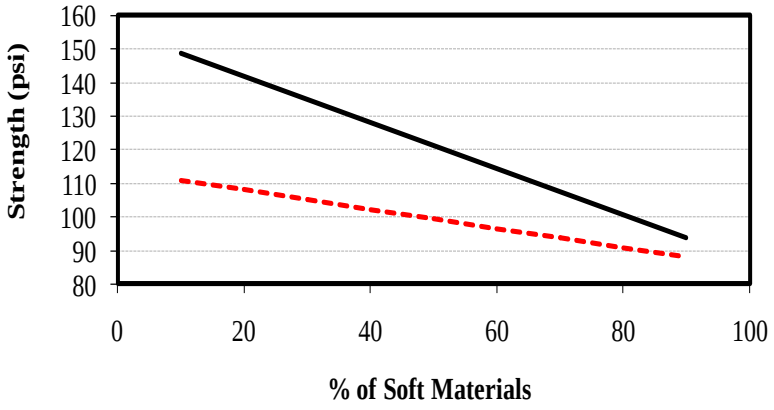

(c) Superpave Mixture

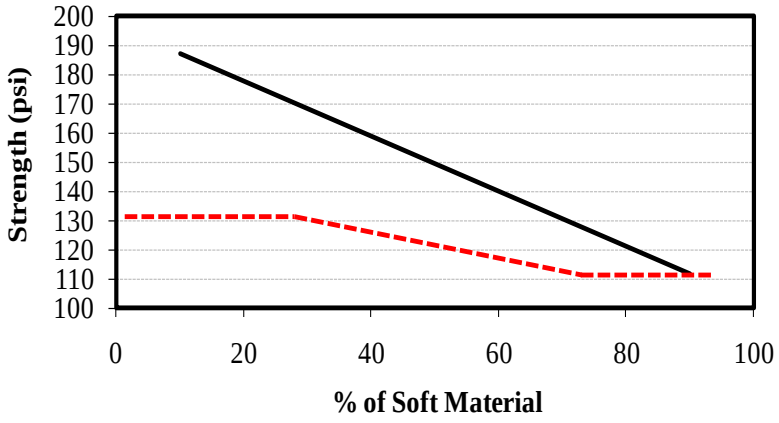

(d) Type-D Mixture

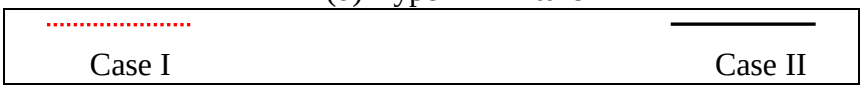

Figure 4.14. continued.

Table 4.1 summarizes the expected reduction in mixture strength given a specific percentage of soft aggregate and the ratio of the two aggregates used in the mixtures. The ratio of the two aggregates' strength was calculated based on the bonding strength used in the discrete element model (Chapter III). For Case I the ratio of the hard limestone to the soft limestone is 1.70, while for Case II the ratio of the sandstone to the soft limestone is 2.13. The reduction in the strength is calculated as the strength of the mixture with 100%

hard aggregate minus the strength of the blend (at the specific blending ratio) divided by the strength of the mixture with 100% hard aggregate (reported as a percentage).

When comparing the different mixtures for the two blending cases (Table 4.1), the Superpave-C and the Type-D mixtures showed almost identical percent reduction at the same soft aggregate percentages. This can be seen in Figure 4.15, which shows these percentages plotted against each other; the points almost fall on the equality line with $R^2 = 0.96$, a slope of almost unity (1.01), and an intercept close to zero (-1.3).

Table 4.1. The Influence of Blending on Mixture Strength.

Percentage of Soft Aggregate	Aggregate Strength Ratio (Hard/Soft)	Mixture Type			
		PFC	CMHB	Superpave	Type-D
20%	Case I: 1.70	16.18	18.93	10.66	11.27
	Case II: 2.13	19.44	14.71	13.42	11.67
40%	Case I: 1.70	15.24	23.76	13.78	14.80
	Case II: 2.13	21.05	18.56	21.00	20.14
60%	Case I: 1.70	19.48	22.08	20.65	19.84
	Case II: 2.13	33.03	32.15	33.00	32.58
80%	Case I: 1.70	19.94	29.99	24.37	24.60
	Case II: 2.13	35.46	42.16	38.32	43.11

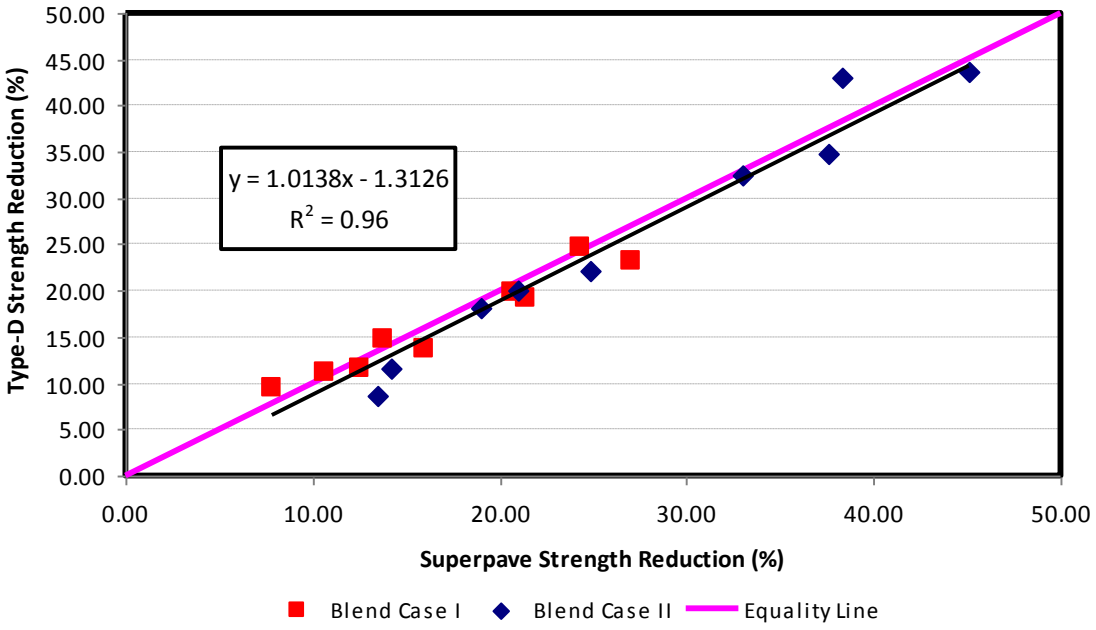

Figure 4.15. Superpave vs. Type-D Strength Reduction (Case I & II).

Comparison with Experimental Laboratory Results

Experimental laboratory tests for blending were done for a blend of soft limestone and sandstone. The percentages were limited to 25%, 50%, and 75%, as it was not feasible due to time constraints to measure the full spectrum of blends as were evaluated in the DEM. Table 4.2 summarizes the results from the laboratory blending results for the IDT strength. The expected trend is a reduction in strength with an increase in the percentage of soft material. However, due to the variability in the laboratory testing results and the limited number of replicates (maximum of three), some points did not follow this trend exactly. Values in Table 4.2 that do not follow the expected trend are marked with an asterisk (*).

This soft limestone–sandstone blend is an identical case to Case II in the DEM analysis. Consequently, the experimental results were compared to the DEM results. The CMHB and PFC results were almost identical to the DEM at 0% and 100% soft material. However, the Type-D and Superpave mixture experimental results at 0% and 100% were different than the DEM results. Therefore, it was necessary to multiply all the experimental results (at all blending percentages) with a factor to match it with DEM results at 0% and 100%. Figure 4.16 shows the experimental results compared to the DEM analysis. The DEM results and the experimental results compare very well and are almost identical (excluding the experimental values with an asterisks [*]).

Table 4.2. Laboratory Blending Results (IDT).

Blend	**Percent of Soft Materials**	**Mixture Strength (psi)**			
		CMHB	**Superpave**	**PFC**	**Type-D**
Soft Limestone/ Sandstone Blend	**0%**	206	226	78	207
	25%	184	190	73	200
	50%	153	217*	72	177
	75%	165*	160	67	199*
	100%	94	125	50	148

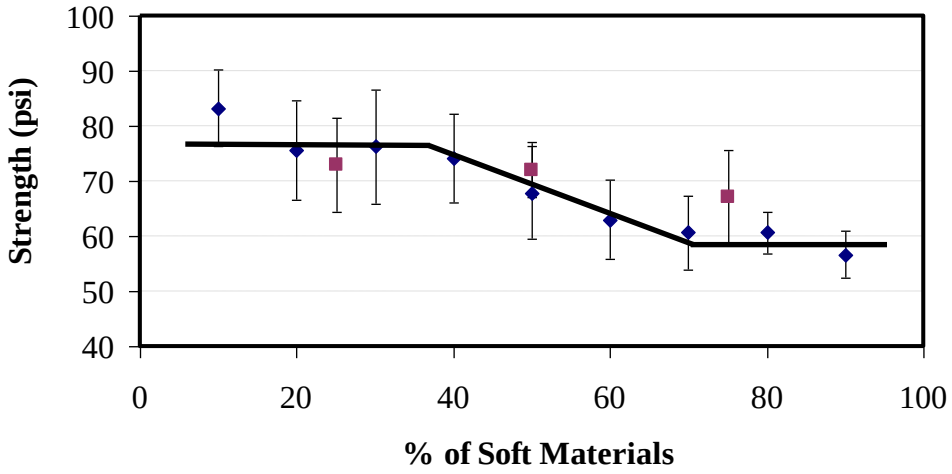

(a) PFC Mixture

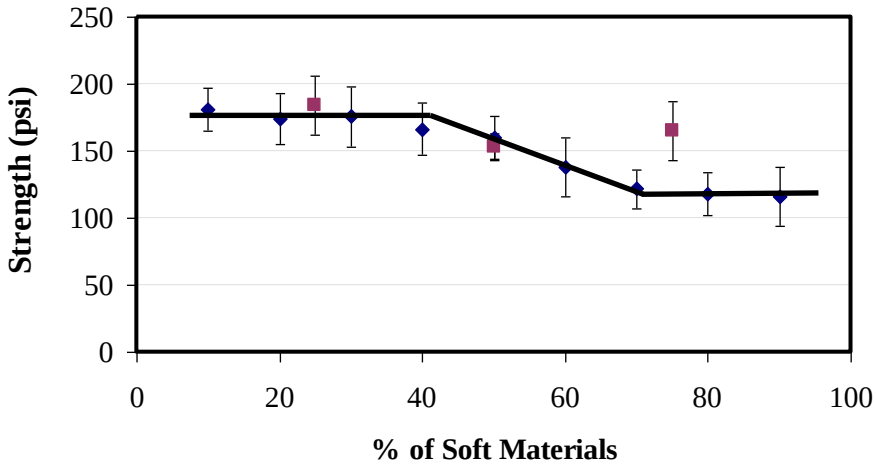

(b) CMHB Mixture

Figure 4.16. Experimental Blending Results Compared to DEM.

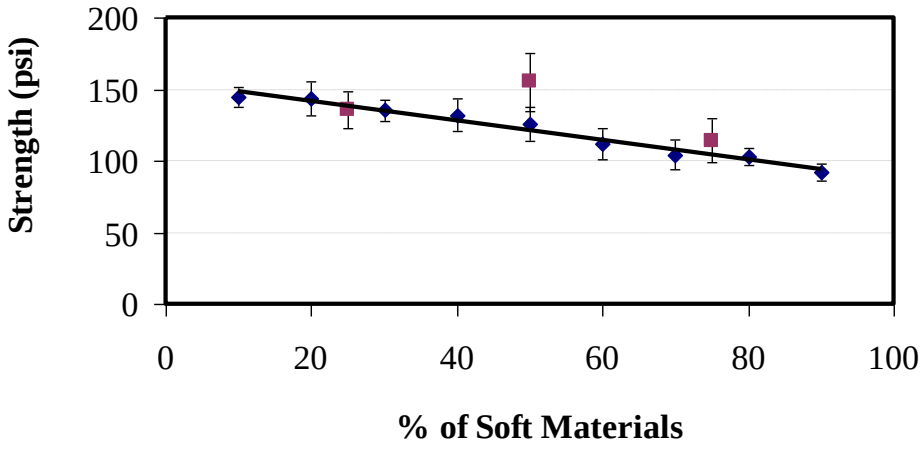

(c) Superpave Mixture

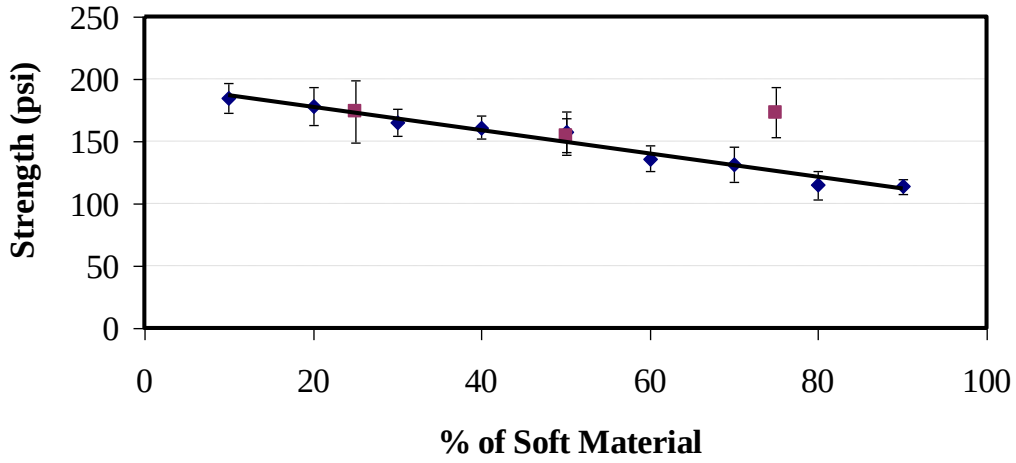

(d) Type-D Mixture

Figure 4.16 Continued.

Other experimental tests, such as the dynamic modulus test, Hamburg wheel (rutting), and flow time, were also conducted for the different mixtures. The results are summarized in Tables 4.3, 4.4, and 4.5 for the modulus, rutting, and flow time, respectively. In order to compare these results to the DEM output, the percent change in

the measurements were calculated (similar to the calculations in Table 4.1) and compared to the percent change in the DEM output. Figures 4.17 through 4.20 summarize the comparison for the CMHB, Superpave, PFC, and Type-D mixtures, respectively. The percent change in DEM compared well with the percent change of the different laboratory tests for all four mixtures.

Table 4.3. Laboratory Blending Results (Modulus).

Blend	Percent of Soft Materials	Dynamic Modulus (ksi)			
		CMHB	Superpave	PFC	Type-D
Soft Limestone/ Sandstone Blend	0%	1231	1169	450	1200
	25%	1185	1184	380	1138
	50%	923	1092	332	1123
	75%	831	1000	232	1077
	100%	662	846	200	1031

Table 4.4. Laboratory Blending Results (Rutting).

Blend	Percent of Soft Materials	Rut Depth (in)			
		CMHB	Superpave	PFC	Type-D
Soft Limestone/ Sandstone Blend	0%	0.147	0.467	N/A	0.147
	25%	0.208	0.653		0.093
	50%	0.160	0.747		0.400
	75%	0.333	0.760		0.600
	100%	0.520	0.667		0.453

Table 4.5. Laboratory Blending Results (Flow Time).

Blend	Percent of Soft Materials	Maximum Strain (μ-in/in)			
		CMHB	Superpave	PFC	Type-D
Soft Limestone/ Sandstone Blend	0%	4900	4400	6750	3500
	25%	6200	4000	N/A	4600
	50%	5000	3900	11500	5500
	75%	7000	4900	8000	6200
	100%	6980	6700	7250	6000

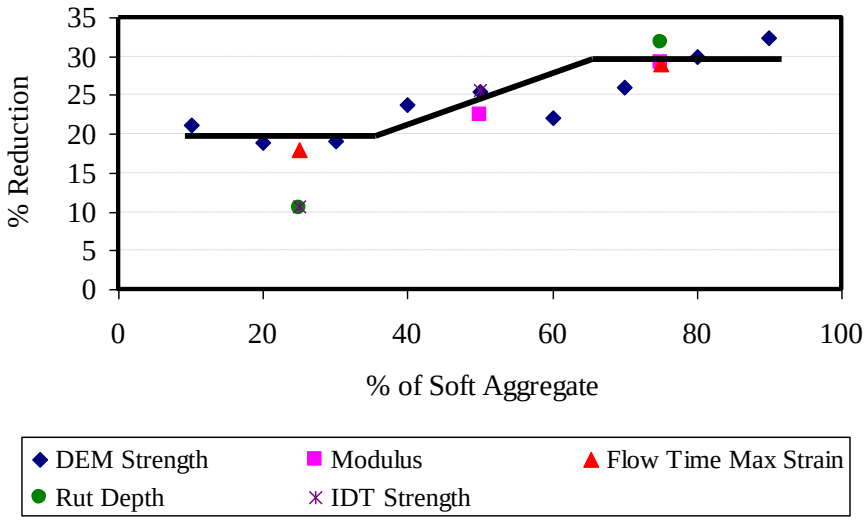

Figure 4.17. Percent Change in Experimental Blending Results Compared to DEM (CMHB Mixture).

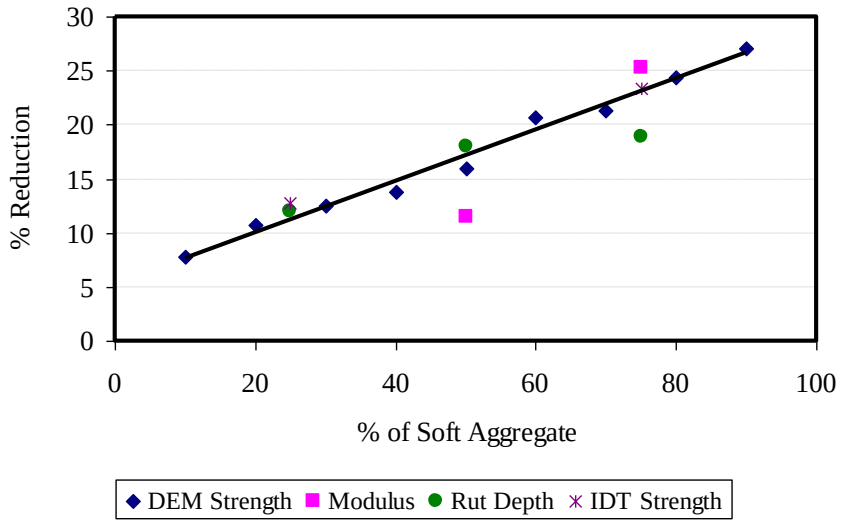

Figure 4.18. Percent Change in Experimental Blending Results Compared to DEM (Superpave Mixture).

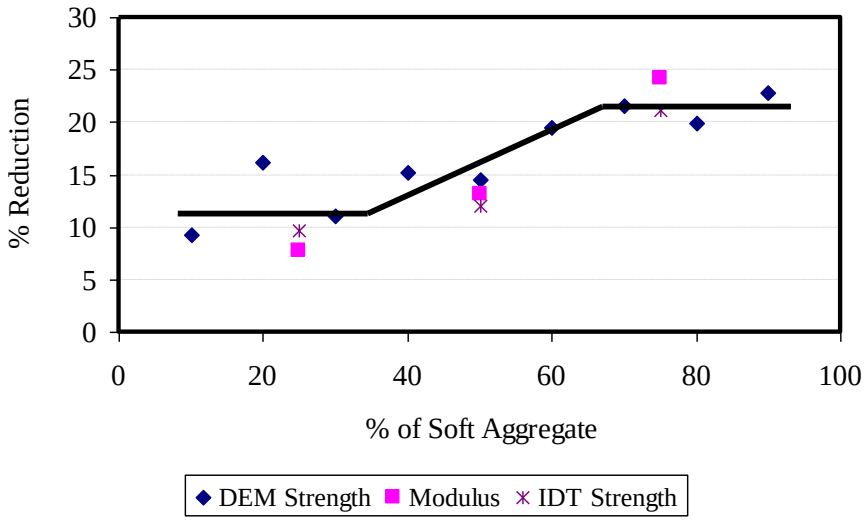

Figure 4.19. Percent Change in Experimental Blending Results Compared to DEM (PFC Mixture).

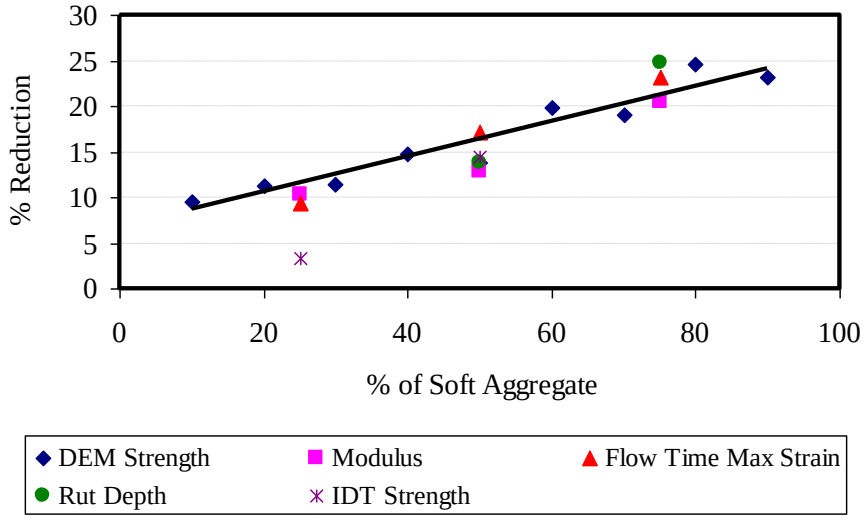

Figure 4.20. Percent Change in Experimental Blending Results Compared to DEM (Type-D Mixture).

Another experimental case of blending hard limestone and granite was performed. However, the strength ratio in this case for granite to hard limestone was 1.36, which does not match with any of the DEM analysis, so a comparison similar to the previous case was not feasible. In addition, due to the small difference in strength between hard

limestone and granite, the different blends of these two aggregates is not expected to give results different than using 100% of either one of these aggregates. This was shown through the experimental results as all tests showed very small differences between the different percentages of blending these two aggregates. Table 4.6 shows an example of the modulus results for CMHB mixture and illustrates how the changes are very small.

Table 4.6. Laboratory Blending Results for the 2nd Experimental Blend (Modulus).

Blend	Percent of Soft Materials	CMHB Mixture	
		Dynamic Modulus (ksi)	% Change
Hard Limestone/ Granite Blend	**0%**	908	---
	25%	1015	11
	50%	877	-3
	75%	954	5
	100%	862	-5

BLENDING CHARTS

It is desirable to estimate the change in the mixture strength at different percentages of blending different aggregates. This section introduces a prediction method to achieve this goal. A contour representation of the strength reduction in the different mixtures' strength due to blending (increasing percentage of soft material) can be produced such that the x-axis represents the soft material percentage, and the y-axis represents the ratio between the hard and the soft material strength. The contour color indicates the percent loss in the mixture strength.

As stated in the previous section, the aggregate strength ratio for Case I was 1.70 and it was 2.13 for Case II. This range is relatively small; consequently, it was decided to add another case with a third aggregate strength ratio. Since the experimental results for

the hard limestone–granite blend (aggregate strength ratio of 1.36) showed minimum/negligible effect of blending on mixture properties, it was decided to add a blending case with a high strength ratio of 6.82. This ratio represents a blend of gravel and soft limestone.

Figure 4.21 (a, b, c, and d) shows the contour representation for the Superpave, Type-D, PFC, and CMHB mixtures, respectively. All four plots were represented in a scale from 0% to 60% reduction in mixture strength. This was necessary in order to make the comparison among the different mixtures easier.

As shown in Figure 4.21, a high aggregate strength ratio reduces the ability of the mixture to accommodate adding soft material for all mixtures. This can be seen in Figure 4.21 by observing that for any specific percent reduction in strength, the high ratio blend case requires less soft material than the low ratio case, and the drop in strength occurs at a faster rate for a higher ratio.

Figure 4.21 a & b shows that the Superpave-C and Type-D mixtures followed almost the same exact trend; as the plots are nearly identical. This further supports the observation that the two mixtures exhibit similar behavior when soft aggregate is blended (Figure 4.15 and Table 4.1).

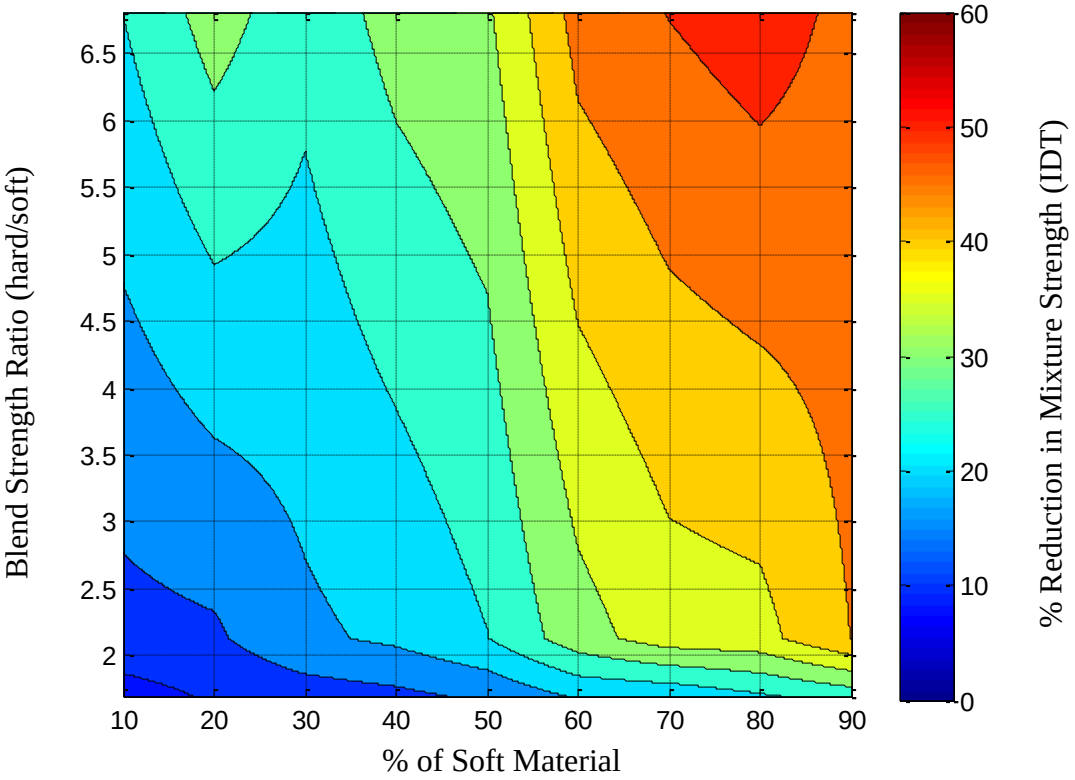

(a) Superpave-C

Figure 4.21. Blending Results (Contour Representation).

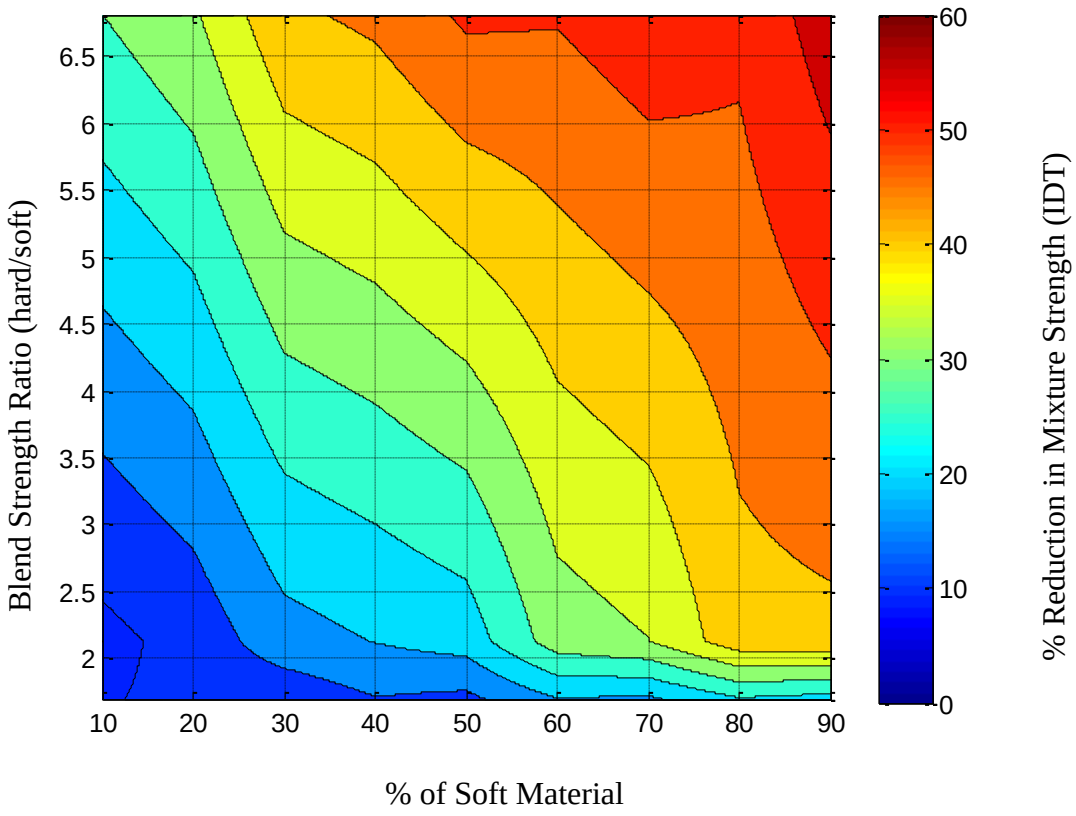

(b) Type-D

Figure 4.21 continued

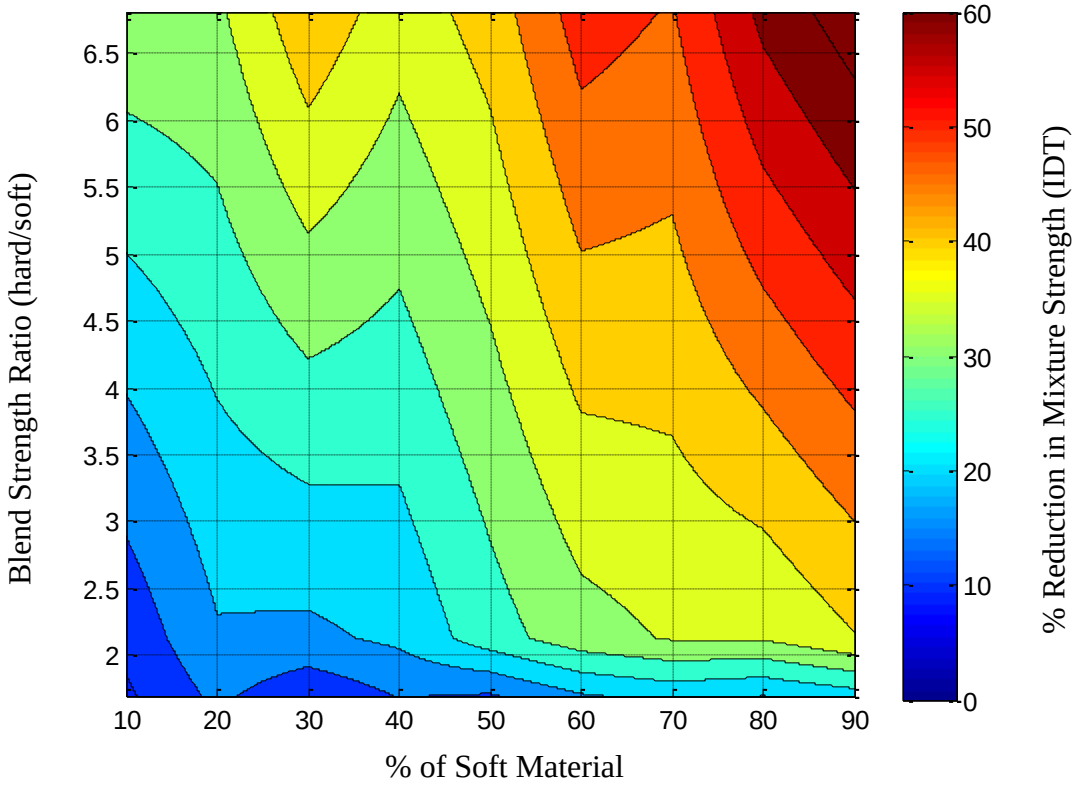

(c) PFC

Figure 4.21 continued

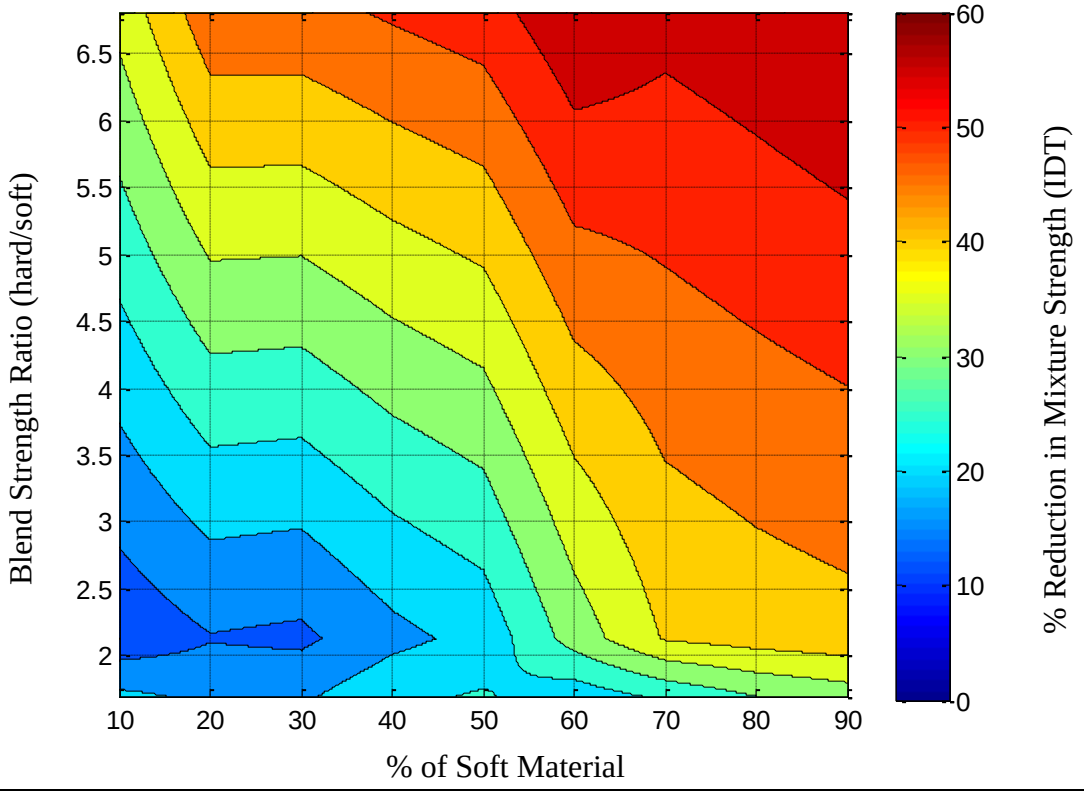

(d) CMHB

Figure 4.21 continued

SUMMARY

The impact of aggregate blending on the strength of asphalt mixtures using DEM was studied. The analysis showed that both the mixture type and strength of aggregates used in the blend are important factors in determining the influence of blending on performance. The following guidelines were developed for blending:

- Dense-graded mixtures such as Superpave and Type-D are more sensitive to blending soft aggregates than open-graded (PFC) and gap-graded (CMHB) mixtures.
- The PFC and CMHB mixtures can accommodate about 40% soft limestone without a decrease in strength. This percentage could vary depending on

aggregate strength, but it is the minimum value that was obtained from the analysis conducted in this study.

- There is almost no benefit to using 30% or less hard limestone or sandstone when the remaining aggregate is soft limestone.

The DEM results compared reasonably well to experimental measurements of the properties of mixtures with different blending percentages. The results revealed that there is a minimum aggregate strength ratio for blending to be useful. This minimum ratio is about 1.36. On the other hand, a ratio of 1.70 showed a change in mixture strength when different percentages of soft aggregate were used. As discussed previously, the influence of using soft aggregate on the mixture depends on the mixture type.

Blending charts were developed to estimate the percentage change in mixture strength based on the ratio of strength of the blended aggregates and the percentages of these aggregates. In addition to these factors, the blending charts clearly demonstrate that the change in strength is a function of the mixture design.

CHAPTER V

A PROBABILISTIC APPROACH FOR THE ANALYSIS OF AGGREGATE RESISTANCE TO FRACTURE IN ASPHALT MIXTURES

INTRODUCTION

Crushing or fracture of aggregate particles was studied by many researchers in the area of geotechnical engineering. These studies analyzed both the crushing of single particles under compression loading, and the crushing of particles within a granular medium. McDowell and Bolton (1998) conducted a study of the micromechanical behavior of crushable soil particles. In this study, single particles were loaded between two flat plates to measure the strength of particles of different size and mineralogy (Figure 5.1). The study showed that aggregate particle strength is not constant even for the same size and aggregate mineralogy, but it has a standard deviation around an average mean value. The authors suggested the use of Weibull statistics to represent the variability of aggregate strength.

Nakata et al. (1999) studied sand particle crushing in using the triaxial test using a probabilistic approach. In this study single aggregate crushing was carried out for different material sizes using different sources. Figure 5.2 shows a schematic of the machine used to crush single aggregate particles. The authors examined the different cases of the loading-displacement relationships, and summarized them in three general shapes. Figure 5.3 shows a schematic of these three general cases. The authors defined two types of forces that control the behavior of single aggregate crushing. The first one

called crushing force F_c is defined as the first point at which load slippage occurs, i.e., the first peak on the load-displacement curve, which corresponds to the breaking of asperities. The second force F_f marks the failure point which is defined as the peak force of the load-displacement curve that causes a major splitting of the particle. The experimental results by Nakata et al. (1999) were described well by the Weibull distribution.

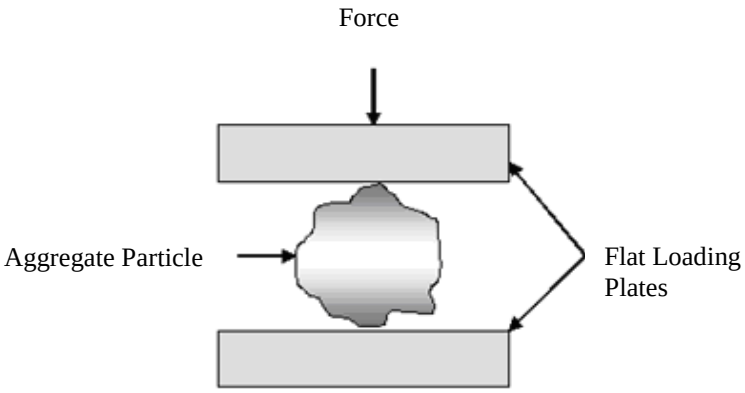

Figure 5.1. Schematic of Particle Strength Test.

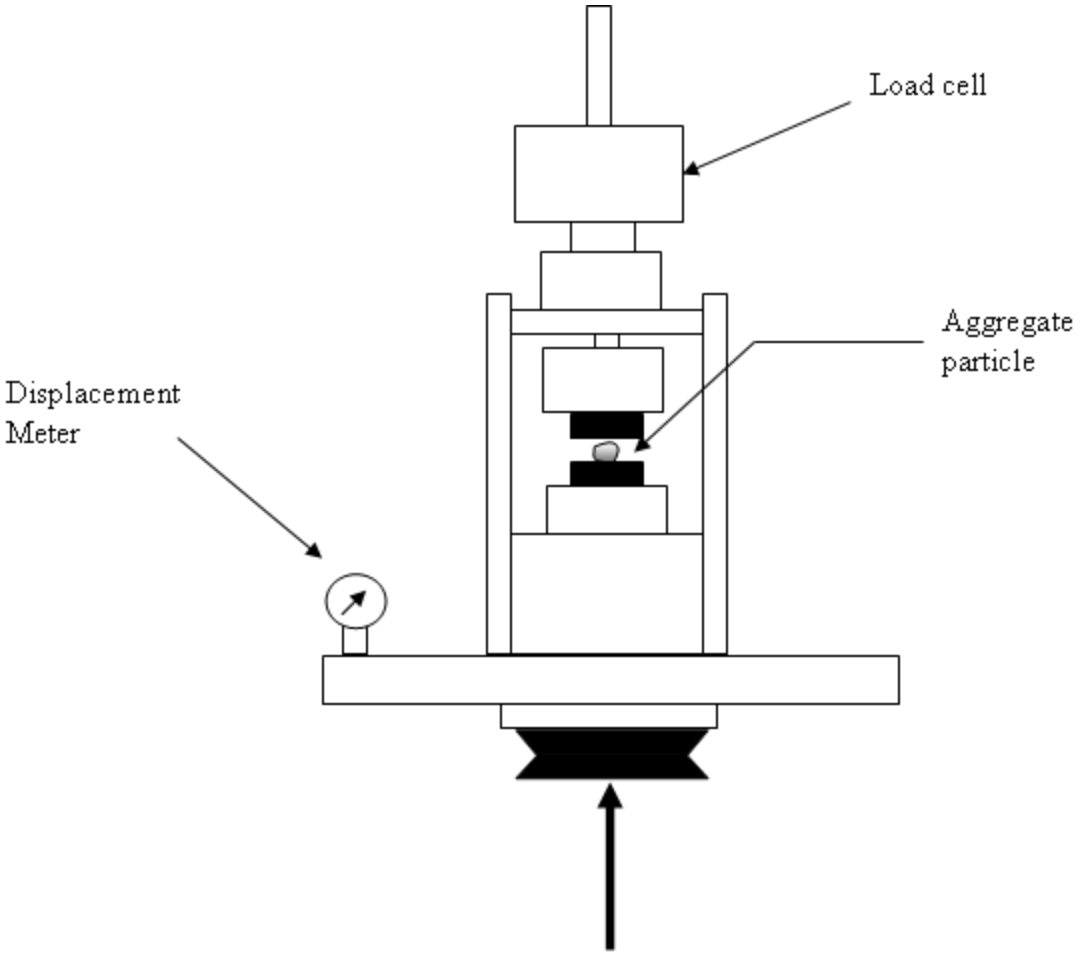

Figure 5.2. Schematic of Single-Particle Crushing Test (after Nakata et al. 1999).

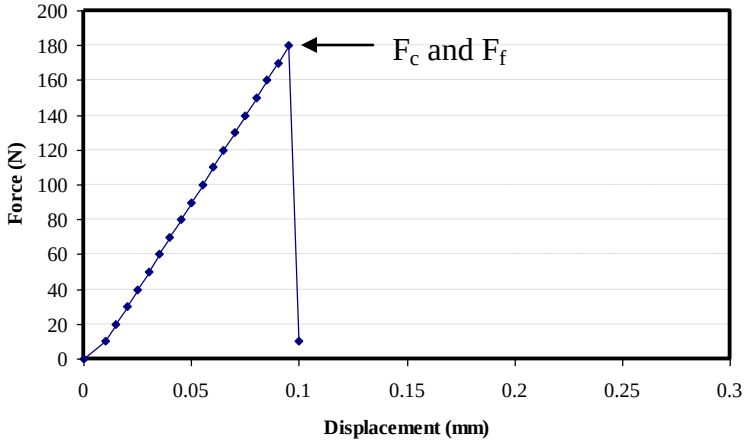

(a)

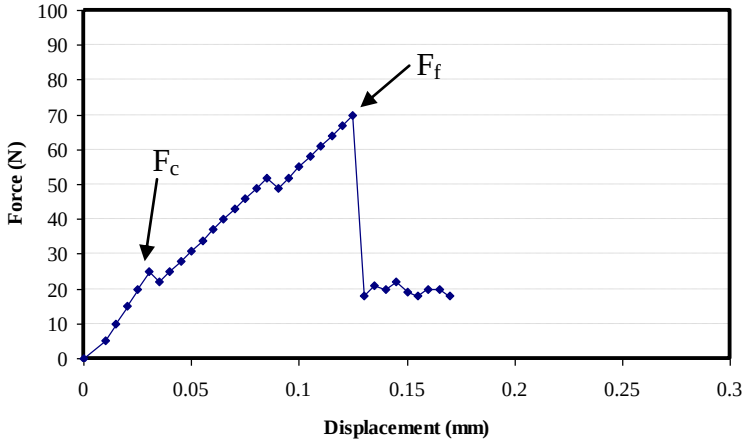

(b)

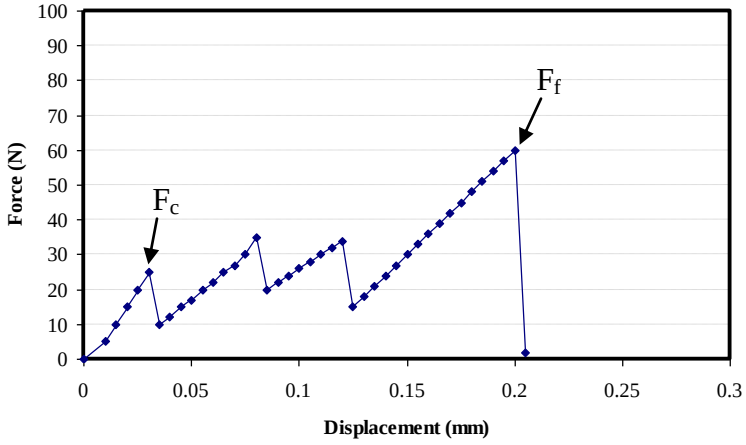

(c)

Figure 5.3. Single Particle Crushing Load-Displacement Relationship.

Cheng et al. (2003) used DEM to simulate particle crushing under uniaxial compression and isotropic compression modes. The authors used a three dimensional discrete element model to simulate these tests. In these simulations, a representation of an aggregate particle was first generated as a sphere. Then, the shape was altered by randomly deleting twenty percent of the discrete elements of each aggregate particle. The authors expected this random deletion to introduce strength variability within aggregate particles. The simulations results matched the crushing strength results from laboratory samples of sand grains.

Marketos and Bolton (2007) utilized DEM to quantify the extent of crushing in granular materials. They used DEM along with probabilistic analysis to predict crushing within granular media. The approach was based on combining a distribution of particle strength with a distribution of internal forces developing within the granular system due to loading to define a crushing probability as the probability of a particle to exhibit an internal force that is greater than its strength.

OBJECTIVES AND SCOPE

The approach used by Marketos and Bolton (2007) is extended in this chapter to study the crushing probability of aggregate particles within asphalt mixtures. The approach presented in this chapter has the following unique features that are different than the work of Marketos and Bolton (2007):

- The approach presented in this chapter utilized actual images of particles in the DEM. This approach allowed accounting for the influence of actual particle shape on their resistance to crushing.

- The crushing was analyzed within an asphalt mixture medium in which the properties of the matrix phase plays an important role in the resistance to crushing. In addition, mixtures with different internal structure distributions were included in the analysis.
- Crushing is analyzed in this chapter by bond loss rather than by removing DEM elements as was done by Marketos and Bolton (2007).
- Several probability distributions were examined to determine the best distributions that fit internal forces and particle strength.

DESCRIPTION OF ANALYSIS APPROACH

This chapter includes an approach that combines probabilistic, analytical and numerical techniques in order to relate aggregate gradation and mechanical properties to the resistance of aggregate structure in asphalt mixture to fracture. The discrete element model developed in chapter III of this dissertation was used as the framework in developing this approach. The discrete element model requires the properties of the aggregates and matrix phases as an input, and it provides the internal forces in a mixture. These internal forces are obtained at the three loading levels considered in chapter III. Case I is at the peak force, Case II is at an intermediate force equal to 50% of the peak force, and Case III is at a force of 2 kN (450 lb).

The discrete model was used to analyze eight combinations of aggregate types and gradations as shown in Table 5.1. These combinations include five Superpave mixtures with hard limestone, soft limestone, sandstone, gravel, and granite; one PFC mixture with hard limestone; one CMHB mixture with hard limestone; and one Type-D

mixture with sandstone. This selection allowed for comparison of the results of different aggregates for the same mixture type, as well the different mixtures with the same aggregate type.

Table 5.1. Aggregate and Mixtures Selection.

Mixture Type	**Aggregate Type**
PFC	Hard limestone
CMHB	Hard limestone
Superpave	Hard limestone
	Soft limestone
	Granite
	Gravel
	Sandstone
Type-D	Sandstone

In the discrete element model, aggregate breakage within an asphalt mixture is represented by the loss of bond among DEM elements (aggregate-aggregate bond only). The loss of bond occurs when the contact force between any two elements reaches the bond strength. Aggregate strength was obtained from single particle crushing using a compression machine. Consequently, in order to analyze aggregate breakage within asphalt mixtures, two separate events needed to be represented using probability distribution functions. The first one is the internal force distribution at contact points between two elements, and the second one is the strength bond of that contact from the single crushing test. The approach developed in this study can be summarized in the following steps (Figure 5.4):

1. The DEM was used to simulate asphalt mixture response under loading and obtain the internal forces within the aggregate structure. The internal forces were obtained at three different levels of loading without allowing for particle breakage.
2. Statistical analysis was conducted to determine the probability density function (PDF) that fits the internal force distribution.
3. A single aggregate crushing test was used to measure the strength of aggregate particles.
4. Statistical analysis was conducted to determine the PDF that fits the aggregate strength distribution.
5. The distribution of aggregate strength obtained from step 4 was used as an input to the discrete element model. The discrete element model was then used to analyze particle fracture within the mixture.
6. The PDFs for the internal forces and aggregate strength (from steps 2 and 4) were used to derive a mathematical representation of the probability of aggregate fracture within the mixture.
7. The mathematical expression obtained in step 6 was then verified by comparing it to the DEM simulation output from step 5.

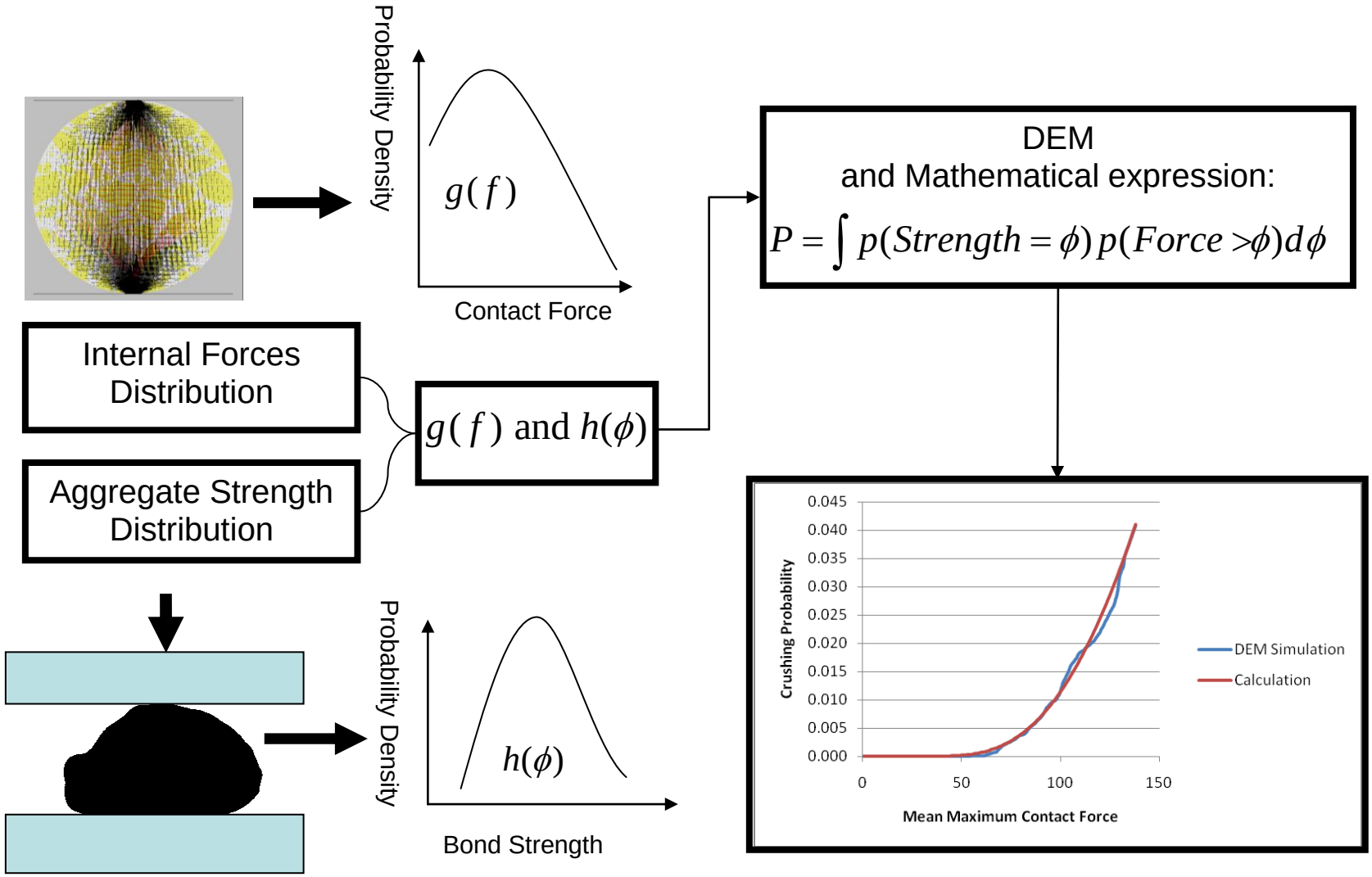

Figure 5.4. Chart Diagram Summarizing the Analytical Approach Steps.

INTERNAL FORCES DISTRIBUTION

A probabilistic distribution of internal forces within aggregate particles can be obtained using DEM analysis at different loading levels. The internal force distribution will vary depending on aggregate structure and matrix properties. Marketos and Bolton (2007) used the following equation to fit the PDF for the internal force distribution:

$$g(f) = (f + a)^b e^{-cf-d} \tag{5.1}$$

where f is the internal force and g(f) is PDF. It is expected that the constants (a, b, c, and d) will change based on aggregate strength, gradation, and matrix (or binder) properties.

As previously discussed in Chapter III, four different forces develop at each contact point under loading: two shear forces and two normal forces. As the contact bond will break once any of the four forces reaches the bond strength, the maximum contact force is considered in deriving a fracture probability relationship.

The contact forces were obtained at the three stages of loading discussed in Chapter III (Case I is at the loading force that corresponds to the mixture strength [peak force], Case II is at the loading force that corresponds to 50% of the mixture strength, and Case III is at 2000 N). The internal forces were obtained without allowing for aggregate breakage or bond loss. This was achieved by assigning very high values for the bond strengths which were equal to ten times the bond strength values of the both the matrix and aggregate of calibrated mixtures.

Figure 5.5 a, b, and c show the probability density distributions of the maximum contact forces for the three stress levels for the hard limestone Superpave mixture. As expected, higher contact force values were obtained at higher stress levels. Each of the

distributions was normalized by dividing them by the mean contact force at that loading level. Figure 5.5 d, e, and f show the probability density for the normalized maximum contact force.

The next step was to fit equation 5.1 to these probability density distributions by using the built-in nonlinear regression function of the SPSS (Statistical Package for the Social Sciences) software. It was found that the same set of PDFs (a, b, c, and d in equation 5.1) could be used to fit the data of the three normalized forces distributions. Figure 5.6 represents an example of the data and PDF for the hard limestone Superpave mixture case. For this case the function coefficients were: a = 2.03, b = 64, c = 24, and d = 49. The same analysis was done for the other seven aggregate-mixture type combinations. Probability density distributions similar to Figure 5.5 were obtained for the eight mixtures and aggregate types and are presented in Appendix A. Figure 5.7 shows the fitting of equation 5.1 to all eight different cases; while Table 5.2 summarizes the coefficients for the eight mixtures. Table 5.2 also includes the R-squared values for all cases as obtained using the SPSS software. The high R-squared values (greater than 0.93) indicate that the PDF fit the data very well.

The PDF coefficients are different among the different cases (Table 5.2). The coefficients did not follow a certain trend in relation to aggregate or mixture type. It seems that each of the four constants is affected by both the mixture type and aggregate type. However, Table 5.2 shows that the Superpave and Type-D mixtures had almost the same exact fitting constants for the same aggregate (sandstone).

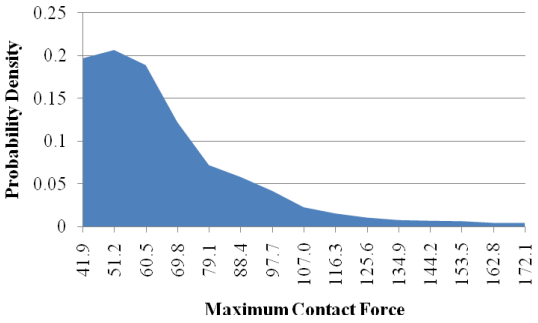

(a) Stress level I

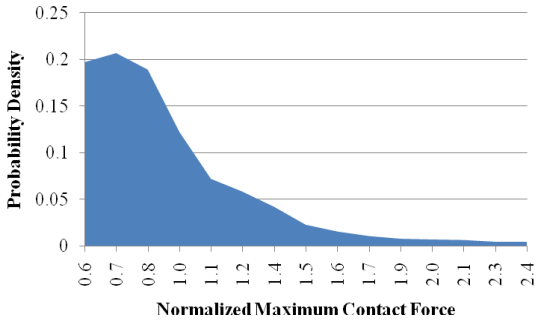

(d) Stress level I – normalized

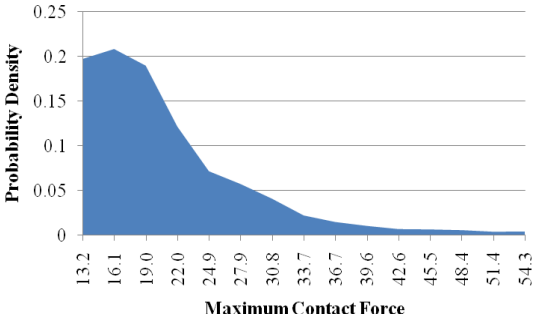

(b) Stress level II

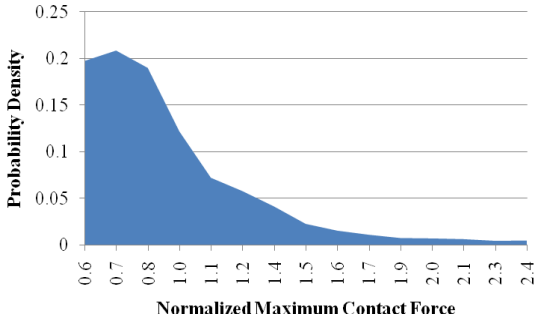

(e) Stress level II – normalized

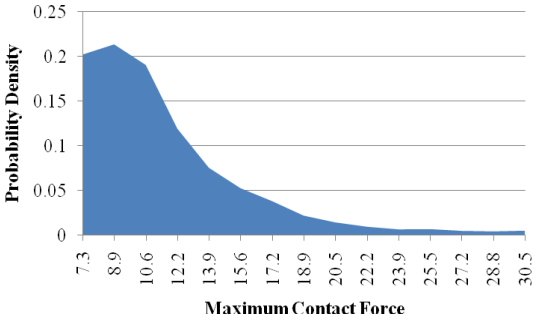

(c) Stress level III

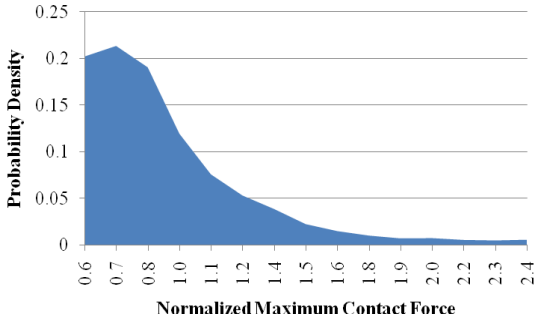

(f) Stress level III – normalized

Figure 5.5. Maximum Contact Force Probability Density (Hard Limestone Superpave Mixture).

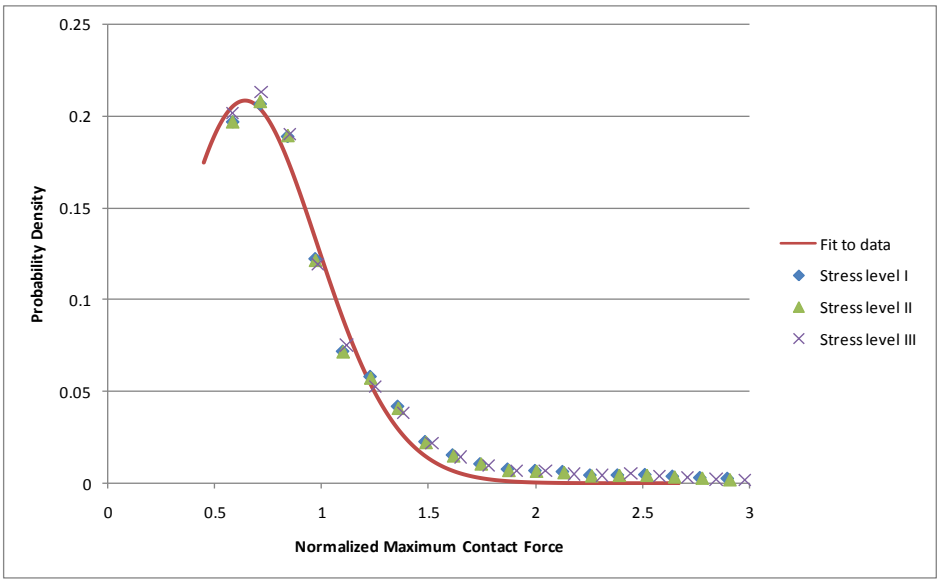

Figure 5.6. Normalized & Combined Maximum Contact Force Probability Density (Hard Limestone Superpave Mixture).

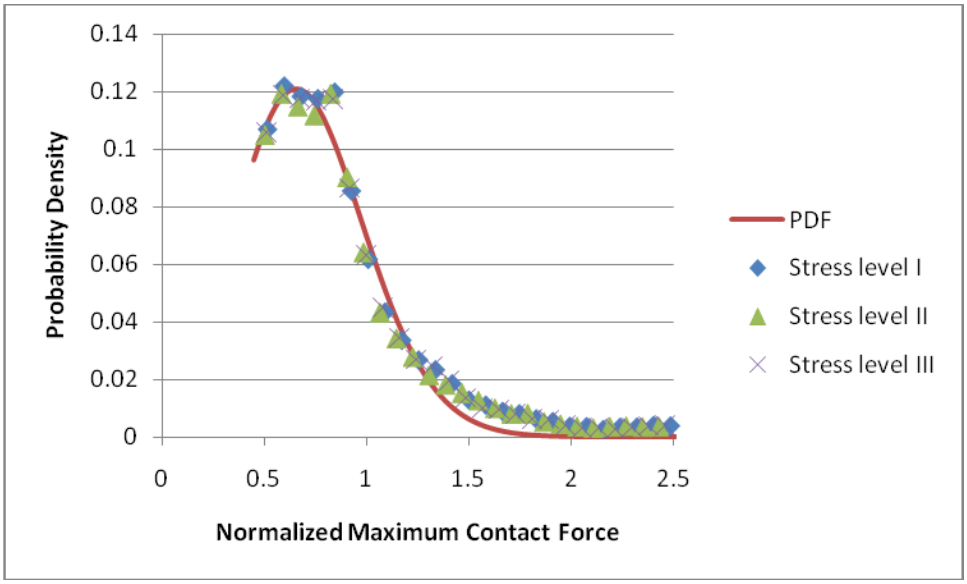

(a) Sandstone Type-D

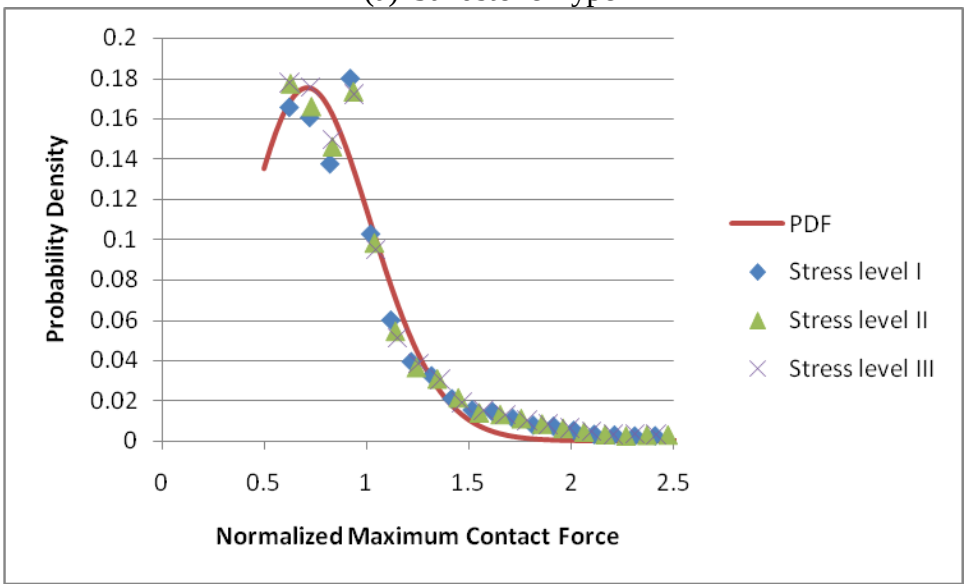

(b) Sandstone Superpave

Figure 5.7. Normalized & Combined Maximum Contact Force Probability Density (All Eight Cases).

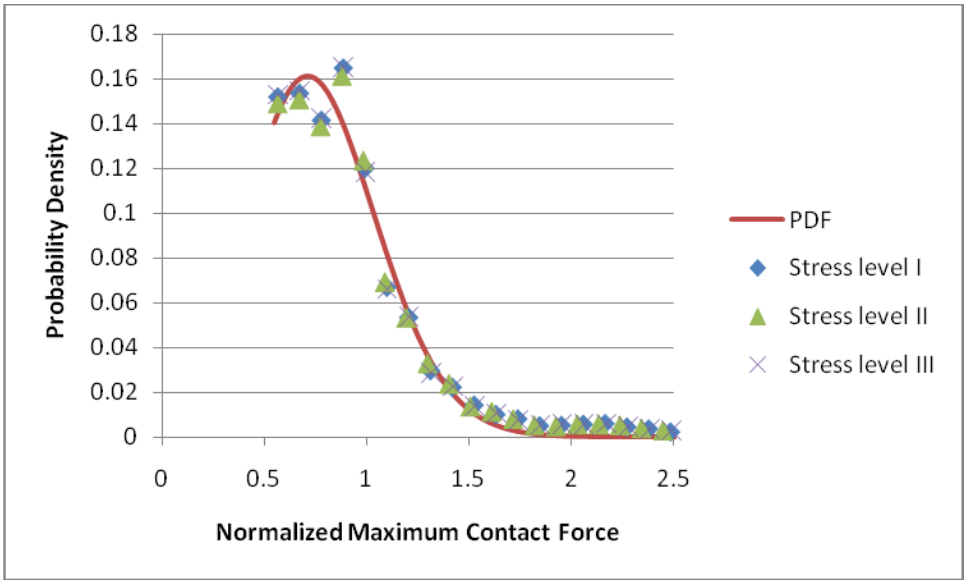

(c) Soft Limestone Superpave

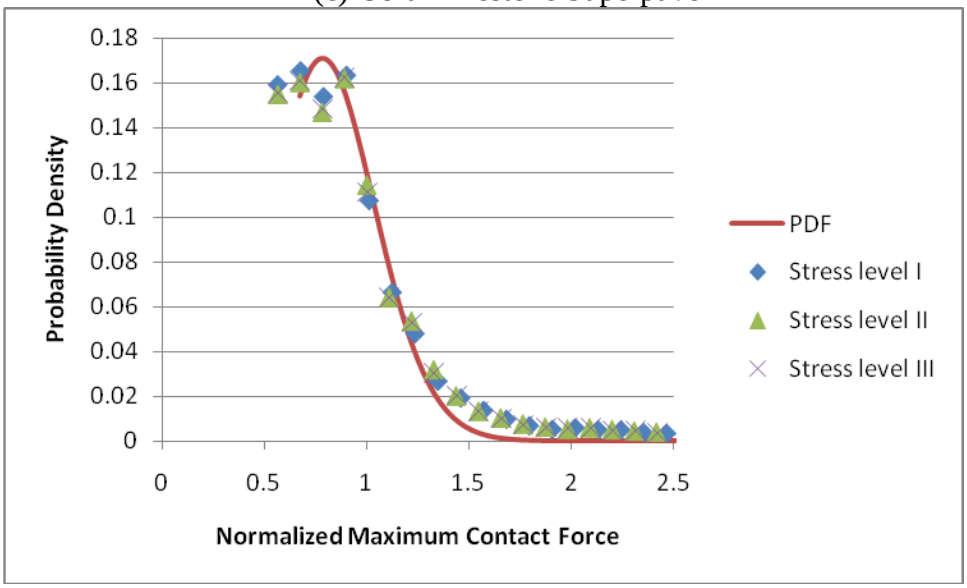

(d) Granite Superpave

Figure 5.7 continued.

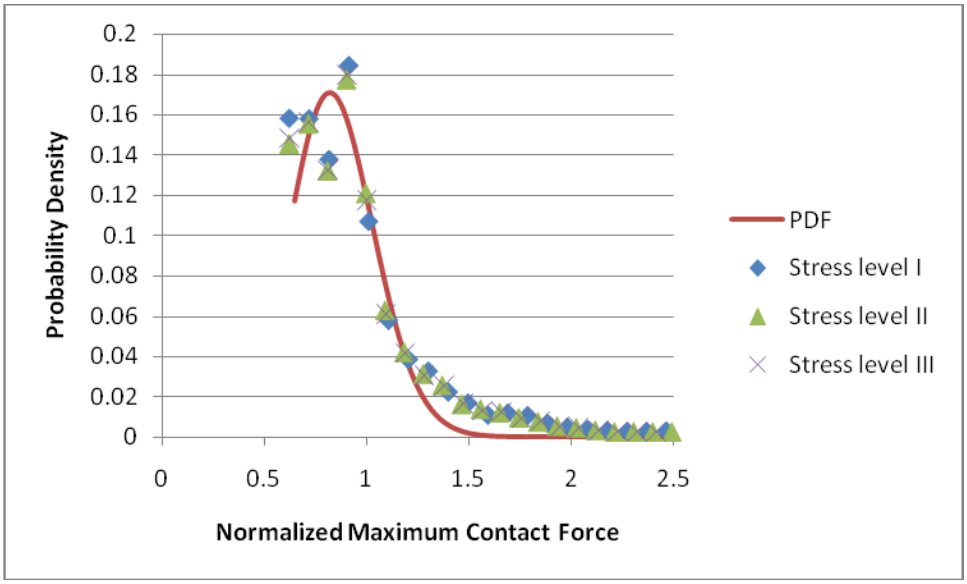

(e) Gravel Superpave

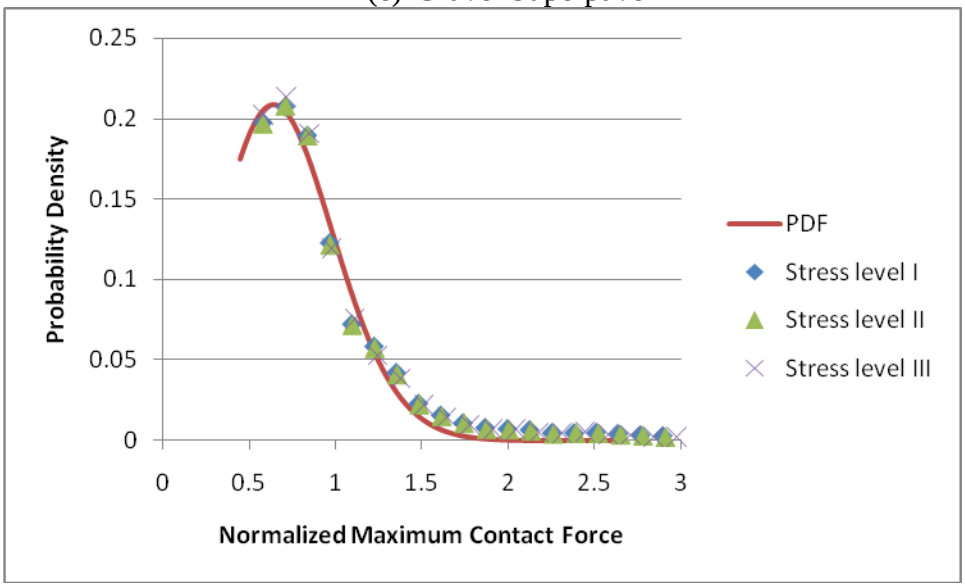

(f) Hard Limestone Superpave

Figure 5.7 continued.

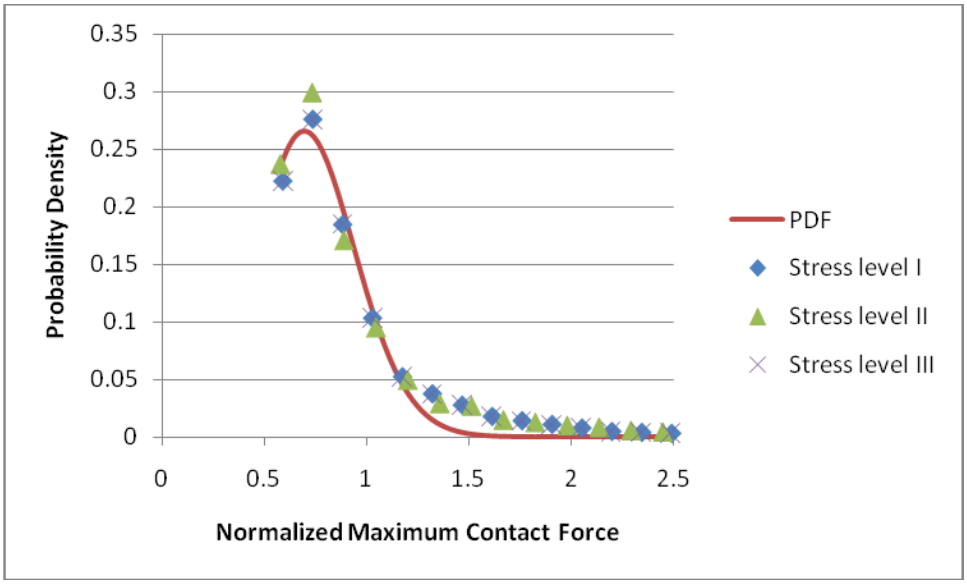

(g) Hard Limestone PFC

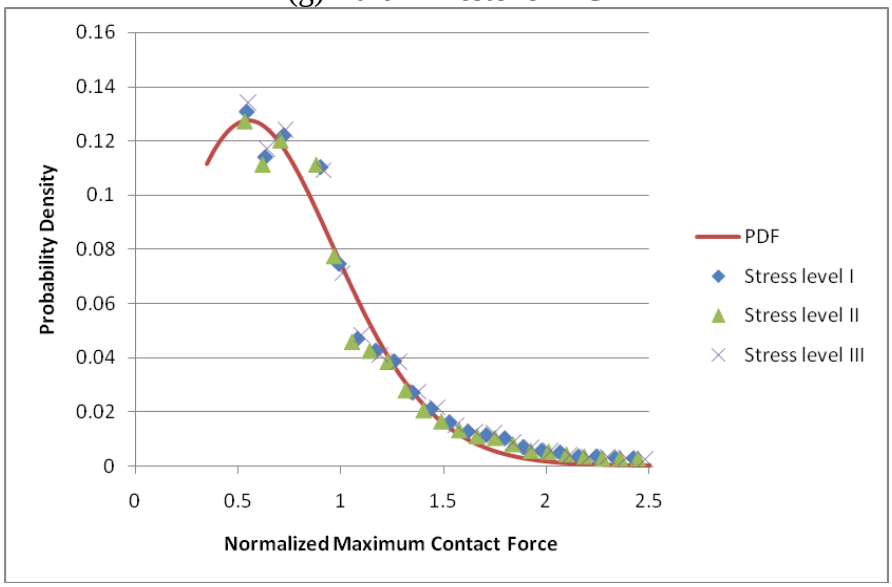

(h) Hard Limestone CMHB

Figure 5.7 continued.

Table 5.2. Internal Forces Fitting Constants.

Aggregate Type	Mixture Type	A	B	c	d	R^2
Hard limestone	PFC	1.40	78	37	33	0.979
Hard limestone	CMHB	1.42	24	12	12	0.980
Hard limestone	Superpave	2.03	64	24	49	0.989
Soft limestone	Superpave	1.36	82	38	34	0.983
Granite	Superpave	1.43	79	36	37	0.965
Gravel	Superpave	1.10	89	46	22	0.934
Sandstone	Superpave	1.78	68	27	45	0.970
Sandstone	Type-D	1.89	66	26	47	0.984

AGGREGATE STRENGTH DISTRIBUTION

The previous section covered the first two steps of the analysis approach proposed in this chapter. This section will cover the next two steps (3 & 4 in page 94) that are concerned with finding the aggregate strength distribution and fitting a PDF for the strength values.

Aggregate strength distribution was obtained by measuring strength of aggregate particles instead of aggregate bulk masses. To this end, a single aggregate particle was crushed. Figure 5.8a shows the machine that was used to test the strength of single aggregates particles between two flat plates. The machine loading cell had a maximum capacity of 30000 lb, and the loading rate of 2 in/min was applied.

One hundred twelve particles passing the 1/2 in. sieve size and retained on the 3/8 in. sieve size from each of the five aggregate sources were tested. Fifty six of these particles were tested positioned vertically, while another group of fifty-six particles were tested positioned horizontally, Figure 5.8 b & c show an illustration of the two positions. For the horizontally positioned aggregates, the upper plate was lowered down slowly until it came in contact with a particle, after which the loading started. For the vertically positioned aggregates, each particle was held in a vertical position using a wrench. Then, the upper plate was lowered until it came in contact with the aggregate particle, after which the wrench was removed and loading started.

Typical load-displacement curves are shown in Figure 5.3. An example of a load-displacement curve for one of the laboratory tests is shown in Figure 5.9. While Figure 5.10 shows a crushed aggregate particle.

a) Compression Machine Used to Perform Single Aggregate Testing (Model: INSTRON 5583)

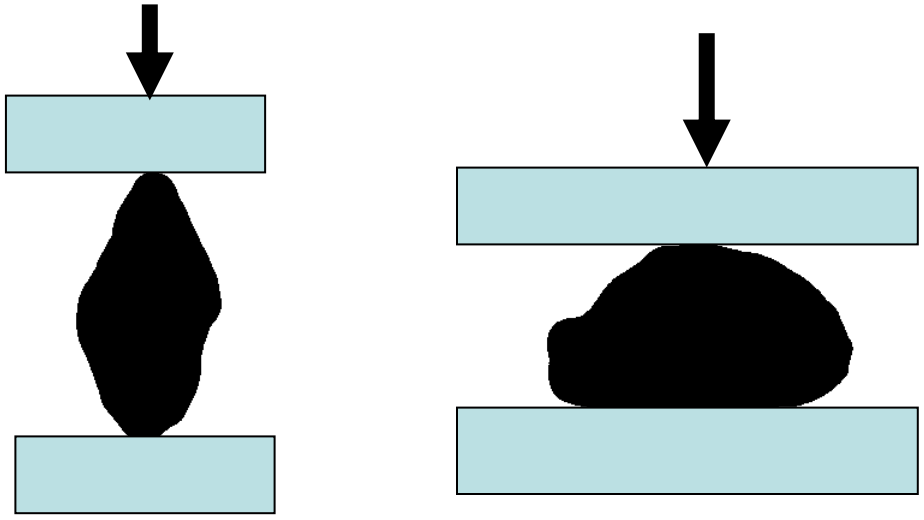

b) Vertically Aligned Aggregate **c) Horizontally Aligned Aggregate**

Figure 5.8. Single Aggregate Crushing Set-up.

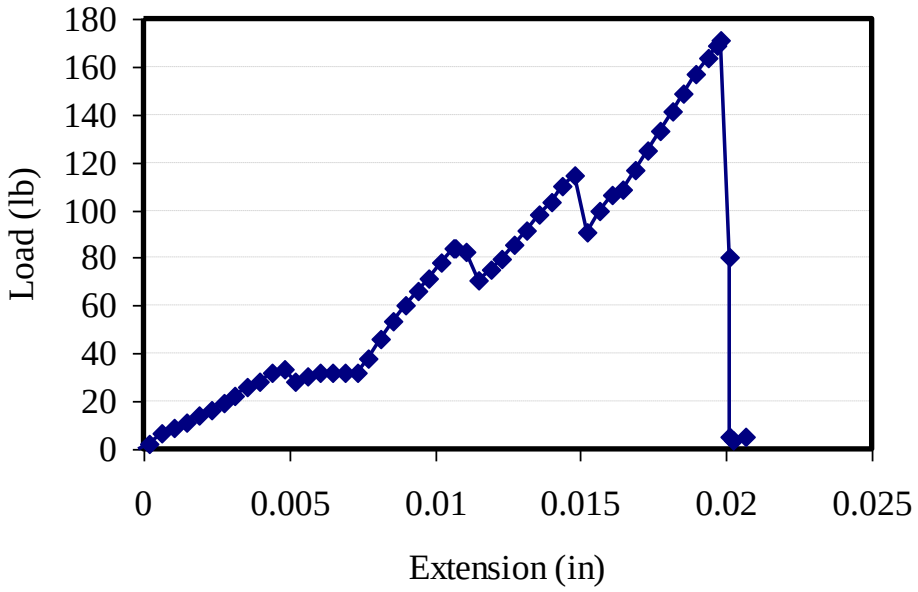

Figure 5.9. An Example of a Single Aggregate Crushing Load-Displacement Curve.

Figure 5.10. A Photo of a Crushed Aggregate Particle.

The averages of the results for each aggregate are shown in Figure 5.11. The results show that the aggregate strength distributions were similar for the tests conducted on particles positioned vertically and horizontally. Figure 5.12 shows an example of the

distributions of the horizontal and vertical strength for the soft limestone. Consequently, it was decided to combine the measurements of both the tests of aggregates in vertical and horizontal positions.

The next step was to fit a PDF to each of the aggregate strength distributions. Statistical software Best Fit 4.0 was used to determine the best function that fit aggregate strength distributions. This software fits the input data to many standard PDFs, including, but not limited to, normal, Gaussian, Weibull, and gamma functions. The software then ranks the distributions based on their goodness of the fit to the input data using chi-squared statistics. The goodness-of-fit test method requires a random sample of size n from the population whose probability distribution is to be estimated. These n observations are arranged in a frequency histogram, with k bins or class intervals. The observed frequency in the i^{th} class interval is denoted as N_i. Using the hypothesized probability distribution, the expected frequency in the i^{th} class interval, denoted E_i is computed. The test statistic is calculated using the following equation:

$$\chi^2 = \sum_{i=1}^{k} \frac{\left(N_i - E_i\right)^2}{E_i} \qquad (5.2)$$

If the population being studied follows the hypothesized distribution, χ^2 has a chi-square distribution with k – p – 1 degrees of freedom, where p represents the hypothesized distribution number of parameters. For a confidence level of 100(1-α)%, the hypothesis that the distribution of the population is the hypothesized distribution would be rejected if the test statistic value calculated using equation 5.2 $\chi^2 > \chi^2_{\alpha,k-p-1}$.

Several distributions were found to fit each of the strength values. However, the normal PDF was found to provide reasonable fitting of all sets of measurements for the five aggregates. Table 5.3 summarizes the chi-square statistics test results for the normal distribution using a 95% level of confidence ($\alpha = 0.05$), and the hypothesis that the probability distribution of the aggregate strength is normal can not be rejected for all five aggregate types.

Figure 5.13 represents the statistical plots of fitting the normal PDF to the strength data as generated by the Best Fit software. The first column (left column) shows the comparison plots which compare the fitted distribution to the input data on a cumulative basis. In Figure 5.13, the red curve represents the fitted normal distribution, while the blue steps represent the aggregate input data. The normal distribution provided reasonable fits for all sets of data. The second column (right column) in Figure 5.13 represents the p-p graph which is a probability – probability graph that compares the distribution of the input data to the distribution based on the fitted function. If the normal PDF fit the data perfectly, this graph should represent an equality line. All five aggregates were very close to the equality line as it shown in Figure 5.13. Table 5.4 summarizes the experimental and the normal distribution parameters (mean: μ and standard deviation: σ) for the five aggregates. It is important to emphasize that the analysis approach developed in this chapter is not limited to the normal distribution as it can incorporate any kind of distribution.

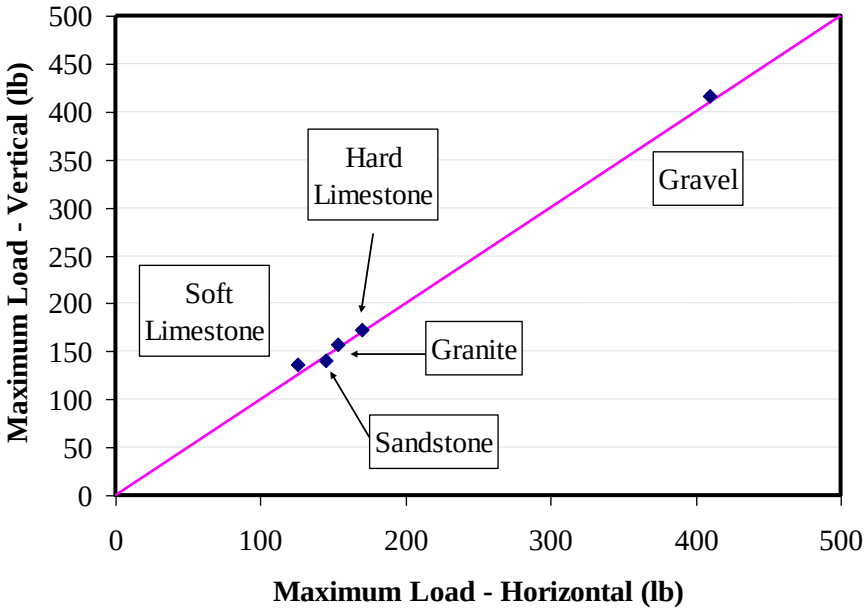

Figure 5.11. Single Aggregate Crushing Average Results.

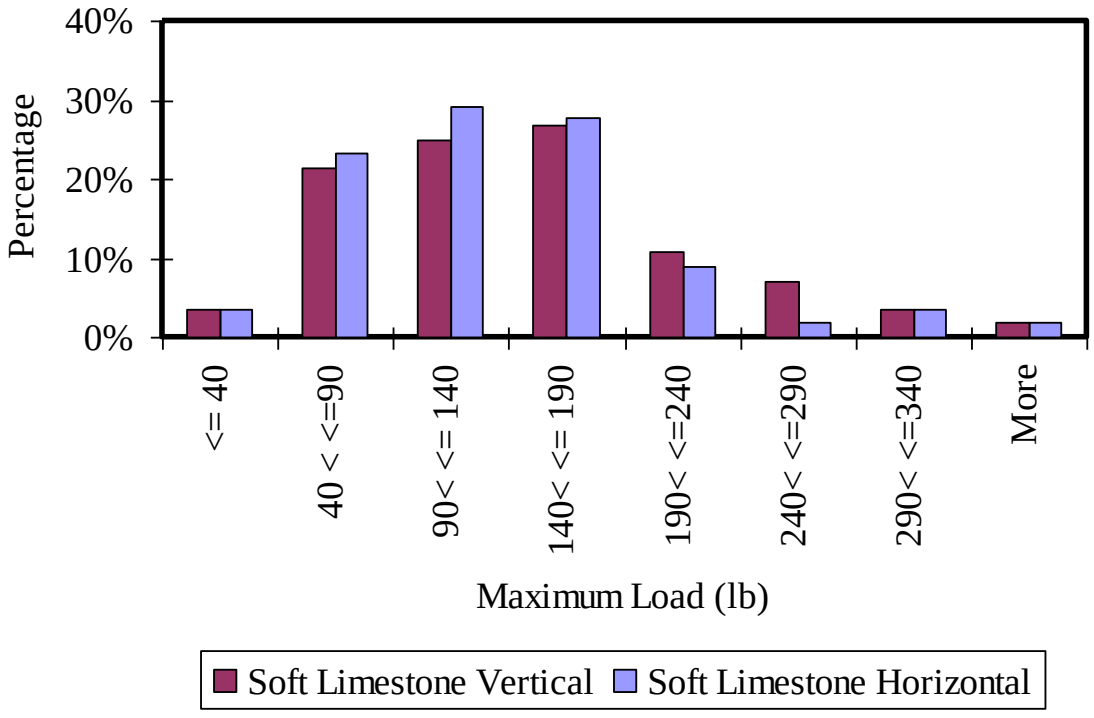

Figure 5.12. Single Aggregate Crushing Results Distribution for the Soft Limestone.

Table 5.3. Chi-square Statistic Test Results.

Aggregate Type	χ^2	$\chi^2_{\alpha,k-p-1}$	Chi-square Test	
			$\chi^2 > \chi^2_{\alpha,k-p-1}$	Normal Distribution Hypothesis
Hard limestone	**0.98**	**2.00**	**No**	**Can't be rejected**
Soft limestone	**1.80**	**4.57**	**No**	**Can't be rejected**
Granite	**2.14**	**12.38**	**No**	**Can't be rejected**
Gravel	**5.00**	**25.06**	**No**	**Can't be rejected**
Sandstone	**1.69**	**5.65**	**No**	**Can't be rejected**

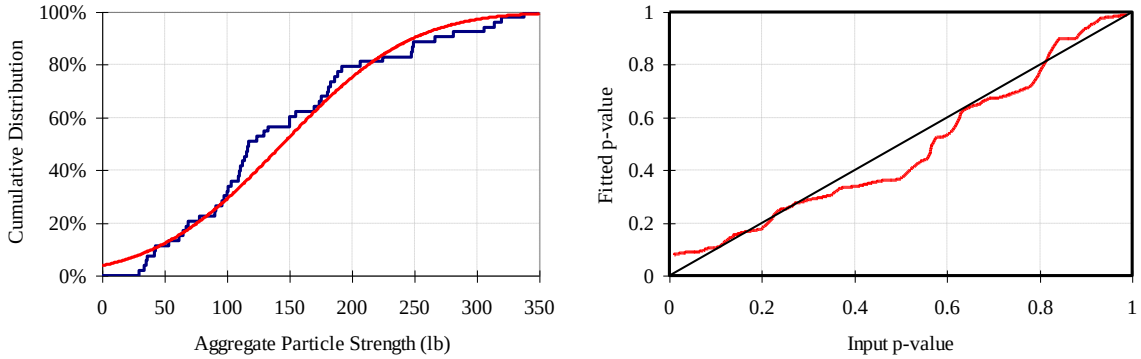

(a) Granite

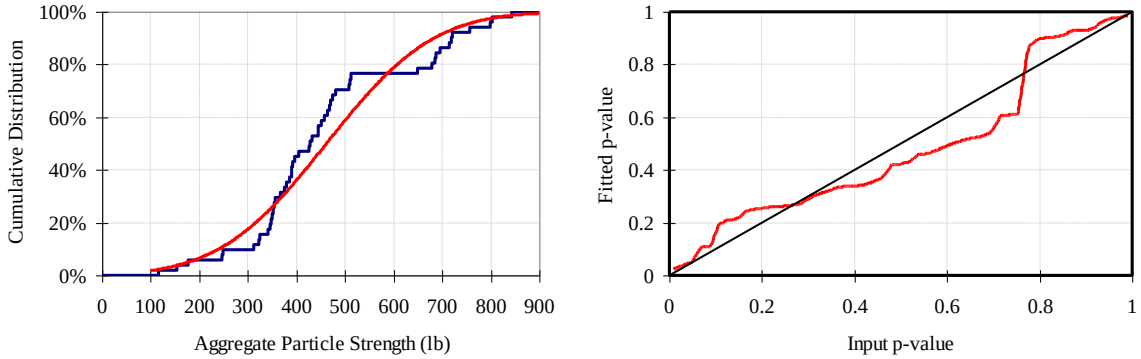

(b) Gravel

Figure 5.13. Normal Distribution Fit to Single Aggregate Crushing Results (Normal Plots & p-value Plots).

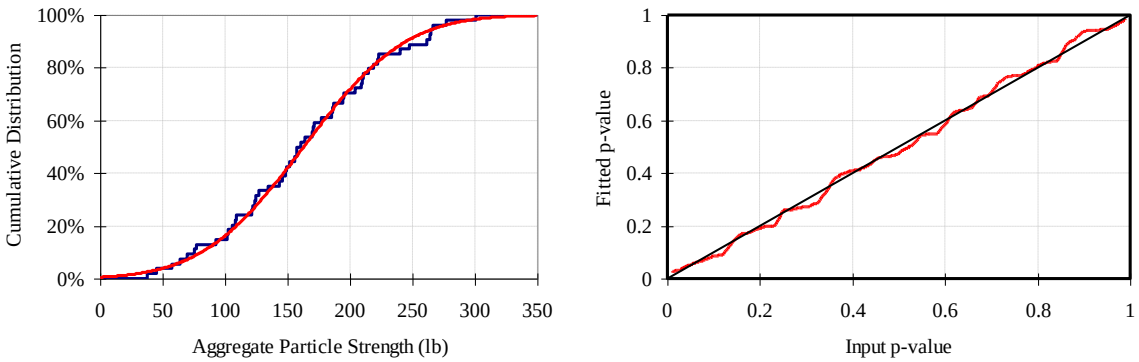

(c) Hard Limestone

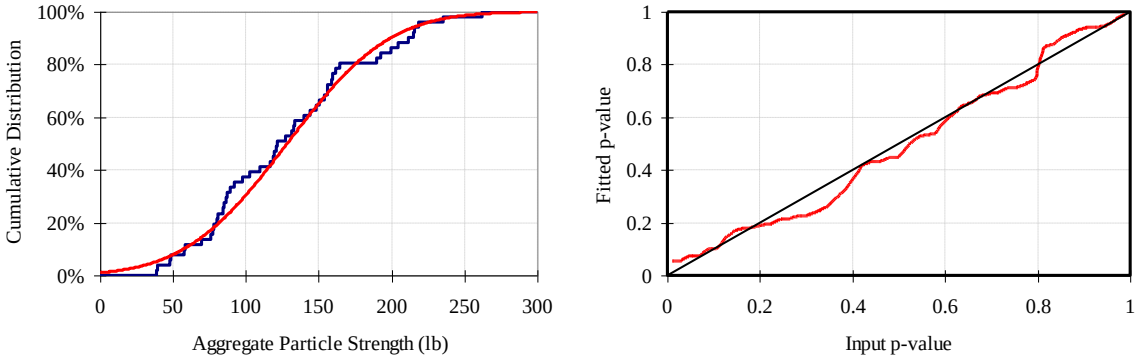

(d) Sandstone

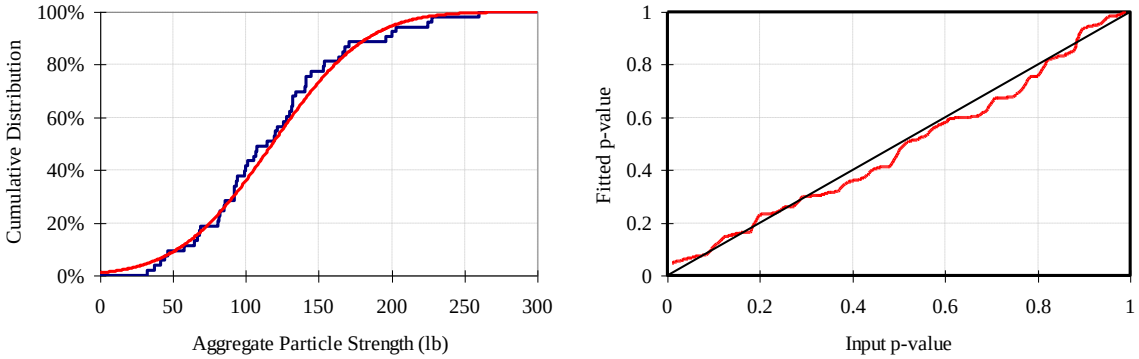

(e) Soft Limestone

Figure 5.13. continued

Table 5.4. Experimental and Normal Fitting Results.

Aggregate Type	Experimental Results		Normal Fitting Results	
	Mean (μ)	Standard deviation (σ)	Mean (μ)	Standard deviation (σ)
Hard limestone	171	76	163	64
Soft limestone	130	70	118	51
Granite	155	91	145	81
Gravel	413	130	393	93
Sandstone	145	68	143	55

AGGREGATE FRACTURE IN ASPHALT MIXTURES

The next step was to use the DEM to predict the fracture of aggregate within the asphalt mixtures. As discussed in the previous section, the normal distribution was selected to represent the aggregate particle strength variability. The DEM was already calibrated for the different aggregates and aggregate gradation cases considered by using an average value for aggregate bond strength as was shown in Chapter III. However, the normal distribution still needed to be incorporated to represent the aggregate strength variability.

A built-in function in PFC2D was used to generate bond strength values that follow a normal distribution with a mean equal to the single "deterministic" bond strength (Chapter III) and a standard deviation based on the aggregate type (Table 5.4). This allowed representing the aggregate strength with a probability distribution with the "deterministic" bond strength calibrated in Chapter III used apposed to the experimental aggregate strength values, since they represented the micro properties of the aggregates, which is the input required for the DEM. Figure 5.14 shows a comparison between the

DEM bond strength and the experimental strength with a strong correlation (R^2 = 0.97). Table 5.5 summarizes the parameters (mean and standard deviation) used in each of the eight different aggregate – mixture type combination cases as well as the maximum and minimum bond strength values which are used in the mathematical derivations of fracture probability as shown in the following section.

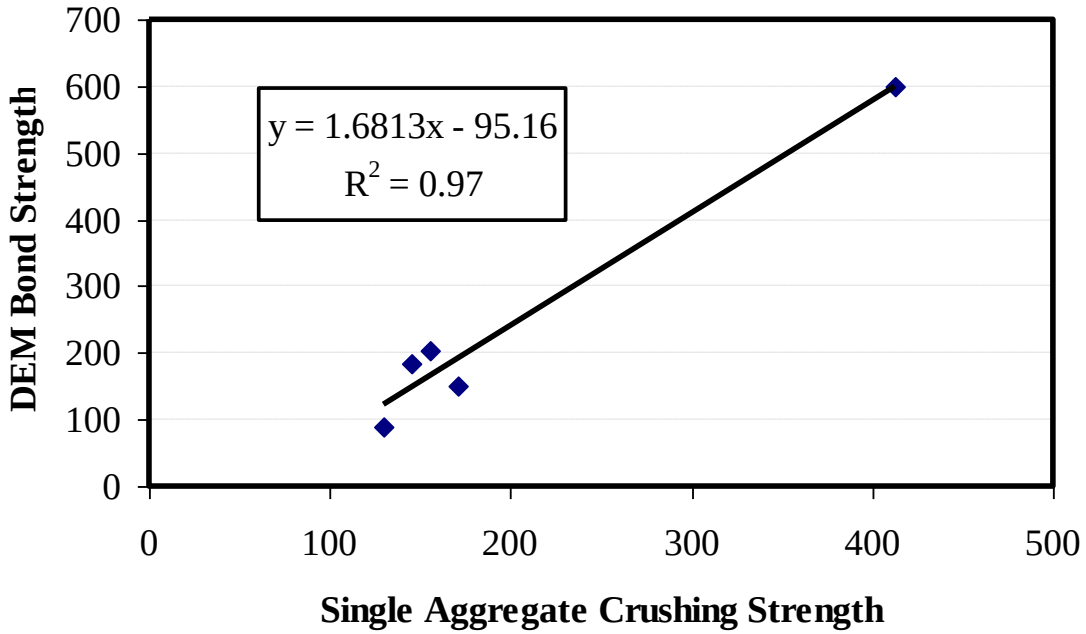

Figure 5.14. DEM Aggregate Bond Strength Compared to Experimental Aggregate Strength.

Table 5.5. Aggregate Variability Input for DEM.

Aggregate Type	Mixture Type	Mean (μ)	Standard deviation (σ)	Minimum bond strength	Maximum bond strength
Hard limestone	**PFC**	149	65	25	327
Hard limestone	**CMHB**	154	65	6	378
Hard limestone	**Superpave**	149	60	0	349
Soft limestone	**Superpave**	90	50	0	269
Granite	**Superpave**	204	65	120	390
Gravel	**Superpave**	600	93	347	872
Sandstone	**Superpave**	185	53	60	361
Sandstone	**Type-D**	185	54	60	380

The distribution of the probability of aggregate breakage in asphalt mixtures can be obtained by deriving the probability of the contact forces exceeding the contact bond strength at the different contacts. The normal PDF (h(ϕ)), which represents the aggregate strength distribution, can be represented as follow:

$$h(\phi)=\frac{1}{\sigma\sqrt{2\pi}}e^{-\frac{(\phi-\mu)^2}{2\sigma^2}} \quad (5.3)$$

The internal force distribution was quantified using equation 5.1, which is re-stated as:

$$g(f)=(f+a)^b e^{-cf-d} \quad (5.1)$$

where g(f) is the probability density function for the maximum internal force distribution based on the data obtained from the DEM,. The probability of breakage within a given

particle with strength φ can be written as the integral shown in equation 5.4 (Marketos and Bolton, 2007):

$$p = \int_{\varphi}^{+\infty} g(f)df \qquad (5.4)$$

where p is the probability of breakage, φ and f are the particle strength and maximum contact force, respectively, both normalized by the mean of the maximum forces of all particles.

However, this expression is the probability of aggregate breakage when all the aggregate particles have the same strength value, "Φ" (or φ if normalized by the mean of maximum contact forces). However, the analysis conducted in this chapter includes the use of a distribution for aggregate strength and not an average value. Therefore, the analysis should be extended to account for aggregate strength distribution. In this case, the probability for breakage to occur at a certain contact is the sum of the products of the probabilities of two independent events: the probability that the bond strength at the contact has a value Φ, and that the internal force at that specific contact is larger than Φ. The summation should cover all the possible values of the bond strength. For continuous distributions for these two independent events, the summation becomes an integral in the limit, and this integral is shown in equation 5.5 (Marketos and Bolton, 2007):

$$P = \int_{Strength_{\min}}^{Strength_{\max}} p(Strength = \phi)\, p(Force > \phi) d\phi \qquad (5.5)$$

The probability of the force exceeding Φ is based on the function g (equation 5.1); however, g is a function of the normalized force (f), and so a change of variable is

required to match Φ, which is a force. This requires replacing (f) by ($F / \overline{F}$), where F is the contact force and $\overline{F}$ is the mean contact force, which leads to equation 5.6:

$$P = \int_{\phi_{\min}}^{\phi_{\max}} h(\phi) \left(\int_{\phi}^{+\infty} g(F/\overline{F}) dF/\overline{F} \right) d\phi \qquad (5.6)$$

Replacing "g" and "h" by their distribution functions from equations 5.1 and 5.3 will result in equations 5.7 and 5.8 respectively:

$$P = \int_{\phi_{\min}}^{\phi_{\max}} h(\phi) \left(\int_{\phi}^{+\infty} (F/\overline{F} + a)^b e^{-c(F/\overline{F})-d} dF/\overline{F} \right) d\phi \qquad (5.7)$$

$$P = \int_{\phi_{\min}}^{\phi_{\max}} \frac{1}{\sigma\sqrt{2\pi}} e^{-\frac{(\phi-\mu)^2}{2\sigma^2}} \left(\int_{\phi}^{+\infty} (F/\overline{F} + a)^b e^{-c(F/\overline{F})-d} dF/\overline{F} \right) d\phi \qquad (5.8)$$

The integral equation 5.8 gives the probability of aggregate breakage within asphalt mixture. This integral can be easily implemented numerically. The probability will be a function of the mean internal force, and the mean internal force is a direct measure of the stress applied to the mixture. In this equation a, b, c, and d are all constants already evaluated for the different mixtures and aggregates (Table 5.1), while μ, σ, maximum strength, and minimum strength are all tabulated in Table 5.5 for the eight different mixtures. Figure 5.14 shows the plot of this equation for the different cases. In each case the DEM simulation was also plotted. For the DEM case, the probability was calculated by dividing the cumulative number of broken bonds by the

total number of existing bonds initially. For this purpose, a subroutine was written in order to track the number of broken bonds within the discrete element model. This routine goes through all the different aggregate contacts within the asphalt mixture, and adds a count of 1 to a "sum" value for every bond strength that exists. As such, this number will represent initially the total bonds within the aggregate. This subroutine is activated for every cycle in the DEM, and the "sum" value represents the number of bonded contacts at that cycle. These values can only decrease because with the loading of the mixture, bonds can only break. And so the difference between the "sum" values for two consecutive cycles is the number of broken bonds.

As shown in the different plots of Figure 5.15, the crushing calculations and the DEM simulation results compare very well for all the different cases initially. However, at higher mean maximum contact force (i.e. higher stress) the two curves diverge for some cases. This can be attributed to the fact that at such high forces the crushing events are not independent anymore which is the underlying assumption in deriving the probability of fracture in Equation 5.8. The fact that a bond is already broken within the mixture will affect where and/or when the next breakage will occur.

Figures 5.8 a and b indicate very similar behavior of the Superpave and the Type-D mixtures for the same aggregate (sandstone) for both the simulation and calculation. The same conclusion was drawn in chapter IV that dealt with blending of different aggregate sources, in which the analysis showed that the two mixtures exhibit very similar behavior. It is also noted that the two mixtures had similar g(f) function coefficients as reported in Table 5.1. The plots in Figure 5.15 also reveal that the eight

different cases had different mean force limits after which breakage started to occur. For the same mixture type, the value of this parameter was significantly affected by the aggregate type. Figure 5.16 shows the Superpave mixture results for the different aggregates. However, for the same aggregate type the change in this parameter from one mixture to another was not as significant as when aggregate type changed for the same mixture. This can be seen in Figures 5.17 and 5.18 showing the comparisons for the hard limestone and sandstone aggregates, respectively.

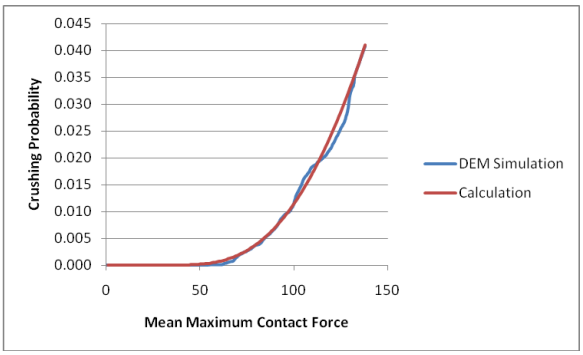

(a) Sandstone Type-D

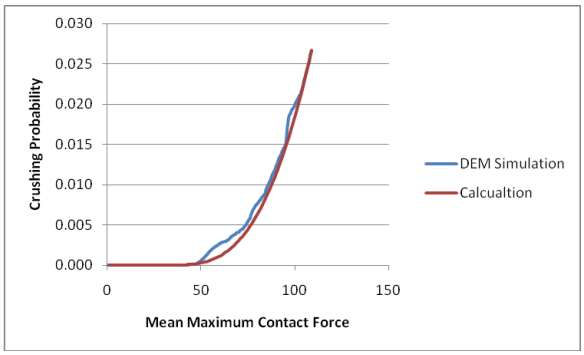

(b) Sandstone Superpave

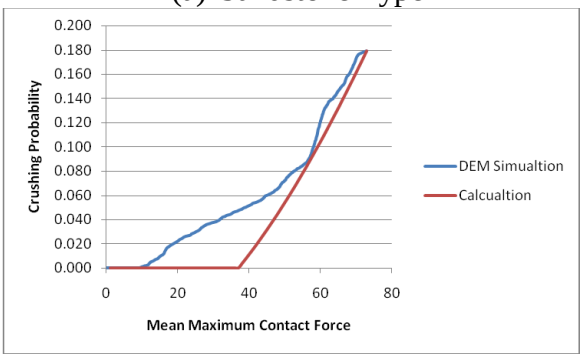

(c) Soft Limestone Superpave

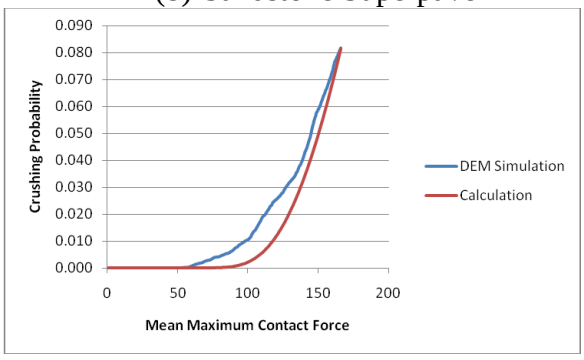

(d) Granite Superpave

Figure 5.15. Probability of Crushing Aggregate within Asphalt Mixtures.

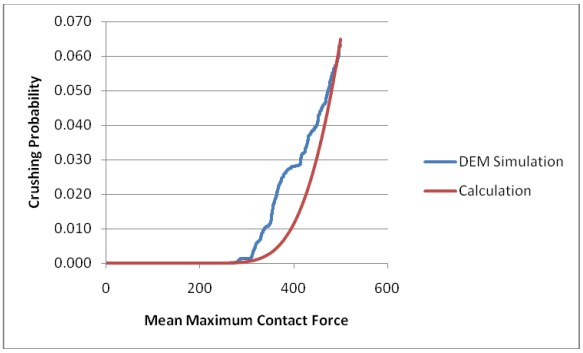

(e) Gravel Superpave

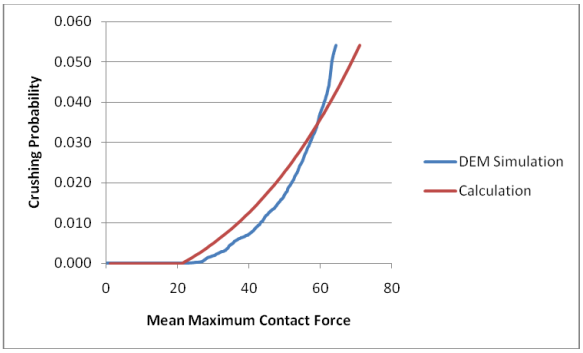

(f) Hard Limestone Superpave

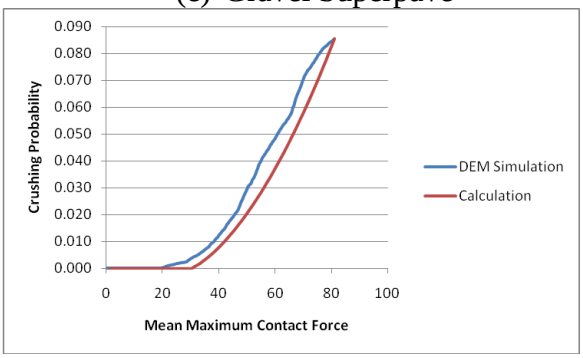

(g) Hard Limestone PFC

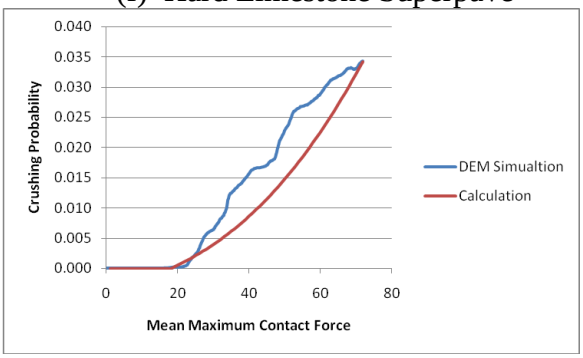

(h) Hard Limestone CMHB

Figure 5.15. continued.

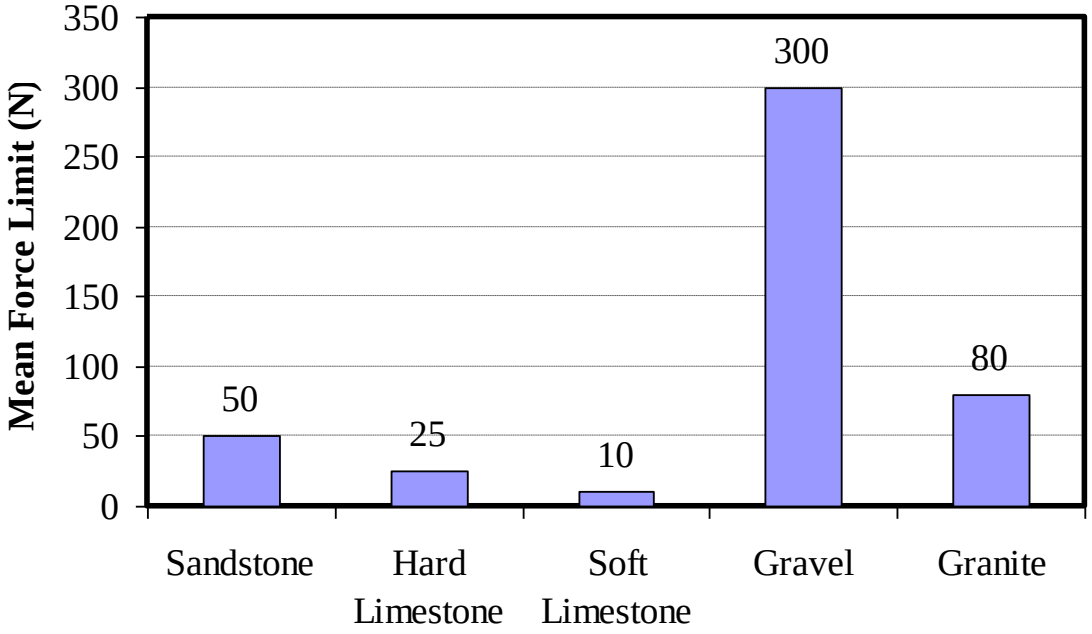

Figure 5.16. Breakage Force Limits for Superpave Mixture.

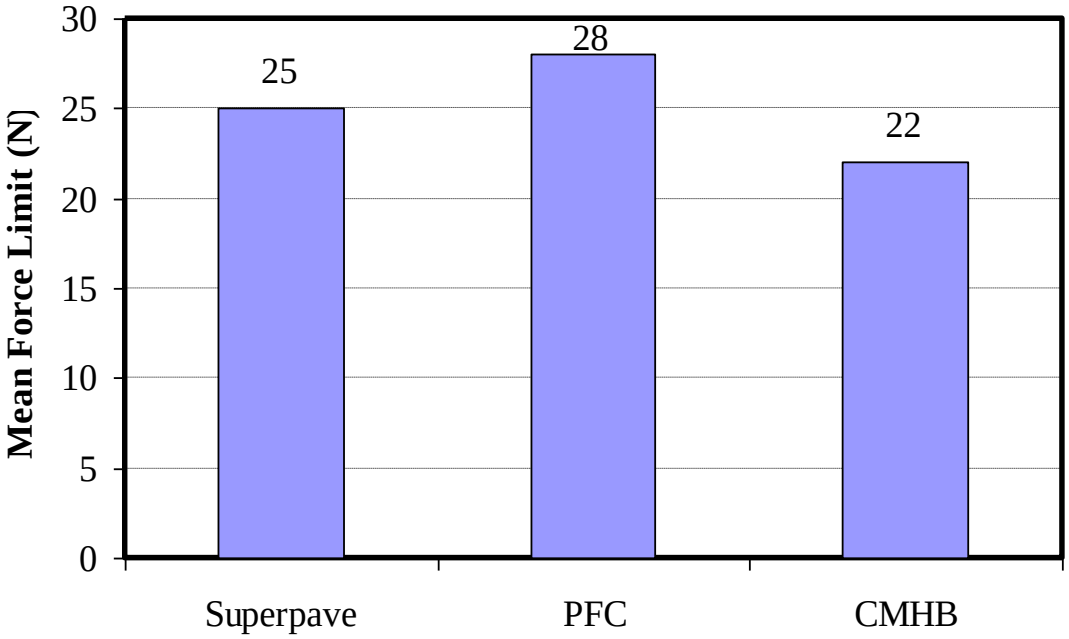

Figure 5.17. Breakage Force Limits for Hard Limestone Aggregate.

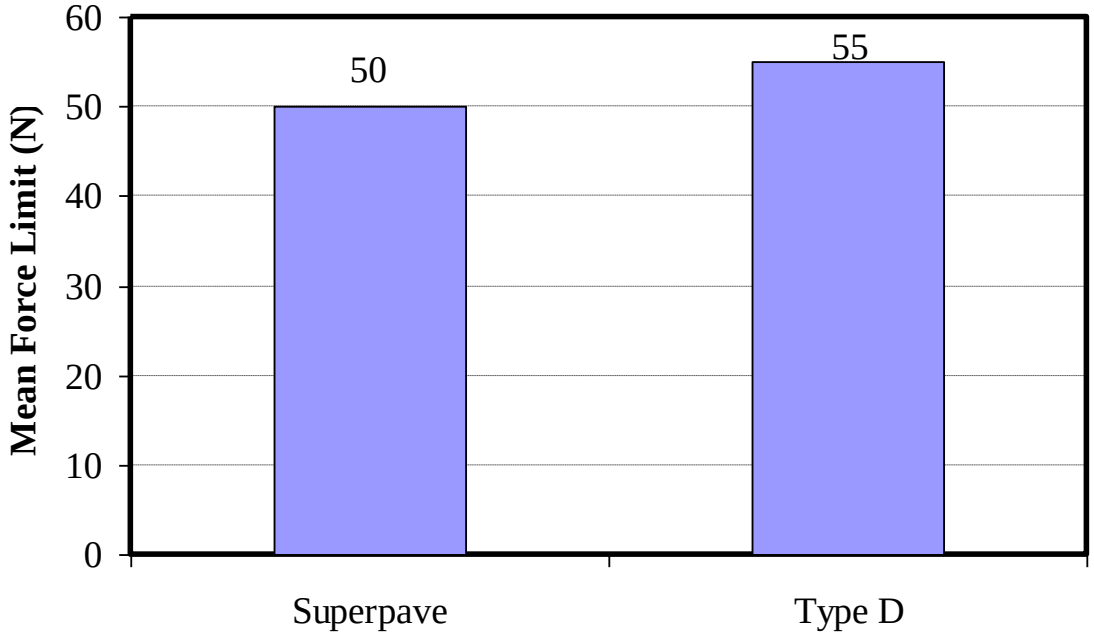

Figure 5.18. Breakage Force Limits for Sandstone Aggregate.

SUMMARY

This chapter presented the development of an approach to analyze aggregate breakage within asphalt mixtures. This approach requires the following inputs: (1) the internal force distribution within the aggregate structure in the asphalt mixture at three different loading levels, (as a function of gradation and binder properties) obtained from the DEM, and (2) the distribution of aggregate strength (as a function of aggregate type) evaluated using a single aggregate crushing test.

Statistical analysis was conducted to determine the PDF that fits the internal force distribution and the PDF that fits the aggregate strength distribution. The output of this approach is a function that provides the probability of aggregate breakage in a mixture. The mathematical approach for deriving the probability of fracture is based on

the probability distribution functions of two different events: contact bond strength and the internal force distribution at the contact points. The PDF of aggregate strength was used as an input to the discrete element model. The DEM was then used to analyze particle fracture within the mixture. The results of aggregate fracture from DEM compared well with the results of the derived PDF of aggregate breakage.

The developed approach is very flexible and can incorporate any types of distributions for the two events. And thus it can be used for different types of mixtures and/or aggregates.

CHAPTER VI

PHYSICAL QUANTIFICATION OF CRACK PATTERNS IN ASPHALT MIXTURES USING DEM

INTRODUCTION

Cracking in asphalt mixtures is a result of the localized internal forces within its structure. Cracking can occur in different patterns: cohesive failure of the bond within aggregate particles, cohesive failure of the bond within the matrix, or adhesive failure at the interface between aggregate and matrix. Different studies attempted to study cracking patterns by treating an asphalt mixture as a binder with rigid inclusions (aggregate filler) (Rodriguez et al 1996, Smith and Hesp 2000, and Hesp et al 2001). These studies explain the relationship between fracture energy and cracking pattern based on crack pinning theory which was developed by Lange (1970) and Evans (1972).

Crack pinning is defined as the slow down of crack propagation as result of its interaction with an inclusion in a multiphase composite material, which causes an increase in the fracture energy compared with the material without the inclusion. Figure 6.1 (Smith and Hesp 2000) shows an illustration of the crack pinning process. As the crack front propagation is intercepted by the inclusions, it gets “pinned” and cannot pass through them since the stress level is insufficient (Hesp et al. 2001). Thus, it bows out between the inclusions until it breaks away. The pinning followed by the bowing causes an increase in the overall length of the crack front due to the change in the crack shape.

Such an increase requires higher energy, and thus the increase in fracture energy occurs (Smith and Hesp 2000). However, the applicability of this theory to asphalt mixtures has to be examined because it was founded based on inclusions at the micro-level and it does not account for the effect of coarse aggregates.

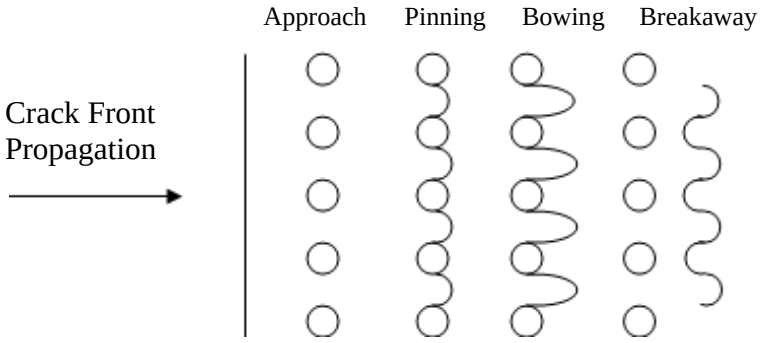

Figure 6.1. Illustration of Crack Pinning (after Smith and Hesp 2000).

Based on input from Lytton at Texas A&M University, Jacobs (1995) used a three phase crack propagation theory to explain crack growth in asphalt mixtures (Lytton 2007). This approach distinguishes between three different types of cracking (Figure 6.2): (1) cracking within the asphalt matrix (binder + fine aggregates) which is a cohesive type of cracking, (2) cracking at the interface between the aggregate particles and the matrix (pealing) which is an adhesive type of cracking, and (3) crack retarding in the case of crack direction change (when a crack tip hits an aggregate particle). The work of Jacobs (1995) differs from crack pinning theory as it does not attribute the increase in fracture energy to plastic energy dissipation at the crack tip due to crack pinning.

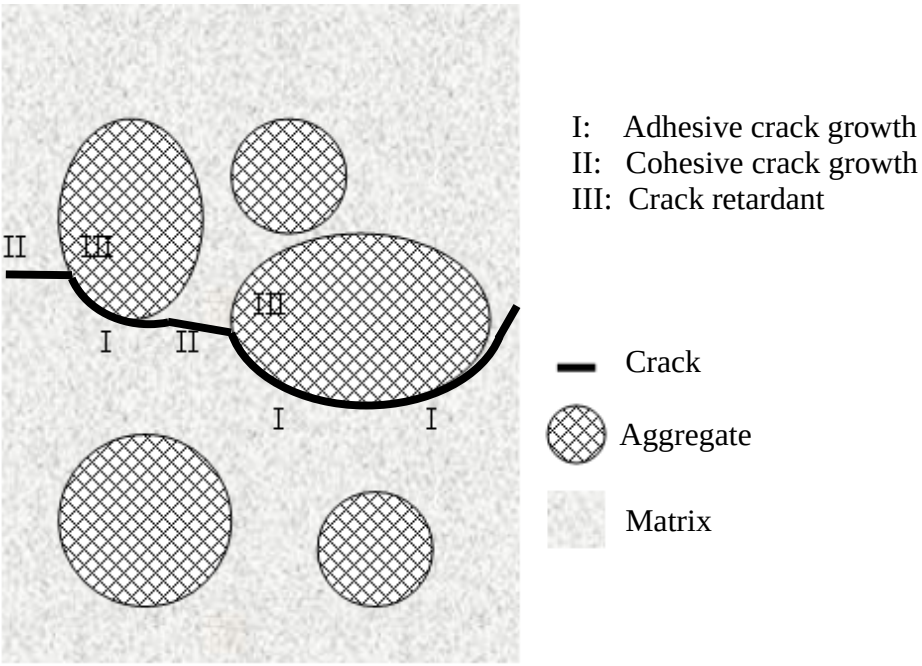

Figure 6.2. Crack Patterns in Asphalt Mixtures (after Jacobs 1995).

OBJECTIVES AND SCOPE

This chapter introduces a physical quantification of crack patterns within asphalt mixtures using the DEM. The discrete element model developed in previous chapters is used with some specific modifications to quantify these crack patterns. The crack patterns are then related to the mixture internal structure and the total energy up to the failure point of the mixture.

As previously discussed in Chapter III, the model, which couples discrete element modeling with image analysis techniques, was calibrated for mixtures with five different aggregates (granite, hard limestone, soft limestone, gravel, and sandstone). Each aggregate was used in mixtures with three or four different gradations (Superpave,

PFC, CMHB, and Type-D) for a total of 17 different mixture cases. Table 3.1 provides a list of mixtures and aggregates.

The method developed in Chapter III distinguishes between discrete elements that belong to the matrix and aggregate phases. In this model, cracking in an asphalt mixture occurs whenever a bond is lost between two discrete elements. A bond between two elements will only break if the internal contact force at that contact exceeds the contact bond strength. Three types of contacts can be defined based on the type of discrete elements involved in the contact: aggregate to aggregate contact, matrix to matrix contact, and matrix to aggregate contact. Figure 6.3 shows an illustration of the three contact types. Figure 6.4 shows the crack patterns that can be developed in a discrete element model of an asphalt mixture. A cohesive crack occurs either within the matrix or the aggregate phases, while an adhesive crack occurs at the interface between these two phases.

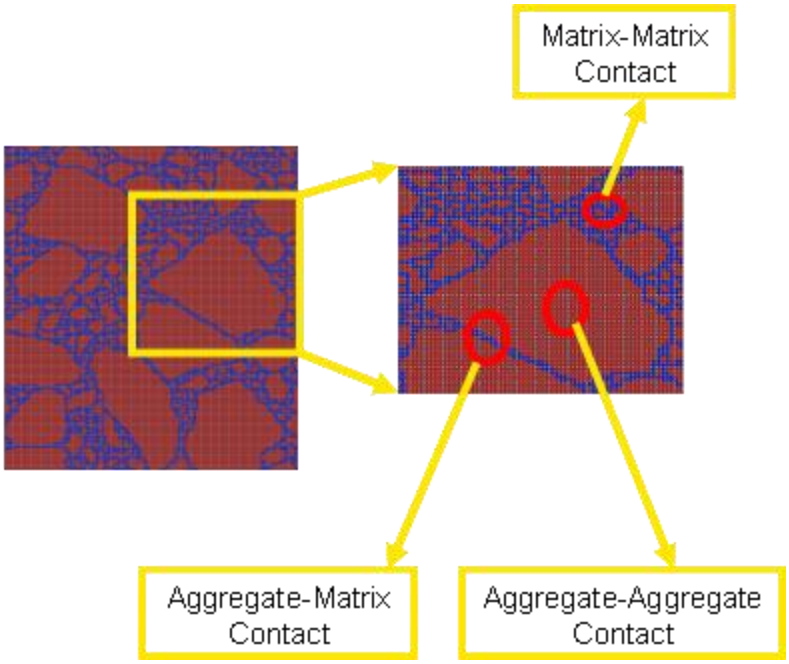

Figure 6.3. Types of Contact in DEM.

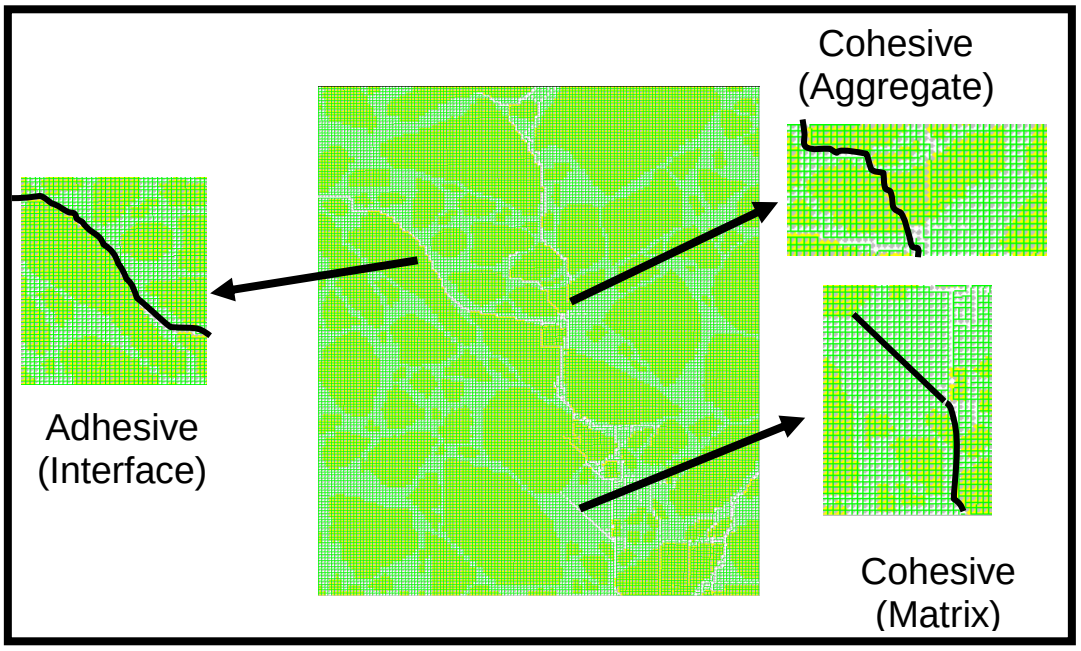

Figure 6.4. Cracking Patterns in DEM.

DEM ANALYSIS OF CRACK PATTERNS

In order to quantify the three types of cracking within the asphalt mixture, a method was developed to analyze the discrete element model results and determine the type of cracking patterns. A brief description of this method is given in this section.

The method checks the types of discrete elements that are in contact; all the discrete elements belong to either the aggregate phase group, or the matrix phase group. And thus it distinguishes between the three contact types discussed previously. After classifying the contact as either an aggregate-aggregate contact, matrix-matrix contact, or an interface contact; the method checks if the contact bond is still active or broken, using a built-in function in the PFC2D. Thus, when this method is applied for an asphalt mixture before starting the simulation (i.e. no loading or cracking) the routine will count the total number of bonded contacts for the three different types. This method is used to count the number of bonded contacts for each of the contact types at different loading levels. The number of broken bonds of each type can be calculated by subtracting current bonded contacts from the original number of bonded contacts. This calculation can be done separately for each of the three contact types in order to separate the three cracking patterns.

The cracking analysis method can be incorporated within the DEM and used at every time step within the loading simulation in order to produce continuous tracking of the cracking patterns. However, this will be costly time wise and will extend the simulation time significantly. Therefore, it was decided to use this routine only at three points of loading in addition to the starting point. The three points were selected to

represent the three loading stages discussed in chapter III. These loading stages were: at the peak force or just before failure (Case I), at an intermediate force equal to 50% of the peak force (Case II), and at a force of 2 kN (450 lb) (Case III). The three cases are illustrated in Figure 6.5.

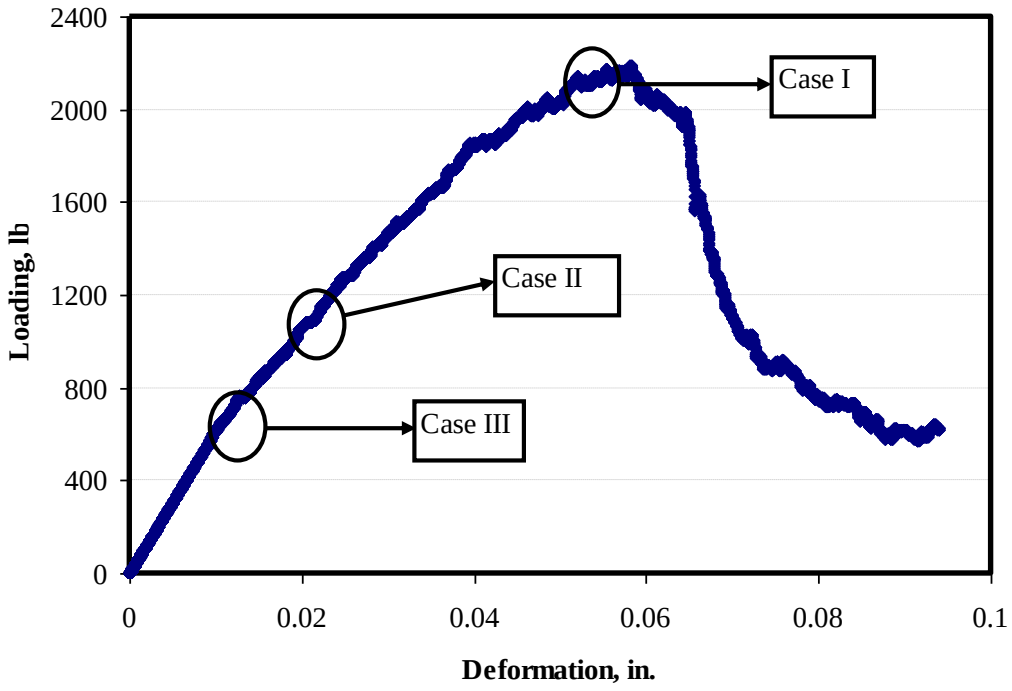

Figure 6.5. An Example of Loading Stages Selected for Analysis.

RESULTS AND ANALYSIS

Tracking of the different cracking patterns using the routine described in the previous section was completed for all 17 mixtures calibrated in this dissertation and for the three loading cases shown in Figure 6.5. As discussed in Chapter III, Cases I and II occurred

at different strain and stress levels depending on the mixture type. Case III was selected at the same stress for all mixtures. Figures 6.6 through 6.10 shows the total number of bonds lost at the Cases II and III loading stages as a percent of the total bonds lost for the Case I loading stage for the hard limestone, soft limestone, granite, sandstone, and gravel, respectively. The load in Case III and Case II was not high enough to produce any cracking for some of the mixtures. Therefore, it was decided to focus the analysis of cracking patterns only on Case I loading. Tensile strength at failure (Table 3.3), is presented in Table 6.1 to facilitate comparing cracking patterns to mixture strength.

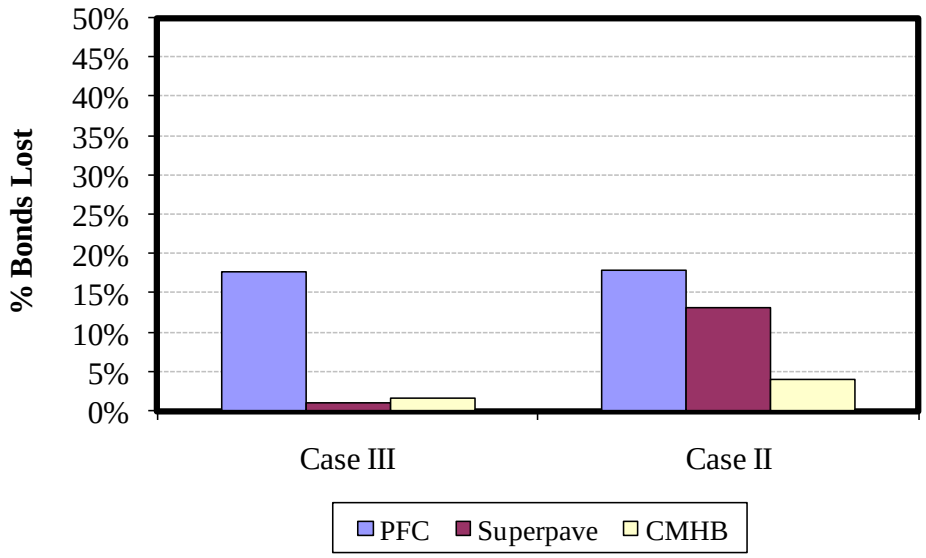

Figure 6.6. Total Bonds Lost as Percentage of Case I Total Bonds Lost for the Hard Limestone.

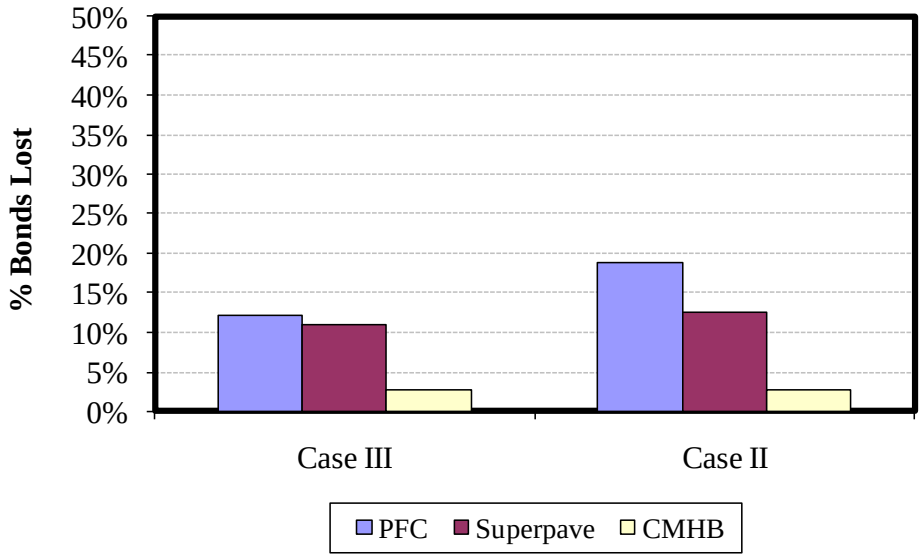

Figure 6.7. Total Bonds Lost as Percentage of Case I Total Bonds Lost for the Soft Limestone.

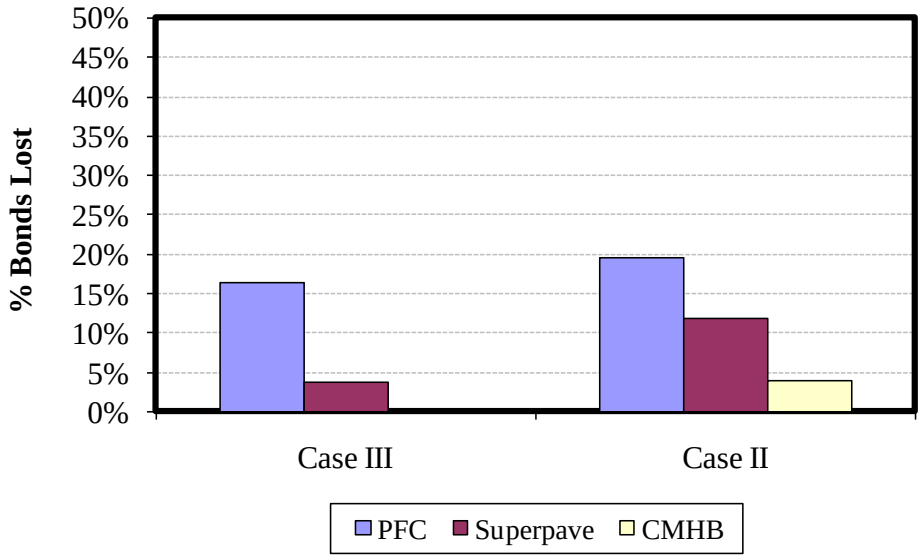

Figure 6.8. Total Bonds Lost as Percentage of Case I Total Bonds Lost for the Granite.

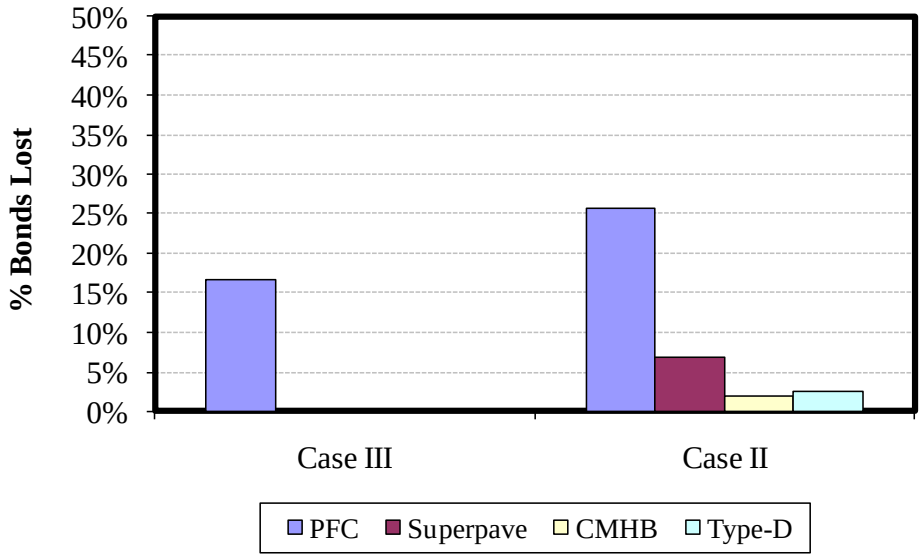

Figure 6.9. Total Bonds Lost as Percentage of Case I Total Bonds Lost for the Sandstone.

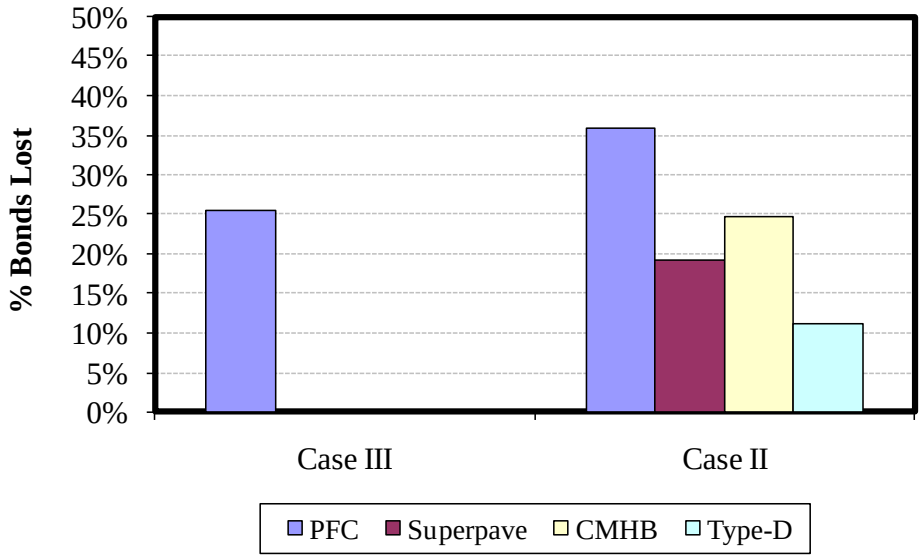

Figure 6.10. Total Bonds Lost as Percentage of Case I Total Bonds Lost for the Gravel.

Table 6.1. Experimental Results of the Asphalt Mixtures. (Table 3.3)

Material	Mixture Type	Tensile strength at failure, kN/m^2
Hard Limestone	CMHB-C	731
	Superpave-C	827
	PFC	455
Granite	CMHB-C	572
	Superpave-C	800
	PFC	421
Soft Limestone	CMHB-C	648
	Superpave-C	862
	PFC	345
Sandstone	CMHB-C	1427
	Superpave-C	1558
	PFC	538
	Type-D	1427
Gravel	CMHB-C	1407
	Superpave-C	1262
	PFC	400
	Type-D	1400

Figures 6.11 through 6.15 summarize the percentages of broken bonds for the hard limestone, soft limestone, granite, sandstone, and gravel aggregates, respectively. These relate each crack type to the total of the three cracking types. For instance, in Figure 6.11 the Superpave-hard limestone mixture has 39% of cracking occurring at the interface between the aggregate and the matrix, 57% of cracking within the matrix phase, and 3% of cracking within the aggregate phase.

The hard limestone results summarized in Figure 6.11 show that the PFC mixture experienced the highest percentage of cracking within the matrix phase (69%) and the lowest percentage at the interface (28%). The Superpave mixture exhibited the opposite of that, where 39% was interface cracking (highest) and 57% was matrix cracking

(lowest). The CMHB mixture came in between these two cases, but closer to the Superpave case. The cracking within the aggregate phase was almost the same for the three mixtures. According to Table 6.1, the hard limestone had the highest strength when used in a Superpave mixture, and the lowest strength when used in a PFC mixture.

Figure 6.12 summarizes the soft limestone results. Again the PFC mixture had the highest matrix cracking and the lowest interface cracking. As in the hard limestone case, the CMHB and the Superpave mixtures had very close percentages of interface cracking; however, the CMHB mixture had 10% of its cracking in the aggregate phase. The PFC mixture had the lowest strength (Table 6.1) while the Superpave mixture had the highest strength for this aggregate type.

The granite aggregate results are shown in Figure 6.13. The CMHB mixture was the only mixture that had cracking within the aggregate phase with the highest interface cracking percentage (41%). As in the previous two cases, the PFC mixture had the highest matrix cracking percentage (74%) and the lowest mixture strength. The Superpave mixture had the lowest matrix cracking, and the second interface cracking.

In addition to PFC, CMHB, and Superpave mixtures; the sandstone and the gravel aggregates (Figures 6.14 and 6.15) were also tested in Type-D mixtures. For the sandstone case the PFC mixture showed the same trend as in the previous cases with the highest percentage of cracking within the matrix phase and the lowest strength. The other three mixtures had similar mixture strength values and the three were comparable. Finally, for the gravel aggregate none of the mixtures had any cracking within the aggregate phase. The Superpave mixture had the second highest matrix cracking

percentage after the PFC mixture and the second lowest mixture strength. The Type-D and the CMHB mixtures had the lowest matrix cracking and the highest mixture strengths.

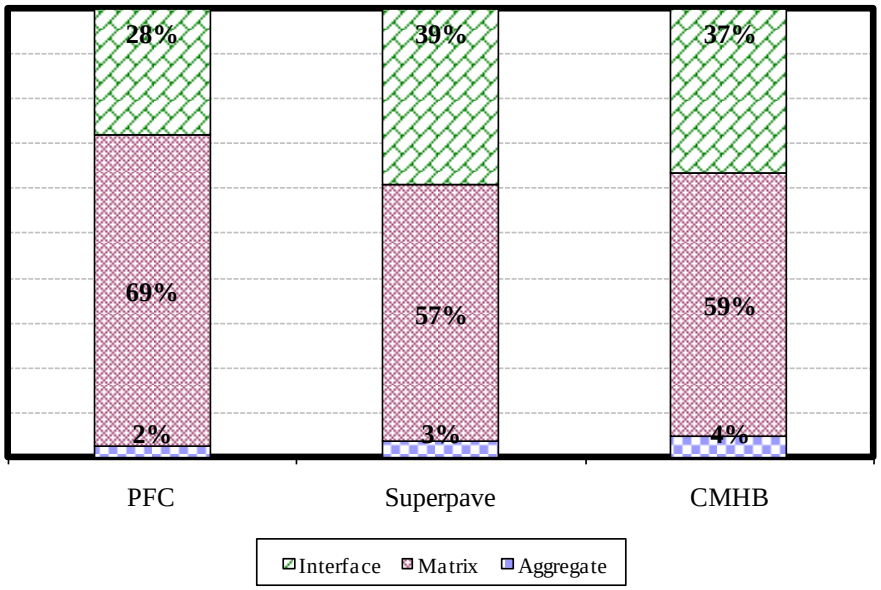

Figure 6.11. Quantifying Crack Patterns for the Hard Limestone.

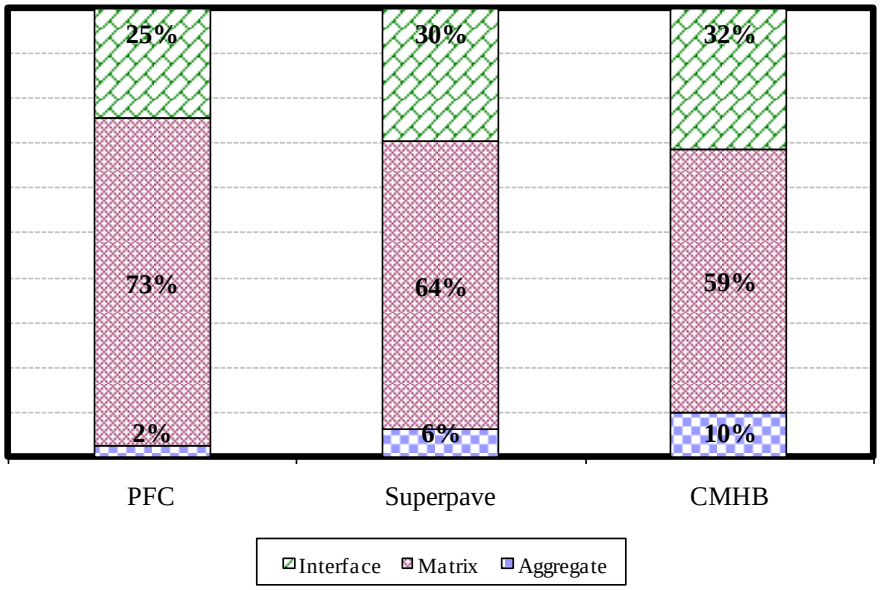

Figure 6.12. Quantifying Crack Patterns for the Soft Limestone.

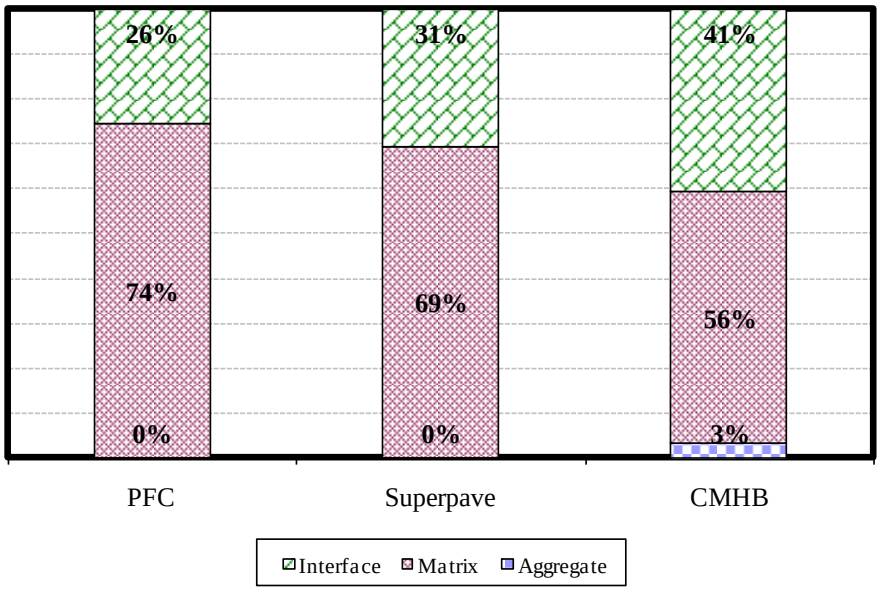

Figure 6.13. Quantifying Crack Patterns for the Granite.

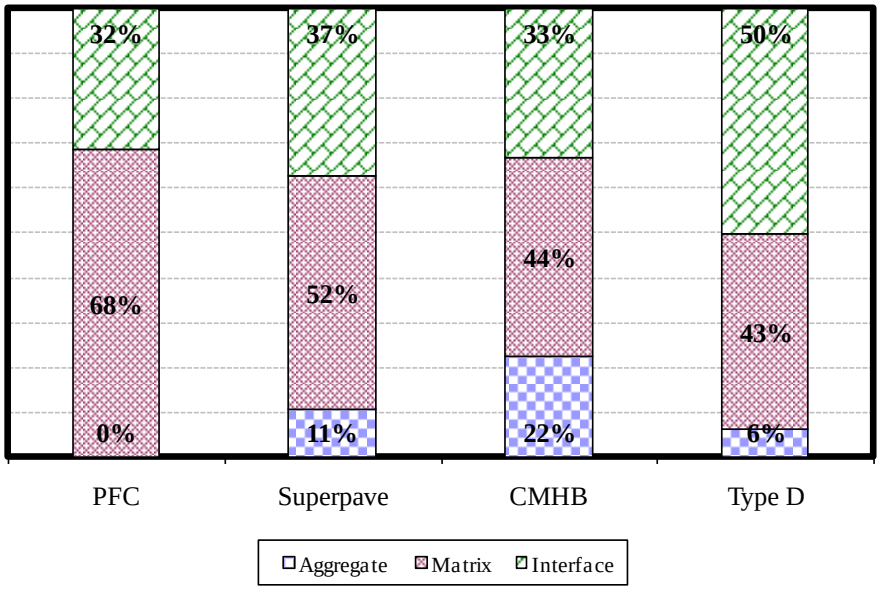

Figure 6.14. Quantifying Crack Patterns for the Sandstone.

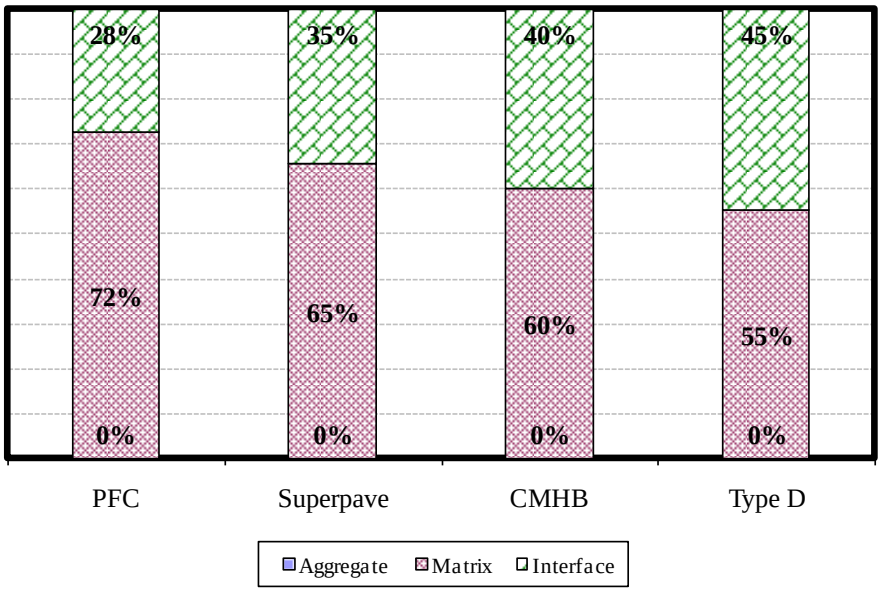

Figure 6.15. Quantifying Crack Patterns for the Gravel.

As shown in Figures 6.11 through 6.15, cracking within aggregate particles occurs; however, this cracking pattern was never the dominant pattern when compared to the other two patterns. The gravel aggregate was the only one that did not encounter any cracking, while both the soft limestone and hard limestone experienced cracking for all the different types of mixtures, with the soft limestone having the highest percentages of aggregate cracking.

Table 6.2 summarizes the ranking of all the different cases discussed in this chapter based on the percent matrix cracking, percent interface cracking, and mixture strength. For all the different aggregates, the mixture with the highest percent of matrix cracking had the lowest mixture strength. Another trend seen for most of the cases is that for the different aggregates, the mixture with highest percent of interface cracking had the highest mixture strength. This can be explained by the crack retardation proposed by Jacobs (1995). Once a mixture loses internal bonds between its contacts, assuming this starts in the matrix phase, cracks start to propagate throughout the mixture, mainly through the matrix phase; however, as the crack front faces an aggregate particle, it will need to either propagate through the aggregate phase, diverge from the aggregate phase and continue through the matrix phase, or propagate through the interface between the matrix and the aggregate. As the analysis of Figures 6.11 through 6.15 and Table 6.2 reveal, the higher the interface cracking is, the higher the strength of the mixture becomes. This indicates that the cracking required higher energy to propagate as a result of being intercepted by an aggregate particle and/or changing from the matrix phase to

the interface. This can be explained by the fact that the bond strength of the discrete element model at the interface is higher than the bond strength within the matrix phase.

Table 6.2. Mixtures Ranking Based on Cracking and Strength.

Material	Mixture Type	Mixture Rank Criteria		
		% Matrix Cracking	% Interface Cracking	Mixture Strength
Hard Limestone	CMHB-C	2	2	2
	Superpave-C	3	1	1
	PFC	1	3	3
Granite	CMHB-C	3	1	2
	Superpave-C	2	2	1
	PFC	1	3	3
Soft Limestone	CMHB-C	2	1	2
	Superpave-C	3	2	1
	PFC	1	3	3
Sandstone	CMHB-C	3	3	2
	Superpave-C	2	2	1
	PFC	1	4	4
	Type-D	4	1	2
Gravel	CMHB-C	3	2	1
	Superpave-C	2	3	3
	PFC	1	4	4
	Type-D	4	1	1

The last analysis was to investigate the relationship between the cracking patterns and the total energy, with the total energy calculated as the area under the stress-strain curve taken up to the point of failure, i.e. to the loading point of Case I. Table 6.3 summarize the total energy values for the 17 different mixtures, along with the ranking of he different mixtures for each aggregate type based on the total energy as well as the percent of interface cracking. Table 6.3 reveals that the total energy ranking was exactly

the same as that based on the percent interface cracking. This result indicates that the percent interface cracking is better related to the total energy of the mixture rather than the strength.

Table 6.3. Mixtures Total Energy and Its Ranking.

Material	Mixture Type	Total Energy (kJ/m^3)	Total Energy Rank	% Interface Cracking
Hard Limestone	CMHB-C	0.455	2	2
	Superpave-C	0.702	1	1
	PFC	0.279	3	3
Granite	CMHB-C	1.278	1	1
	Superpave-C	0.721	2	2
	PFC	0.270	3	3
Soft Limestone	CMHB-C	1.940	1	1
	Superpave-C	1.474	2	2
	PFC	0.282	3	3
Sandstone	CMHB-C	1.496	3	3
	Superpave-C	1.956	2	2
	PFC	0.349	4	4
	Type-D	2.690	1	1
Gravel	CMHB-C	1.407	2	2
	Superpave-C	1.590	3	3
	PFC	0.271	4	4
	Type-D	1.902	1	1

SUMMARY

The discrete element model developed Chapter III was modified in this chapter in order to track the different cracking patterns within asphalt mixtures. The modified model successfully captured three different cracking patterns: matrix phase cracking, aggregate phase cracking, and interface cracking. This model was then used to quantify cracking

patterns for the 17 different mixtures in this study. This was achieved by developing a method that can track and count broken aggregate-aggregate bonds, matrix-matrix bonds, and aggregate-matrix bonds.

The results showed that the PFC mixture encountered the highest matrix phase cracking and had the lowest mixture strength for all the different aggregates. The results revealed that higher percentages of interface cracking are associated with higher mixture strength. This can be explained by crack retardation at the interface of a matrix with an aggregate particle. Cracking within the aggregate phase occurred in most of the cases, but not for the gravel aggregates. This aggregate cracking was the highest in the soft limestone mixtures. This finding indicates that the strength of the aggregate plays a significant role on whether the aggregate particles will be able to sustain the internal forces applied within the asphalt mixtures.

CHAPTER VII

CONCLUSIONS AND RECOMMENDATIONS

CONCLUSIONS

This study deals with the development of an approach for modeling the combined effects of aggregate gradation, shape, stiffness, and strength on asphalt mixture performance utilizing the Discrete Element Method (DEM) along with image processing techniques. The interaction between these different properties is difficult to study through experimental testing only, and thus numerical and analytical approaches are useful to investigate such a difficult problem.

The literature review presented in this dissertation demonstrated that aggregate properties such as angularity, size, strength and toughness, and gradation, play an essential role in influencing asphalt mixture performance. The review also showed that the DEM approach is a useful method to analyze asphalt mixture response as it is capable of accounting for the interaction between the internal structure distribution and aggregate properties in the analysis of asphalt mixture response and performance.

The discrete element model developed in this study was used in simulating the resistance of asphalt mixtures to fracture, and the model allowed for quantification of the internal forces in asphalt mixtures, which cannot be accomplished by conventional experimental methods. The results showed that the PFC mixtures experienced higher stresses than all other mixtures, and thus it is recommended that aggregate strength for PFC mixtures should be about 25% more than the strength of aggregates used in dense

graded or gap graded mixtures. The model was also used to analyze the performance of different aggregates based on internal forces and resistance to fracture. The results can be used to select the appropriate aggregate type given a specific mixture design.

The model was successful to a large extent in representing the influence of the variability of both aggregate properties and internal structure distribution on mixture response. Aggregate variability was considered in this analysis by assigning a distribution for aggregate strength instead of a single average value. Consequently, it was possible to analyze the effect of changes in variability in aggregate properties and their spatial distribution within the mixture on the mixture strength. The variability in mixture strength obtained from the DEM compared fairly well with the variability obtained from laboratory testing.

The impact of aggregate blending on the strength of asphalt mixtures was studied using the discrete element model. The analysis showed that both the mixture internal structure and the strength of aggregates used in the blend influence the optimum percentage of blending without adversely influencing strength. It was interesting to find that some mixtures can accommodate about 40% soft (low strength) aggregate without decreasing mixture strength in comparison to the use of 100% hard (high strength) aggregates, while some mixtures showed a trend of a linear decrease in strength with the increase of the amount of soft (low strength) aggregate used. However, all the mixture types showed that there is no benefit to using less than 30% of the high strength aggregate because at this level the low strength aggregate will control the mixture response.

The percent change in the different experimental tests results were compared to the percent change of the DEM strength results. The experimental tests included the IDT strength, dynamic modulus, Hamburg wheel (rut depth), and flow time maximum strain. The DEM results compared reasonably well to experimental measurements of the properties of mixtures with different blending percentages. The results revealed that there is a minimum aggregates strength ratio for blending to be useful in enhancing mixture strength. This minimum ratio is about 1.36. Charts were developed to estimate the percentage change in mixture strength based on the ratio of the strength of the blended aggregates and the percentages of these aggregates.

A probabilistic-analytical approach was used to analyze aggregate breakage in asphalt mixtures. This approach incorporates the internal force distribution obtained from the discrete element model and the distribution of aggregate strength to predict the probability of aggregate breakage in a mixture. The output of this approach is a mathematical expression that represents the probability of aggregate breakage as a function of loading level, and it can be evaluated numerically. The analysis approach is based on the hypothesis that fracture probability is a function of two different events: contact bond strength and the internal force distribution at the contact points. The approach is very flexible and can include any types of distributions for the two events. It can be used to estimate the probability of aggregate fracture for different types of mixtures and/or aggregates. The results of aggregate breakage from DEM compared well with the results of the derived probability of aggregate breakage.

The discrete element model was used to track the different cracking patterns (cohesive: aggregate-aggregate, cohesive: matrix-matrix, and adhesive: matrix-aggregate) in asphalt mixtures. The cracking patterns in asphalt mixtures were dependent on aggregate properties and mixture internal structure. For all the different aggregate types, the PFC mixture experienced the highest cracking percentage within the matrix. For the different mixtures, gravel was the only aggregate that did not encounter any cracking, while both the soft limestone and hard limestone experienced cracking for all the different types of mixtures. The analysis showed that the mixtures with highest percentage of cracking on the interface had the highest total energy.

RECOMMENDATIONS

These following recommendations are based on the results presented in this dissertation:

- The model developed is capable of ranking the performance of different aggregates for a specific mixture as well as ranking the different mixtures for one aggregate. Consequently, the model is a useful tool to investigate which mixture can be used in certain areas given the availability of local aggregate sources.
- The blending charts developed in chapter IV can be used to establish guidelines for allowable percentages of blending soft (low strength) aggregates. However, verification with more experimental data is needed to assure that these charts can be used for soft materials other than the soft limestone used in this study.
- The analytical approach presented in chapter V to determine the probability density function (PDF) of aggregate fracture in asphalt mixtures is flexible as it

can include any mathematical function that describes aggregate strength distribution. It is recommended to use this approach to generate PDFs for a wide range of aggregates. These functions can then be used to optimize the selection of aggregates and designs of asphalt mixtures.

- The cracking patterns quantified in chapter VI showed that mixtures with very high cracking within the matrix phase have the lowest mixture strength, and that mixtures that encountered crack retardation followed by interface cracking had a higher strength ratio. It is recommended to investigate different combinations of binders, aggregates, and mixture designs in order to recommend a set of such combinations that would produce more of the "favorable" cracking patterns that are associated with higher mixture strength.
- It is recommended to continue research efforts that combine analytical and numerical approaches to develop a virtual testing environment of asphalt mixtures. This virtual environment would be useful to account for the interaction between the properties of the mixture constituents and mixture design and the influence of this interaction on mixture performance. Once the model is calibrated it can be used to run as many simulations as required. Thus, the virtual testing environment would be an inexpensive means to evaluate the influence of changing different material and design factors on the mixture response, as it provides precise control over almost every single factor.

REFERENCES

Abbas, A. R. (2004). "Simulation of the micromechanical behavior of asphaltic mixtures using the discrete element method." Ph.D. Dissertation, Washington State University, Pullman, WA.

Abbas, A., Masad, E., Papagiannakis, T., and Harman, T. (2007). "Micromechanical modeling of the viscoelastic behavior of asphalt mixtures using the discrete-element method." *International Journal of Geomechanics* ASCE, 7(2), 131-139.

Abbas, A., Masad, E., Papagiannakis, T., and Shenoy, A. (2005). "Modelling asphalt mastic stiffness using discrete element analysis and micromechanics-based models." *International Journal of Pavement Engineering*, 6(2), 137-146.

Aho, B. D., Vavrik, W. R., and Carpenter, S. H. (2001). "Effect of flat and elongated coarse aggregate on field compaction of hot-mixture asphalt." *Transportation Research Record. 1761*, Transportation Research Board, Washington, DC; pp 26–31.

Barksdale, R. D., Pollard C. O., Siegel, T., and Moeller, S. (1992). "Evaluation of the effect of aggregate on rutting and fatigue of asphalt." *Technical Report FHWA-AG-92-8812*. Georgia Department of Transportation, Atlanta, GA.

Cheng, Y. P. H. (2004). "Micromechanical investigation of soil plasticity." Ph.D. Dissertation, Churchill College, University of Cambridge, UK.

Cheng, Y. P., Nakata, Y., and Bolton M. D. (2003). "Discrete element simulation of crushable soil." *Geotechnique*, 53(7), 633-641.

Cheung, L. W, and Dawson, A. R. (2002). "Effects of particle and mixture characteristics on performance of some granular materials." *Transportation Research Record 1787*, Transportation Research Board, Washington, DC; pp 90-98.

Collins R. J. (1976). "Waste products as a potential replacement for aggregates." *Proc., 4th International Ash Utilization Symposium*, St. Louis, MO, March 24-25, pp. 93-113.

Cundall, P. A. (1971). "A computer model for simulating progressive large scale movements in blocky rock systems." *Proc., Symposium of the International Society of Rock Mechanics,* Nancy, France, Vol. 1, Paper No. II-8.

Cundall, P. A., and Hart, R. (1992). "Numerical modeling of discontinua." *J. Engr. Comp.,* 9, 101-113.

Cundall, P. A., and Strack, O. D. L. (1979). "A discrete numerical model for granular assemblies." *Geotechnique*, 29(1), 47-65.

Dai, Q., and You, Z. (2007). "Prediction of creep stiffness of asphalt mixture with micromechanical finite-element and discrete-element models." *Journal of Engineering Mechanics* ASCE, 133 (2), 163-173.

Evans, A. G. (1972). "The strength of brittle materials with a second-phase dispersion." *Philosophical Magazine,* 26, 1327-1344.

Foltz, R. B., and Truebe, M. (2003). "Locally available aggregate and sediment production." *Transportation Research Record 1819*, Transportation Research Board, Washington, DC; pp. 185–193.

Guerrero, S., and Vallejo, L. E. (2005). "Discrete element method evaluation of granular crushing under direct shear test conditions." *Journal of Geotechnical and Geoenvironmental Engineering* (ASCE) 131(10), 1295-1300.

Hand, A. J., Stiady, J. L., White, T. D., Noureldin, A. S., and Galal, K. (2002). "Gradation effects on hot-mixture asphalt performance." *Journal of the Association of Asphalt Paving Technologists*, 70, 132-175.

Harra, G. W. (1962). "Degradation of aggregates." *Pacific Builder and Engineer*, 68(9), 86-86.

Hesp, S. A. M., Smith, B. J., and Hoare, T. R. (2001). "Effect of the filler particle size on the low and high temperature performance of asphalt mastic and concrete." *Journal of the Association of Asphalt Paving Technologists*, 70, 492-508.

Jacobs, M. M. J. (1995). "Crack growth in asphaltic mixtures." Ph.D. Dissertation, Delft University of Technology, Delft, Netherlands.

Kim, H., Wagoner, M. P., and Buttlar, W. (2008). "Simulation of fracture behavior in asphalt concrete using a heterogeneous cohesive zone discrete element model." *Journal of Materials in Civil Engineering* ASCE, 20(8), 552-563.

Lange, F. F. (1970). "The interaction of a crack front with a second-phase dispersion." *Philosophical Magazine*, 22, 983-992.

Lytton, R. (2007). personal communication.

Mahmoud, E., and Masad, E. (2007). "Experimental methods for the evaluation of aggregate resistance to polishing, abrasion and breakage." *Journal of Materials in Civil Engineering* ASCE, 19(11), 977-985.

Marketos, G., and Bolton, M.D. (2007). "Quantifying the extent of crushing in granular materials: A probability-based predictive method." *Journal of the Mechanics and Physics of Solids*, 55(10), 2142-2156.

Masad, E. (2003). "The development of a computer controlled image analysis system for measuring aggregate shape properties." *Final Report*, National Cooperative Highway Research Program NCHRP-IDEA Project 77, National Research Council, Washington, D.C.

McDowell, G. R., and Bolton, M. D. (1998). "On the micromechanics of crushable aggregates." *Geotechnique*, 48(5), 667-679.

McDowell, G. R., and Harireche, O. (2002). "Discrete element modeling of soil particle fracture." *Geotechnique,* 52(2), 131-135.

Nakata, Y., Hyde, A. F. L., Hyodo, M., and Murata, H. (1999). "A probabilistic approach to sand particle crushing in the triaxial test." *Geotechnique*, 49(5), 567–583.

Pan, T., Tutumluer, E., and Anochie-Boateng, J. (2006). "Aggregate morphology affecting resilient behavior of unbound granular materials." *Transportation Research Record 1952*, Transportation Research Board, Washington, D.C.; pp. 12-20.

Particle Flow Code in 2-Dimensions (PFC2D) Manual (2004), Version 3.10, Itasca Consulting Group, Minneapolis, MN.

Prowell, B. D., Zhang., J., and Brown, E. R. (2005). "Aggregate properties and the performance of superpave designed hot mixture asphalt." *NCHRP Report 539*, Transportation Research Board, National Research Council, Washington, D.C.

Rajaram, V., and Hoagberg, R. K. (1984). "Inventory of aggregates in an expanding urban area." *Bulletin of Engineering Geology and the Environment*, 29(1), 315-319.

Rakshvir, M., and Barai, S. V. (2006). "Studies on recycled aggregates-based concrete." *Waste Management & Research*, 24(3), 225-233.

Rodriguez, M. G., Morrison, G. R., van Loon, J. R., and Hesp, S. A. M. (1996). "Low temperature failure in particulate-filled asphalt binders and asphalt concrete mixtures." *Journal of the Association of Asphalt Paving Technologists*, 66, 520-569.

Sanders, C. A., and Dukatz, E. L. (1992). "Evaluation of percent fracture of hot-mixture asphalt gravels in Indiana." *Effect of Aggregate and Mineral Filler on Asphalt Mixture Performance*, R. C. Meininger, ed., American Society for Testing and Materials, STP 1147. Philadelphia, PA.

Smith, B. J. and Hesp, S. A. M. (2000). "Crack pinning in asphalt mastic and concrete: regular fatigue studies." *Transportation Research Record No. 1728*, Transportation Research Board, Washington, D.C.; pp 75-81.

Tutumluer, E., and Pan, T. (2008). "Aggregate morphology affecting strength and permanent deformation behavior of unbound granular materials." *Journal of Materials in Civil Engineering* ASCE, 20(9), 617-627.

USGS (U.S. Geological Survey) (1999). "Natural aggregates – Foundation of America's Future." *USGS Fact Sheet FS 144-97*, U.S. Department of Interior.

Wu, Y., Parker, F., and Kandhal, P. S. (1998). "Aggregate toughness/abrasion resistance and durability/soundness tests related to asphalt concrete performance in pavements." *Transportation Research Record 1638*, Transportation Research Board, Washington, D.C.; pp. 85–93.

You, Z., and Buttlar, W. G. (2004). "Discrete element modeling to predict the modulus of asphalt concrete mixtures." *Journal of Materials in Civil Engineering* ASCE, 16(2), 140-146.

You, Z., and Buttlar, W. G. (2005). "Application of discrete element modeling techniques to predict the complex modulus of asphalt—aggregate hollow cylinders subjected to internal pressure." *Transportation Research Record 1929*, Transportation Research Board, Washington, DC; pp 218–226.

APPENDIX A

MAXIMUM CONTACT FORCE PROBABILITY DENSITY PLOTS

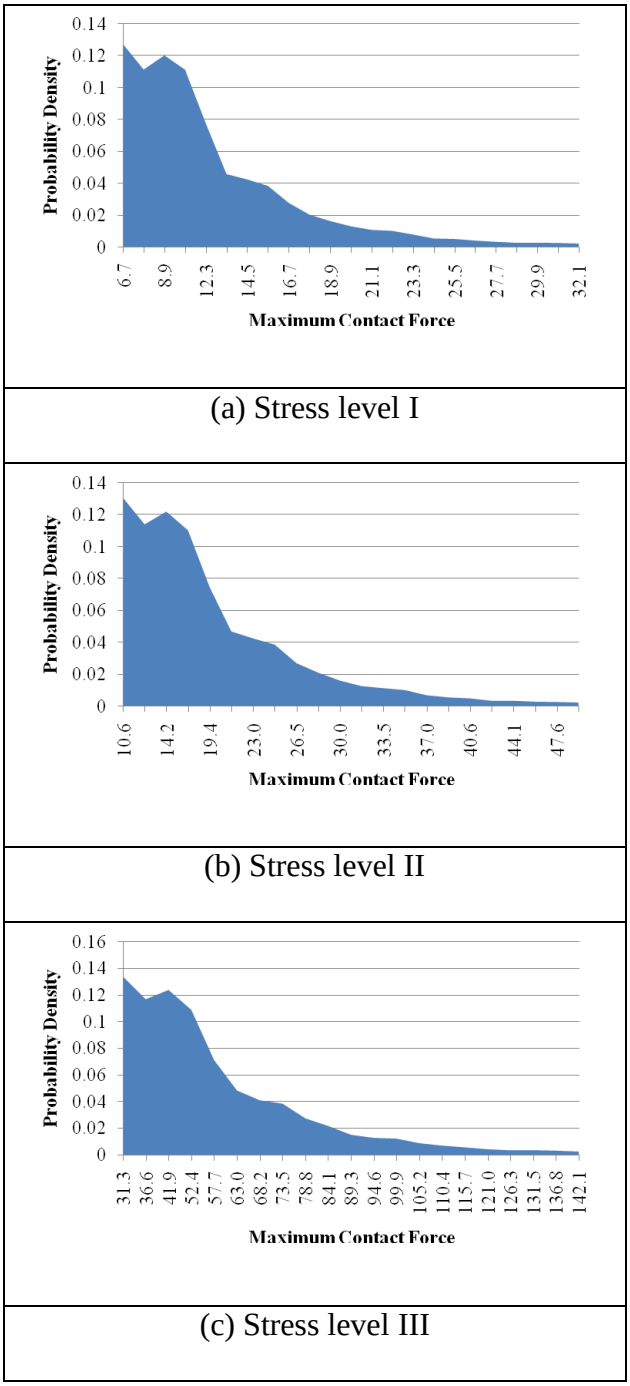

Figure A.1. Maximum Contact Force Probability Density (Hard Limestone CMHB Mixture).

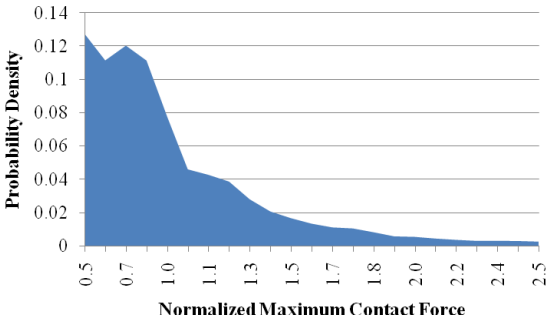

(a) Stress level I – normalized

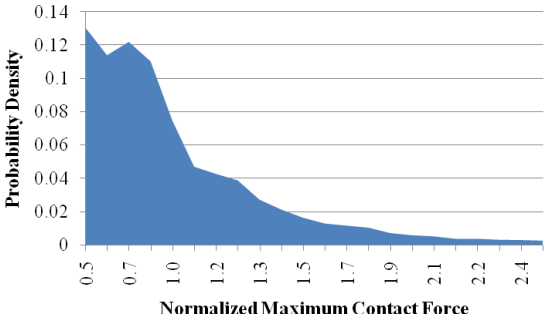

(b) Stress level II – normalized

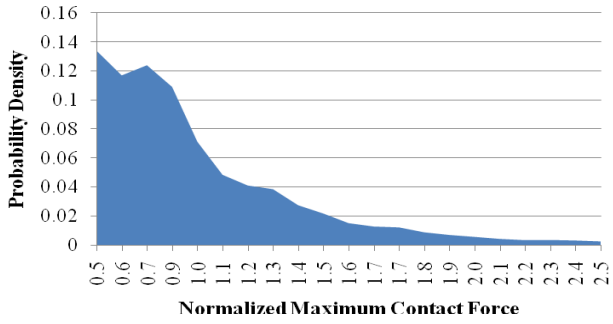

(c) Stress level III – normalized

Figure A.2. Normalized Maximum Contact Force Probability Density (Hard Limestone CMHB Mixture).

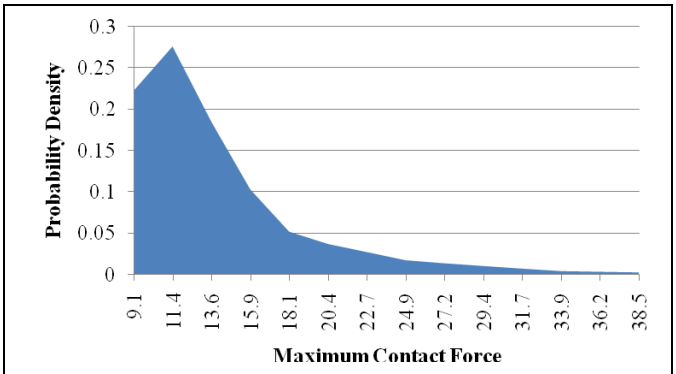

(a) Stress level I

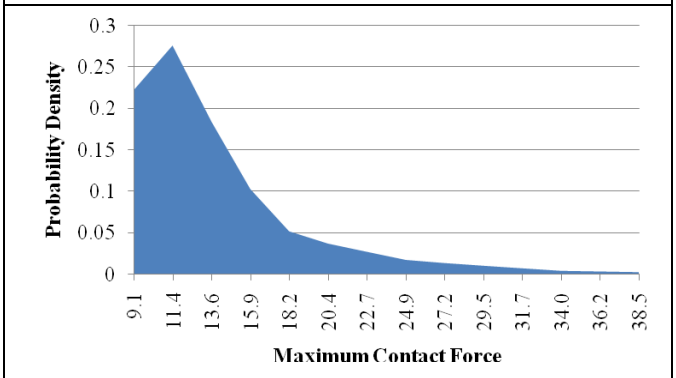

(b) Stress level II

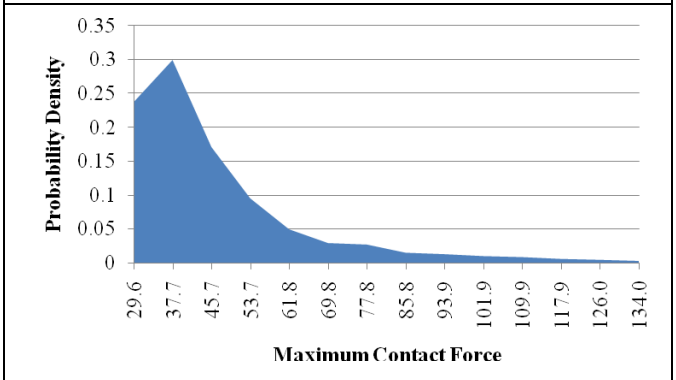

(c) Stress level III

Figure A.3. Maximum Contact Force Probability Density (Hard Limestone PFC Mixture).

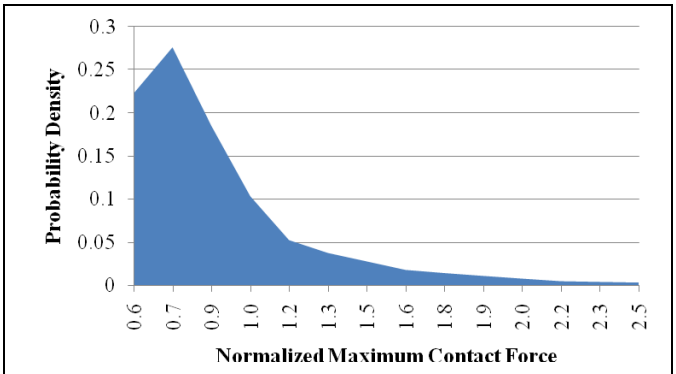

(a) Stress level I – normalized

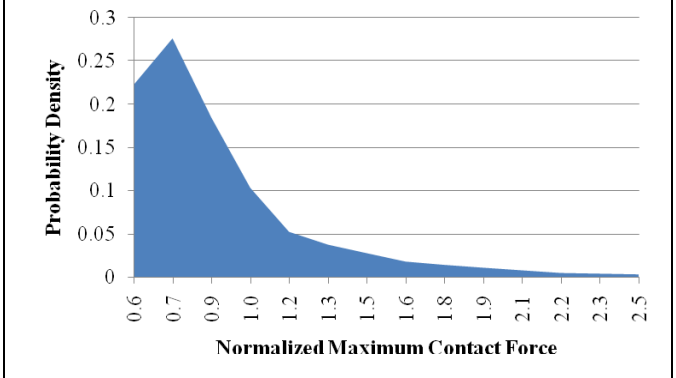

(b) Stress level II – normalized

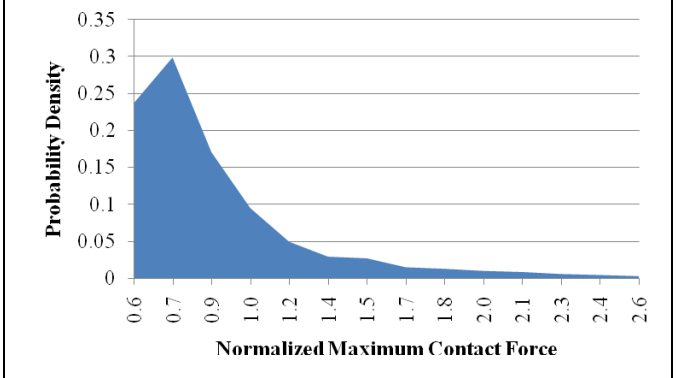

(c) Stress level III – normalized

Figure A.4. Normalized Maximum Contact Force Probability Density (Hard Limestone PFC Mixture).

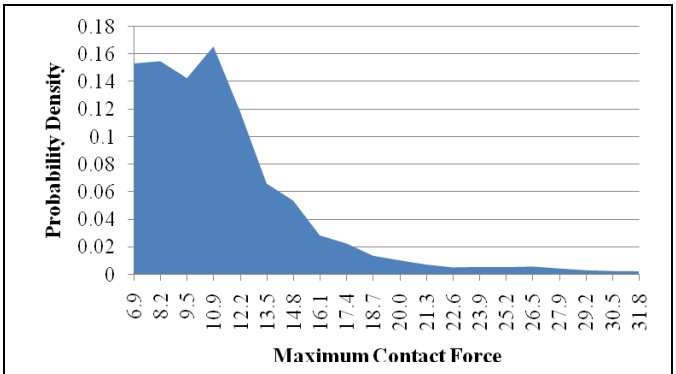

(a) Stress level I

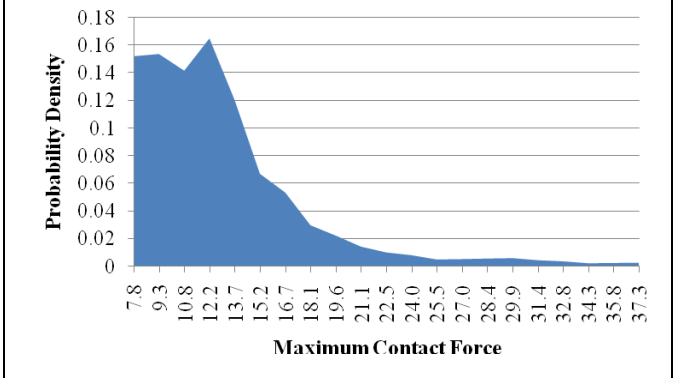

(b) Stress level II

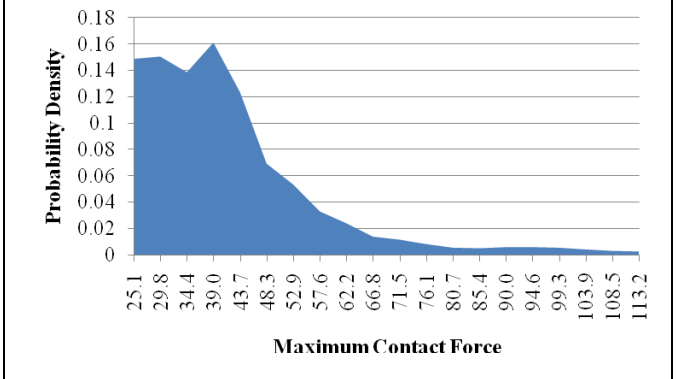

(c) Stress level III

Figure A.5. Maximum Contact Force Probability Density (Soft Limestone Superpave Mixture).

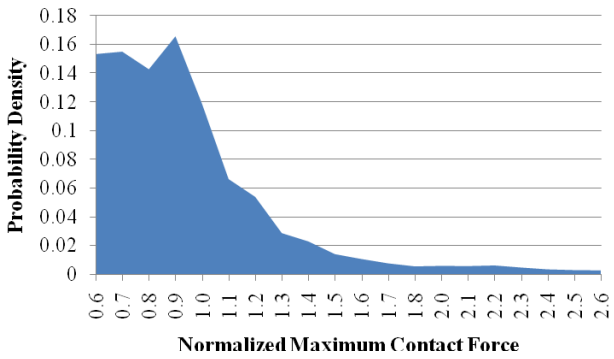

(a) Stress level I – normalized

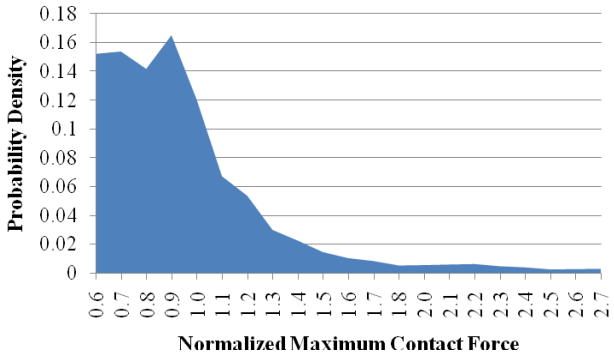

(b) Stress level II – normalized

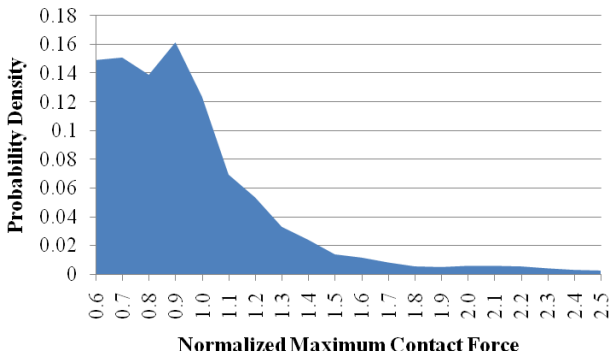

(c) Stress level III – normalized

Figure A.6. Normalized Maximum Contact Force Probability Density (Soft Limestone Superpave Mixture).

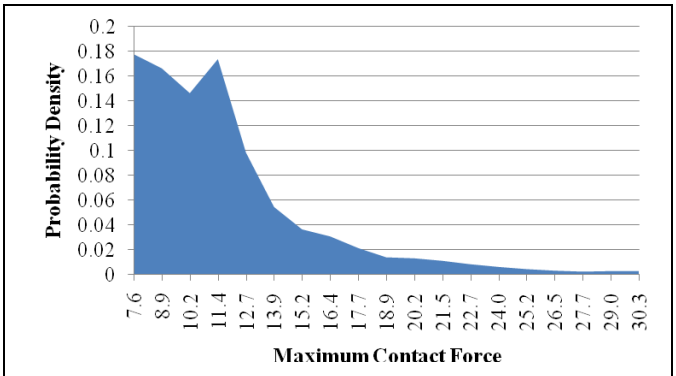

(a) Stress level I

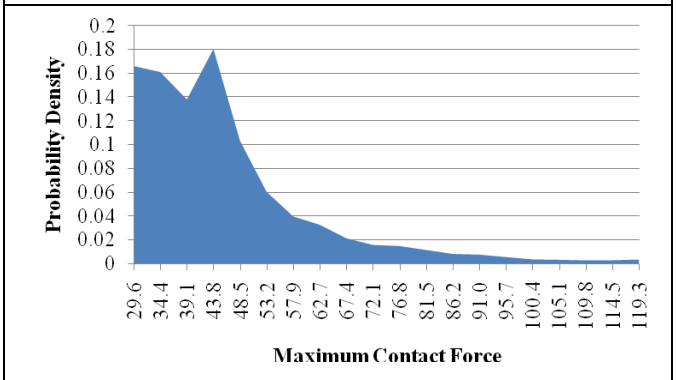

(b) Stress level II

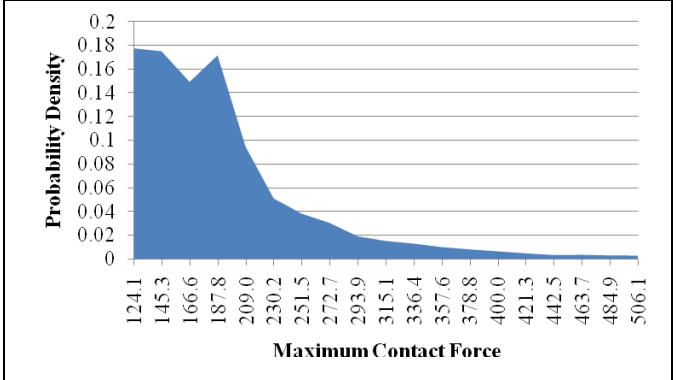

(c) Stress level III

Figure A.7. Maximum Contact Force Probability Density (Sandstone Superpave Mixture).

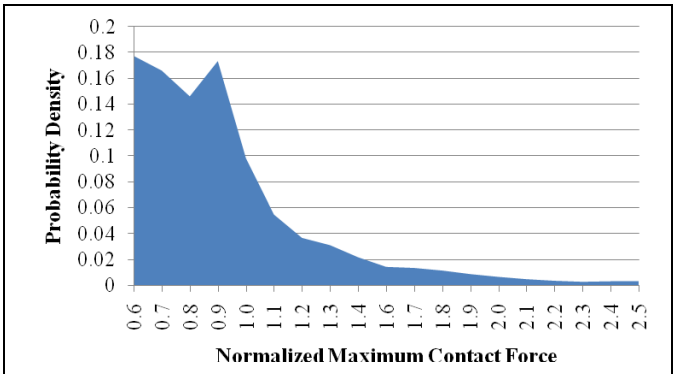

(a) Stress level I – normalized

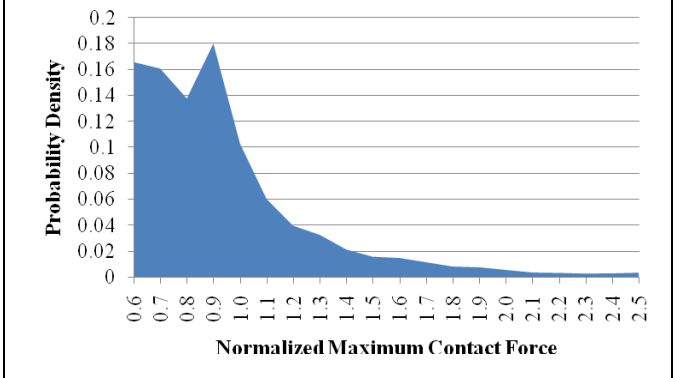

(b) Stress level II – normalized

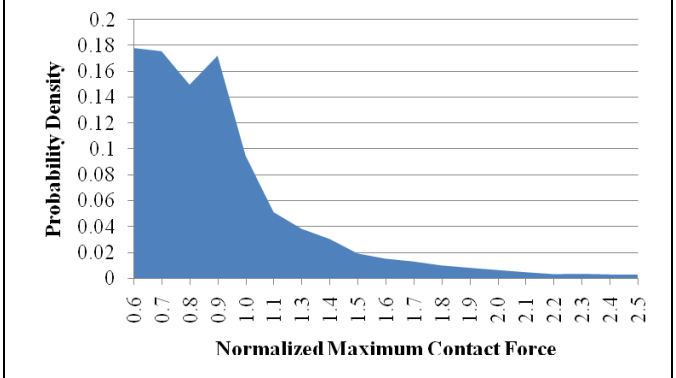

(c) Stress level III – normalized

Figure A.8. Normalized Maximum Contact Force Probability Density (Sandstone Superpave Mixture).

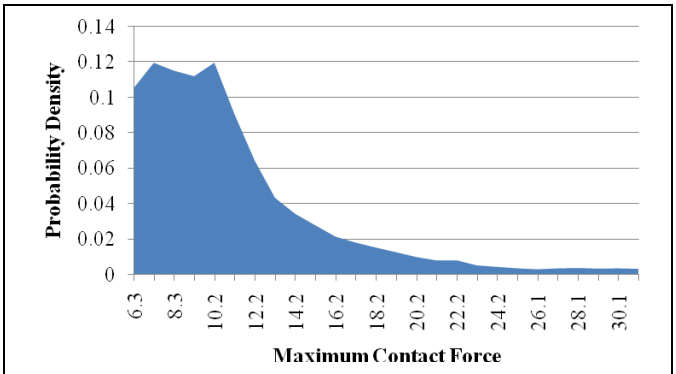

(a) Stress level I

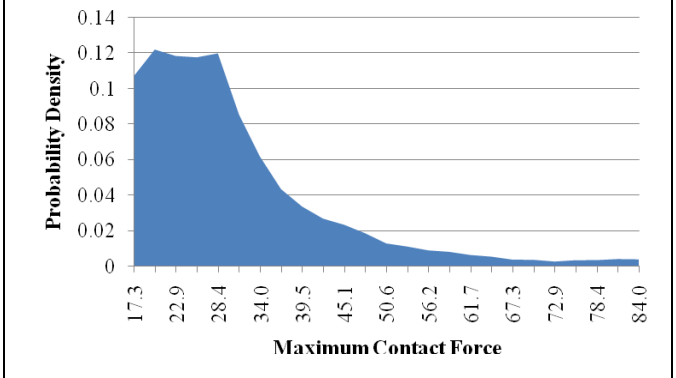

(b) Stress level II

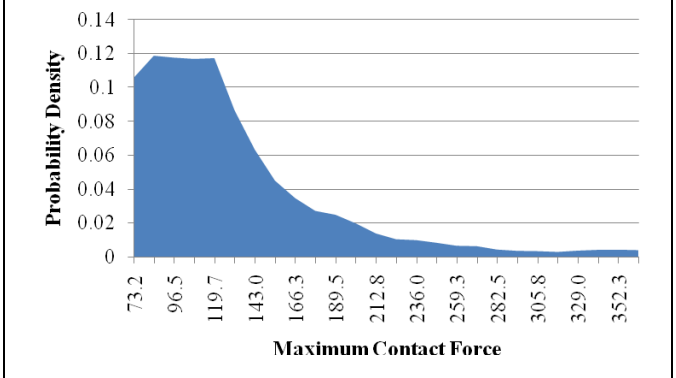

(c) Stress level III

Figure A.9. Maximum Contact Force Probability Density (Sandstone Type-D Mixture).

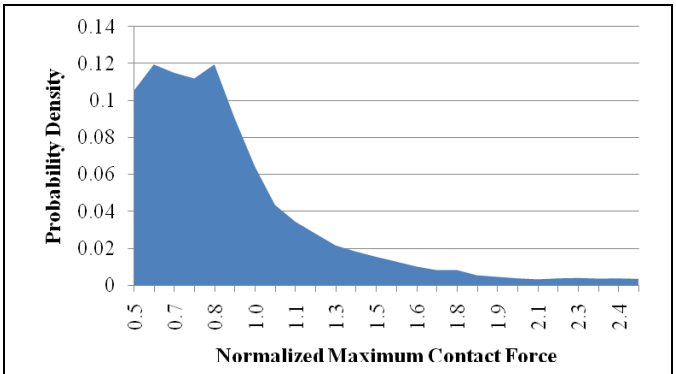

(a) Stress level I – normalized

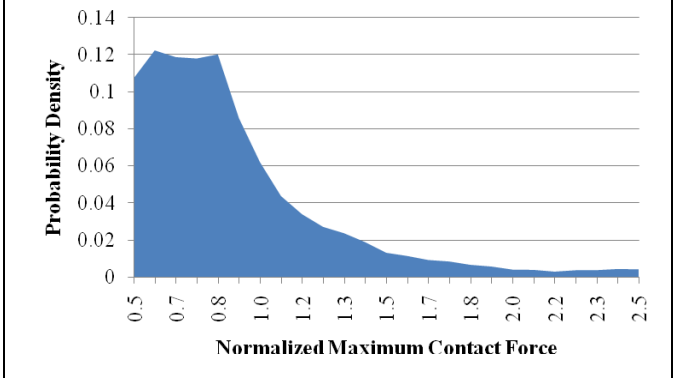

(b) Stress level II – normalized

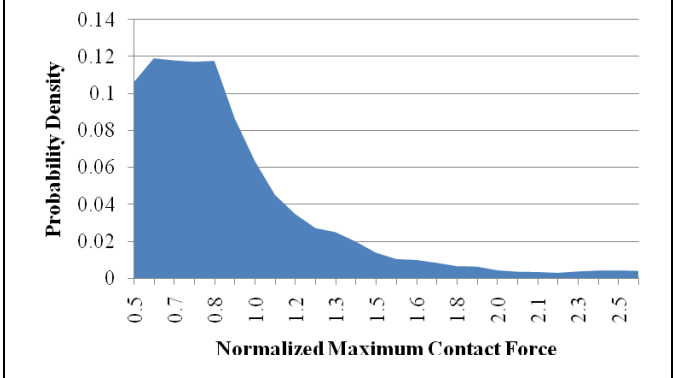

(c) Stress level III – normalized

Figure A.10. Normalized Maximum Contact Force Probability Density (Sandstone Type-D Mixture).

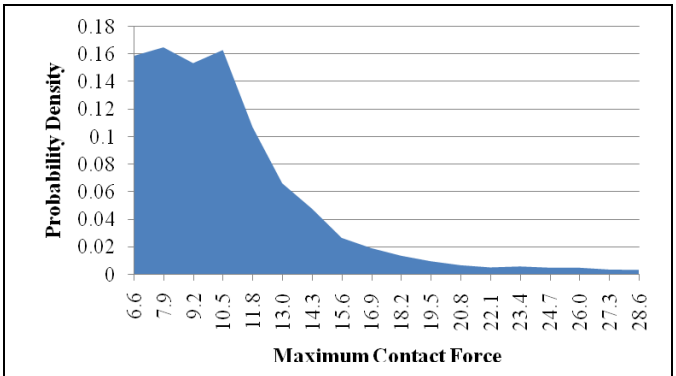

(a) Stress level I

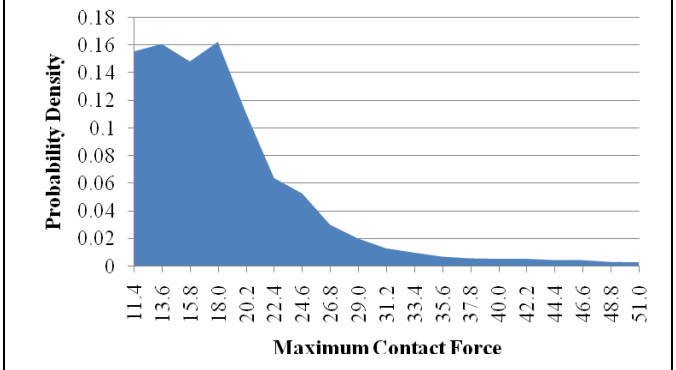

(b) Stress level II

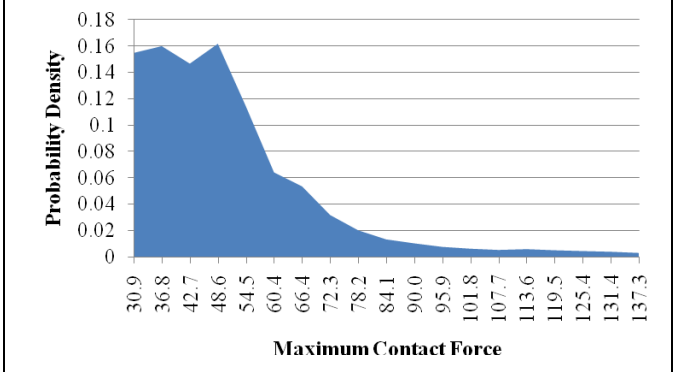

(c) Stress level III

Figure A.11. Maximum Contact Force Probability Density (Granite Superpave Mixture).

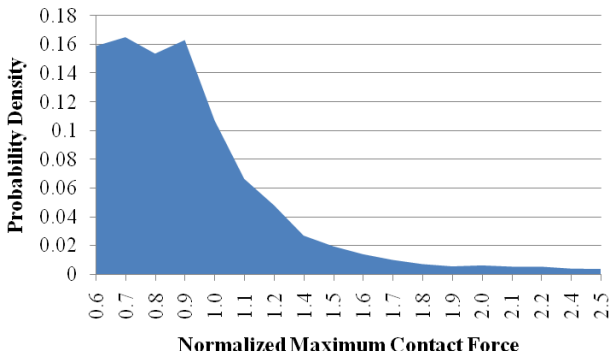

(a) Stress level I – normalized

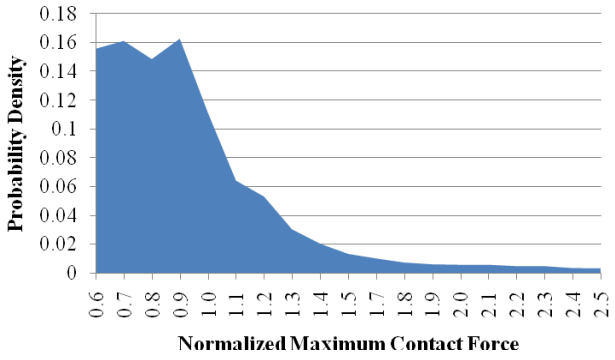

(b) Stress level II – normalized

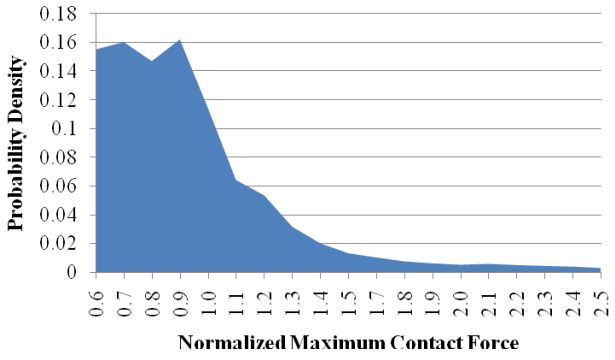

(c) Stress level III – normalized

Figure A.12. Normalized Maximum Contact Force Probability Density (Granite Superpave Mixture).

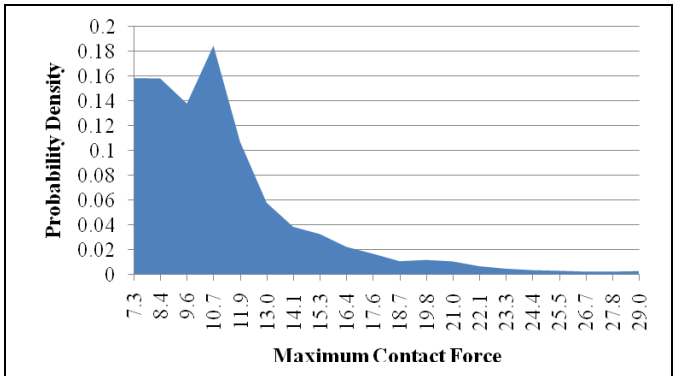

(a) Stress level I

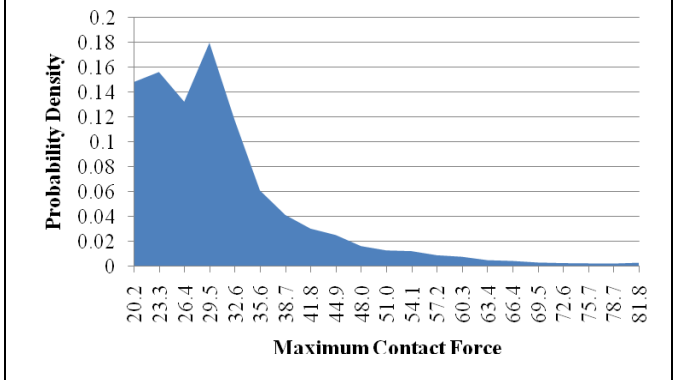

(b) Stress level II

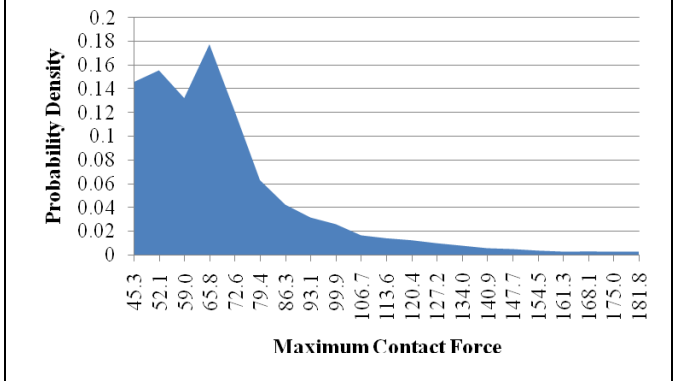

(c) Stress level III

Figure A.13. Maximum Contact Force Probability Density (Gravel Superpave Mixture).

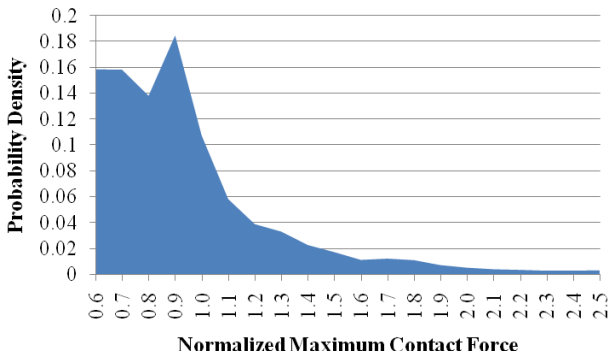

(a) Stress level I – normalized

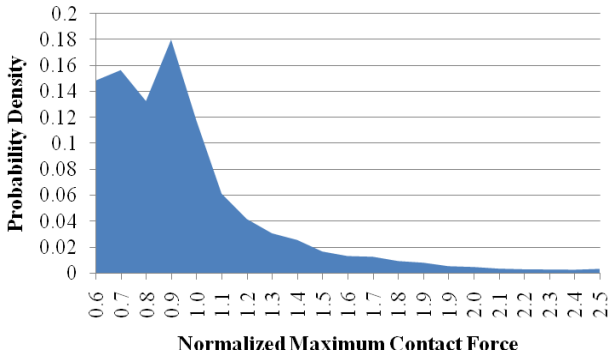

(b) Stress level II – normalized

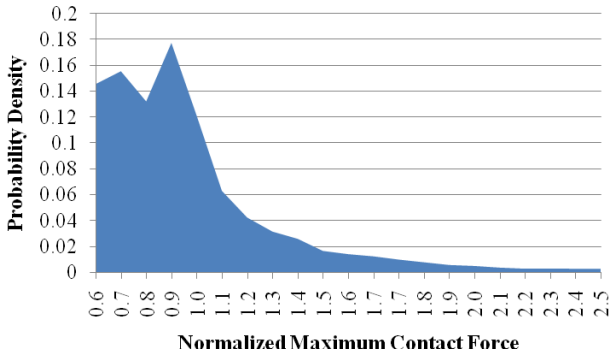

(c) Stress level III – normalized

Figure A.14. Normalized Maximum Contact Force Probability Density (Gravel Superpave Mixture).

VITA

Name:	Enad Muhib Ahmad Mahmoud
Address:	67 Uqba Bin Nafe' street, B-2, Jabal Amman – Fifth Circle, Amman, Jordan
Email Address:	enad81@yahoo.com
Education:	B.S., Civil Engineering, University of Jordan, Amman, 2003 M.S., Civil Engineering, Texas A&M University, 2005 Ph.D., Civil Engineering, Texas A&M University, 2009